LOAD BEARING REGENERATIVE REPAIRS FOR THE CARTILAGINOUS SOFT TISSUE OF THE INTERVERTEBRAL DISC

By

James W. S. Hayami

A thesis submitted to the Department of Chemical Engineering

in conformity with the requirements for

the degree of Doctor of Philosophy

Queen's University

Kingston, Ontario, Canada

(August, 2014)

Abstract

Cartilaginous load bearing soft tissues such as the nucleus pulposus in the intervertebral disc are affected by degenerative diseases and physical injury, which if not treated early can initiate a progressive decline in joint function and result in lower back pain. Early treatment options to repair the nucleus pulposus, regain immediate joint function, and aid in the regeneration of *de novo* tissue are necessary to restore the health and function of symptomatic joints. To satisfy the regenerative design criteria, a cellular hydrogel based approach was chosen and methods were examined to improve mechanical properties while maintaining an injectable and *in situ* formable scaffold. To improve the stiffness and fatigue resistance of the hydrogels, low molecular weight acrylated *star*-copolymers composed of D,L-lactide or trimethylene carbonate with ε-caprolactone were mixed with an aqueous solution of methacrylated glycol chitosan to form a hydrogel-elastomer co-continuous morphology. After photo-cross-linking, the elastomer phase contributed the majority of the initial stiffness to the co-continuous scaffolds. Hydrolysis of the elastomer phase, controlled the decrease in the co-continuous scaffold modulus from fast (2 – 3 weeks) to slow (> 2 months) by changing D,L-lactide to trimethylene carbonate in the ε-caprolactone based elastomers. The slower degrading trimethylene carbonate based elastomer phase was able to maintain an approximate 1200 kPa equilibrium modulus in the co-continuous scaffolds during a 2 month *in vitro* static culture. Methacrylated prepolymers of glycol chitosan, hyaluronic acid, chondroitin sulfate and their blends were examined to improve the initial mechanical properties of the hydrogels and maintain the phenotype of the encapsulated chondrocytes during culture. A co-cross-linked mixture of methacrylated prepolymers, hyaluronic acid and chondroitin sulfate, had an initial equilibrium modulus of 260 kPa, which was maintained along with the highest number of the originally seeded cells (60 %) and cartilaginous matrix accumulation compared to the other hydrogels during a 1 month *in vitro* static culture.

Overall, the development of the co-continuous hydrogel-elastomer morphology was able to produce an injectable cell encapsulating scaffold with an initial modulus greater than 1 MPa and demonstrated regenerative potential that would be suitable for the repair of cartilaginous load bearing soft tissues.

Acknowledgements

I would like to express my sincere gratitude to my supervisors Dr. Brian Amsden and Dr. Stephen Waldman for the support and patience you have both provided throughout my PhD.

I have been here too long to thank everyone I have met along the way, but if we shared a conversation, had a laugh or talked about our research I want to thank you. You have made an impact on my life and it would not have been the same without you. A special thank you goes out to Jillian Brenner, Fei Chen, Jackie Fan, Jake Kaupp, Justin Lee, Aaron McGregor, Moira Vyner, Joanna Weber, and Stuart Young for making my time here extra special.

I would like to thank my parents John and Judy and my brother Robert for all the love and support you have provided me throughout this process. Dad, you taught me that hard work pays off and to see a job through until the end. Mom, your love, patience and compassion showed me all that's good in this world. To my big brother Robbie, you showed me that nothing is truly broken it just has a new purpose. Thank you.

Finally, to my best friend Jenna Usprech, you have been by my side throughout this entire process and I could not have done it without you. Your wonderful outlook on life is contagious and you are a true inspiration to those around you. You are the love of my life. Thank you.

Table of Contents

List of Figures

List of Tables

List of Abbreviations

(Tri)Acrylated Star Co-Polymer	ASCP
2-Aminoethyle Methacrylate	AEMA
Adipose Derived Stem Cell	ADSC
Annulus Fibrosis	AF
Articular Cartilage	AC
Bone Marrow Derived Mesenchymal Stem Cell	BMSC
Chondroitin Sulfate (Methacrylated)	CS (MCS)
Degenerative Disc Disease	DDD
Degree of Methacrylation	DM
Extra-cellular Matrix	ECM
Glycidyl Methacrylate	GMA
Glycol Chitosan (*N*-Methacrylated)	GC (MGC)
Glycosaminoglycan	GAG
Hyaluronic Acid (Methacrylated)	HA (MHA)
Intervertebral Disc	IVD
Load Bearing Soft Tissues	LBST
Mass Concentration	% w/v
Mass Fraction	% w/w
Methacrylic Anhydride	MA
Molecular Weight	MW
Notochordal	NC
Nucleus Pulposus	NP
Pericellular Matrix	PCM
Poly(ethylene glycol)	PEG

Poly(ε-caprolactone-*co*-D,L-lactide)	DLLACL
Poly(ε-caprolactone-*co*-trimethylene carbonate)	TMCCL
Proteoglycan	PG
Total Disc Replacement	TDR
Total Joint Arthroplasty	TJA
Volume Concentration	% v/v

Chapter 1

Introduction

1.1 Research Problem – Nucleus Pulposus Related Back Pain

Treatment for lower back pain is one of the top-ranked, most expensive medical interventions in North America. [1] It is estimated that over $100 billion dollars a year are spent on health care costs related to lower back pain. [2] Individuals that are plagued by chronic back pain often have limited mobility and a reduced quality of life. [2] A review of the literature on lower back pain shows a strong correlation to degeneration within the intervertebral disc (IVD), known as degenerative disc disease (DDD). [3] However, the cause of DDD is not well understood and many studies have been conducted to investigate how the disease progresses. These studies have determined a linkage of DDD to work related repetitive strain, smoking, age, sex, and more recently, genetics. [4] In addition, lower back pain can also be caused by acute injury to the IVD from physical overloading, which results in the herniation of the nucleus tissue into the surrounding nerves.

Most injuries to, or diseases of, the IVD are usually initiated within the central region called the nucleus pulposus. Early signs of degeneration and injury can be diagnosed with MRI and X-ray before the affected disc becomes symptomatic. [4] However, once the disc is symptomatic there are very limited options to repair it successfully. Current repair methods to alleviate discogenic pain use total disc replacements or spinal fusions. However, both of these methods are plagued by issues such as premature degradation of the adjacent discs and facet joints in addition to spinal stenosis to the point where additional surgeries may be required. [5-7] Therefore, an alternative method is needed to repair a symptomatic disc at an earlier stage in the degeneration process where most of the original IVD is still intact. Tissue engineering offers a method that could replace the nucleus pulposus with a cell-laden biodegradable scaffold. A

biodegradable scaffold with mechanical properties similar to the native NP could restore the natural disc height and overall joint biomechanics and ultimately alleviate the pain from the affected disc. In addition, the scaffold could be designed to be replaced by *de novo* tissue once the original materials have degraded *in vivo*.

1.2 Normal Intervertebral Disc Physiology

The intervertebral disc (IVD) is a multi-component soft tissue responsible for the load bearing and articulating movements between the vertebral bodies in the spine (Figure 1.1 (A)). Working from the outside in, the IVD is constructed radially from annulus fibrosus to the central nucleus pulposus (Figure 1.1 (B)). Axially, a hyaline cartilage membrane separates the central nucleus from the bony vertebral bodies (Figure 1.1 (C and D)).

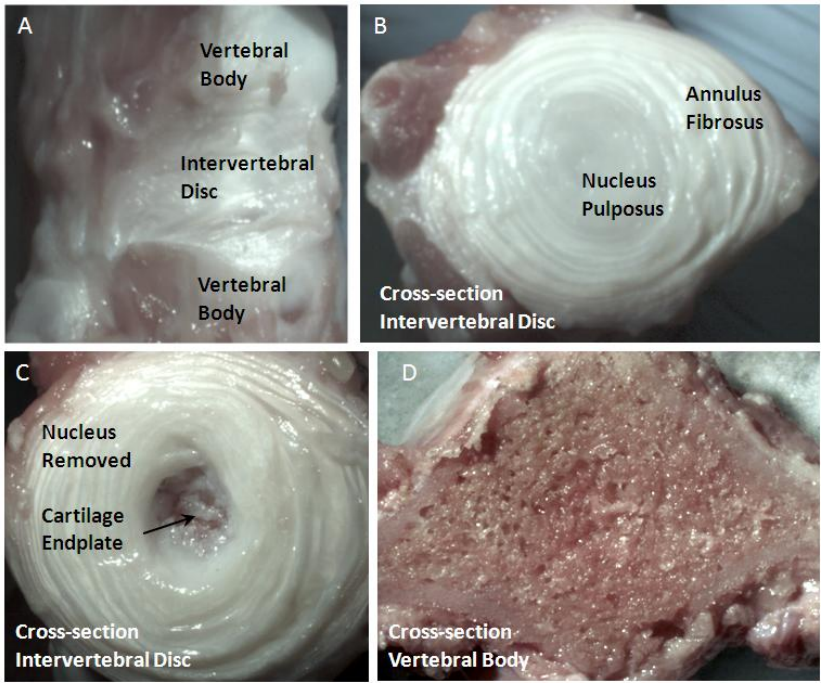

Figure 1.1: Bovine caudal motion segment for (A) lateral view of intact motion segment composed of an intervertebral disc (IVD) and two vertebral bodies. Transverse views of (B) intact IVD with central nucleus pulposus and outer annulus fibrous structures, (C) nucleus pulposus removed to show location of cartilage endplate and (D) cross-section of vertebral body showing porous bony structure filled with marrow (nutrient supply).

The annulus fibrosus is a complex tissue constructed from a series of lamellae, each of which contain well oriented collagen fibre bundles. The collagen fibre bundles are orientated approximately 30 ° from the horizontal, and alternate in direction between each lamellae. The highly defined lamellar structure of the annulus makes it resistant to radial pressure from the NP during axial compression of the spine. The fibre bundles are mainly constructed from collagen type I and have a defined crimp pattern, with a subcomponent of ~ 20 % collagen type II fibrils (outer annulus). [8] The collagen type II content transitions to approximately 70 % content in the inner annulus. Proteoglycans (dry weight) make up ~ 10 % of the outer annulus and ~ 30 % of the inner annulus. [8] Most of the lamellae are non-uniform in thickness and continuity, which leads to a defined inner and outer segment within the annulus. [9] The outer annulus, much like a ligament,

is embedded within the upper and lower vertebral bodies. The inner annulus gradually encapsulates the nucleus, curving inward and up towards the cartilage endplates. In addition to the physical changes within the annulus, vasculature decreases in density from the outer periphery to the nucleus interface, where very little is present.

A hyaline cartilage endplate contacts the upper and lower portion of the nucleus to the IVD. It is very similar in structure and function to articular cartilage and also contains rounded chondrocytes. A very thin layer of calcified cartilage separates the endplates from the bone along with blood capillaries and pockets of bone marrow in the vertebral bodies. [10] The function of the cartilage endplate in the IVD is to maintain the hydrostatic pressure by limiting the movement of water between the internal IVD (nucleus) and the vertebral bodies. [10]

The nucleus pulposus (NP) is often described as a soft gelatinous tissue, which is high in proteoglycan content and reinforced by a dense network of collagen fibrils. The NP has very limited vasculature present throughout the tissue and it is speculated that the cells receive nutrients via diffusion through both the cartilage endplates and annulus fibrosus. [11-13] It has been suggested that the IVD disc space is "immune-privileged" due to its avascular nature. [14-16] The main components found in the nucleus are proteoglycan (PG) molecules, which comprise ~ 70 % of the dry weight of the nucleus, of which the main PG is aggrecan. Collagen is the second most prevalent protein in the nucleus, with a typical collagen to proteoglycan ratio being around 1:20. [17] The main collagen present in the NP is type II and makes up ~ 80 % of collagen present in the nucleus. [8] Collagen type II fibrils form a loosely packed network in the nucleus, which trap PGs (mainly aggrecan) that have aggregated with hyaluronic acid. PG molecules and their negatively charged glycosaminoglycan subunits can complex with water and allow for a high water content (~ 80 %) to fill the interconnecting spaces within the matrix. [8] Hydrostatic pressure in the disc results in an increased disc height and stability of the spine as the annulus resists the pressure of the expanding nucleus.

The cell types found in the NP varies during early childhood to adolescence. Initially a notochordal cell population, which appears as clusters and form gap junctions between themselves, are the major cell type present in the NP tissue. [18] During adolescence the larger notochordal cells are replaced by the smaller NP cells, which are similar in appearance to the rounded chondrocytes located in hyaline cartilage. [19, 20] The NP cells are also similar in function to chondrocytes in that they synthesize proteoglycans and collagen type II fibrils, but to a much lesser extent than the original notochordal cells. [19]

1.3 The Degenerative Disc

The degenerative disc disease (DDD) process has been defined as an aberrant cell-mediated response to progressive structure failure. [21] Almost all adults are afflicted by some degree of DDD that most often results in lower back pain. The first tissue to be affected in the IVD is the centrally located nucleus pulposus. Some of the more noticeable and consistent degenerative changes within the NP begin to appear immediately after adolescence in both the cells and ECM. [22]

It has been speculated that the degenerative changes in NP tissue are linked to the loss of the notochordal cells during adolescence. [22] One possible reason for the loss of the notochordal cell population is a reduction in the transport ability for nutrients and waste removal through the cartilage endplates with time. [13] However, fractures to the cartilage endplates, which increase metabolite transport into the disc space can also result in DDD. [23, 24] The remaining adult NP cell population can be phagocytic, apoptotic and senescent, especially in areas where degenerative structural damage has occurred in the ECM of the nucleus. [25, 26] Therefore, there is a link between the changing NP cell population and structural changes to the IVD tissues, but how this directly plays into the DDD pathway is not known.

Age related degenerative effects on the NP tissue have also been reported. During the degenerative process, the PG aggregates within the nucleus become more fragmented, resulting in a loss of nucleus hydration (87 % to 74 % between childhood and old age). [8] The collagen network becomes stiffer due to a loss of collagen type II fibrils (80 % to 30 % of collagen dry weight after 60 years of age) and increased cross-linking between the fibrils and sugar molecules. [8] Ultimately, these changes in the NP physiology are often accompanied by a loss in the disc height and the mechanical stability of the spine, which eventually presents itself as lower back pain.

Many studies have looked for a link between DDD and other factors such as environmental risks, age, gender and genetics. Studies examining the spine with MRI and autopsy specimens have shown that there is a linear increase in disc degeneration with age (more specifically between 2 to 88 years of age). [27-29] Gender and environmental factors have not been strongly linked with DDD due to conflicting results. Genetic factors may also play an important role in disc degeneration. Heritability of disc degeneration in the lumbar spine region has been estimated at 74 % (95 % confidence interval, 64 – 80%). [30] In another study with 115 male monozygotic twins, 61 % of the variability in disc degeneration could be explained by familial aggregation compared to 7 % for physical loading 9 % for age. [31] Although a strong link between genetic factors and disc degeneration has been established, a complete mechanism involving all of the genes involved and the corresponding pathophysiology has not been elucidated. Therefore, DDD is best classified as a multi-factorial disease similar to osteoarthritis.

1.4 Current Repair Strategies for the Degenerative Disc

Once a degenerated or injured disc has become symptomatic it is often too late for conservative non-surgical methods to be effective. The most common surgical approach to treat a symptomatic disc is to perform a nucleoplasty or discectomy, where the central nucleus and other

herniated soft tissues are removed. However, removing a large portion of the IVD can lead to joint instabilities. Joint instabilities can then lead to rapid wear on the other IVD components (AF, endplates and ligaments) and vertebral bodies. Spinal fusion is one option which has gained popularity in recent years; an increase in spending from 1992 to 2003 of $ 75 to $ 482 million for spinal fusion surgeries was seen in the US alone. [32] Total disc replacements (TDR) have also been approved for degenerative disc repair and have demonstrated a slight improvement over spinal fusions due to the maintenance of an articulating joint. However, the non-regenerative repair can limit the lifetime of a TDR if the activity level of the individual is high. Although all of these surgical treatments can relieve the immediate pain, they do not reflect the original IVD architecture, resulting in altered biomechanics. [33] Therefore, the altered biomechanics of current surgical treatments result in higher loads within the adjacent discs and can cause them to degrade prematurely. [5, 6]

Another repair strategy for damaged discs is to replace only the nucleus pulposus, provided that enough of the surrounding IVD components are still intact. This type of repair would be suitable for early onset DDD where only the nucleus tissue has started to degrade, resulting in decreased disc height. By only replacing the nucleus, more of the natural biomechanics of the IVD joint would be maintained, thus preventing premature degradation to the adjacent discs. Various attempts at a permanent NP repair approach have been investigated and a select few have progressed into clinical trials. [34-37] However, a non-regenerative NP replacement will never become fully integrated into the IVD space and, due to a limited material life-time, may lead to device failure in the future. Therefore, a naturally regenerating NP replacement that can adapt to the ever changing mechanical and physiological properties of the NP tissue is of great interest in the field of tissue engineering.

Chapter 2

Literature Review

The focus of this study will be placed on developing a regenerative replacement for the nucleus pulposus. To date there are relatively few published works that review the field of load bearing soft tissues and, more specifically, nucleus pulposus tissue engineering. [38-40] Possible repair strategies for a regenerative IVD are shown below in the generalized schematic (Figure 2.1).

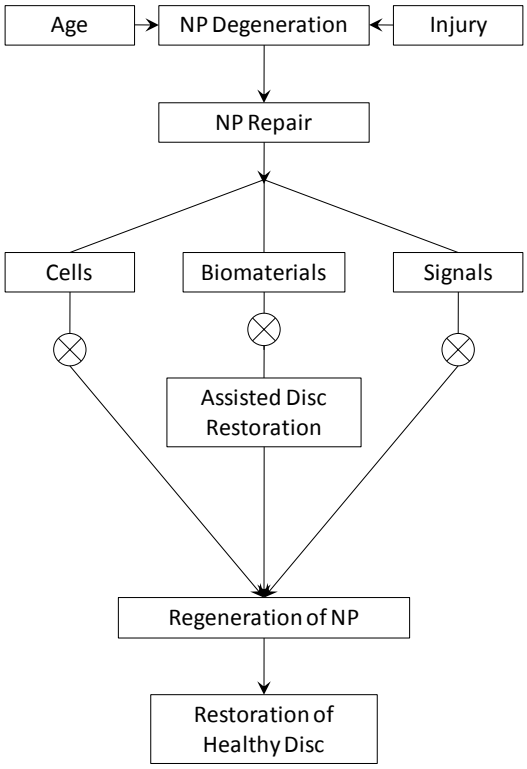

Figure 2.1: Possible strategies for NP repair to ultimately restore IVD function of the affected joint. The three main components of a NP tissue engineering approach includes cells, biomaterials and signals (chemical or mechanical), which can be used individually or combined.

2.1 Scaffold Design Criteria

For a load bearing tissue like the NP, a scaffold based approach will be crucial in providing a functional replacement immediately upon implantation. The scaffold should be injectable to allow for a minimally invasive surgery and quick recovery time. Sufficient mechanical properties will ensure that the scaffolds can be subjected to physiological loading after implantation. Fabricating a functional scaffold that can incorporate a cell based therapy approach will also be required for producing *de novo* tissue over time. Therefore, cell choice will be important in producing the specific NP-like tissue within the scaffolds. External signals such as mechanical stimulation and chemical growth factors may also be beneficial in enhancing the functionality of the tissue that is accumulated within the scaffolds. Biodegradable materials used to construct the scaffold will also permit the scaffold to gradually transfer load bearing duties to the *de novo* tissue. Careful material selection is critical in fulfilling as many of the design criteria as possible, which will help to improve the odds of achieving a successful scaffold design. This literature review will highlight some of the important properties required for a successful injectable NP implant as well as some issues that previous scaffold designs have encountered.

2.2 Mechanical Requirements for a Nucleus Pulposus Replacement

In order to replace the NP there has to be a guideline set to determine suitable mechanical properties for the scaffold. In a study by Wilke *et al.*, a pressure transducer was implanted into the lumbar spine of a healthy individual with a fully intact intervertebral disc (IVD). [41] The normal pressure within the IVD space when at rest was 0.2 MPa and reached a maximum of 2 – 3 MPa under various physical activities. Other studies have been conducted to determine the modulus of explanted annulus-confined bovine NP and unconfined human NP tissue, which were in the range of 310 ± 40 to 5 ± 3 kPa, respectively. [42, 43] In addition, the effect of degeneration on the overall

modulus of NP tissue has been investigated and it was found that the soft fluid-like NP changed to a drier solid-like tissue, which increased in stiffness as the degeneration progressed in samples that were obtained from patients ranging from 16 – 90 years of age. [44, 45] Other attempts have been made to model the mechanical properties of the NP using finite element analysis, which predicted an optimal modulus for the NP replacement would be between 1 – 4 MPa. [34, 46] For the purpose of this study we have selected a lower boundary of the confined NP tissue modulus (~ 300 kPa) to the upper boundary of 1 MPa. This range in modulus should be sufficient for the scaffold to function as a stand-alone load bearing NP replacement.

2.3 Cell Type/Source

2.3.1 Nucleus Pulposus Derived Cells

The obvious initial choice for a cell type to study in our scaffold system would be NP cells since the cells are already acclimatized to the environment of the IVD space. However, as previously mentioned, the nucleus pulposus has the potential of possessing a double cell population (notochordal (NC) and nucleus pulposus (NP)), which can change with age in some species. Therefore, the type and age of animal tissue and the cells isolated from it must be taken into consideration for a tissue engineering model. In a study by Miyazaki *et al.*, rat, rabbit and bovine animal models were compared for NP tissue in a standard ionically cross-linked alginate hydrogel system. [47] The rat and rabbit models (NC (+)) had much higher cell density in the native tissue than the bovine model (NC (-)). In addition, the NC (+) animal models all demonstrated higher cell activity and GAG production compared to the bovine model when cultured in the hydrogels. A study by He *et al*. also examined the effect of normal and physically induced degeneration on rabbit NP cells to proliferate and gene expression of collagen II and aggrecan. [48] The normal NP cells were more proliferative and could express higher relative gene levels for

collagen II and aggrecan than the degenerated NP cells. Yuan *et al*. also examined young versus old rabbit NP cells and demonstrated better proliferative abilities in 2D culture of the younger NP cells. [49] For this reason, the younger NP cells were chosen for additional studies to encapsulate within collagen microspheres in an attempt to preserve their phenotype *in vitro* over the traditional monolayer culture. [49] These studies highlight some of the possible difficulties in using human adult NP cells for tissue engineering, since there will be no viable NC population and the disc will most likely be in some stage of degeneration. Therefore, an NC (-) model may have benefit for stimulating the senescent adult NP cell population to produce tissue. However, it is likely that a more active and abundant cell source will be required to aid the original host NP cells in the production of functionally engineered NP tissue. Cells from other cartilaginous load bearing soft tissues with similar cell phenotypes could have potential for disc regeneration as well as a co-culture system to enhance the NP cells. Two possible options which will be discussed in the following sections are mesenchymal stem cells or cartilage cells (chondrocytes).

2.3.2 Bone Marrow or Adipose Derived Stem Cells

Many studies have examined the possibility of using mesenchymal stem cells (MSC) for NP tissue regeneration. [50-57] Some of these studies have focused on co-cultures of MSCs with NP cells in an attempt to differentiate the stem cells into a more NP-like cell line. Co-culture experiments have demonstrated that a 75 – 80 % NP cell population was required to directly induce significant stem cell differentiation when co-cultured in a pellet. [52] Soluble factors from the NP cell lines (80 % population) were also able to indirectly induce differentiation of MSCs (20 % population) to a more NP-like phenotype using a transwell monolayer culture system. [58] A similar indirect co-culture setup was also shown to differentiate rat bone marrow derived mesenchymal stem cells (BMSC) into intervertebral disc-like cells after 14 days. [50] A 3D alginate hydrogel co-culture environment was also used to determine if the indirect factors secreted from

the NP cells could induce stem cell differentiation. [59] All of the above studies were able to show the stem cells were able to up-regulate collagen type II and aggrecan and down-regulate collagen type I. These changes in gene expression were indications of a more NP-like phenotype of the stem cells.

Adipose derived stem cells (ADSC) are another viable cell source for NP tissue regeneration, which are more readily accessible than MSCs. [60] ADSCs also have the ability to differentiate into a more NP-like phenotype when in an indirect contact alginate hydrogel, [61] direct contact collagen type II hydrogel, [62] and indirect contact transwell micromass [63] environments.

2.3.3 Cartilage Derived Cells

Chondrocytes are a very similar cell type to adult NP cells but are present in much higher abundance in cartilage tissue and are considered to be a viable cell source to produce NP-like tissue. Rabbit intervertebral discs explants injected with articular chondrocytes have been shown to exhibit a 50 % increase in proteoglycan accumulation over their controls. [64] Chondrocytes can also be isolated from two different types of cartilage: a load bearing hyaline (articular) or elastic (auricular) cartilage. In a study by Chung *et al*. articular (knee) and auricular (ear) chondrocytes from pig were studied in a methacrylated hyaluronic acid (MHA) hydrogel system (2 % w/v) for up to 12 weeks *in vitro*. [65] Interestingly, auricular chondrocytes were able to produce more cartilaginous tissue and significantly improve the compressive modulus of their MHA hydrogels (~ 8 times increase, by 12 weeks) compared to the MHA hydrogels seeded with articular chondrocytes. However, the articular chondrocytes in the MHA hydrogels were more responsive to dynamic mechanical loading than the auricular chondrocytes. After 5 days of stimulated culture the relative gene expression levels (normalized to the free swelling controls) for collagen

II and aggrecan increased approximately 2.5 and 1.5 times for the articular chondrocytes, and slightly below 1.5 for both in the case of the auricular chondrocytes.

2.3.4 Comparative Cell Studies for Cartilaginous Load Bearing Soft Tissues

Other studies by Zeiter *et al*. and Erickson *et al*. have examined multiple cells (articular chondrocytes, NP and BMSC) for viability, ECM accumulation and change in compressive modulus in a variety of hydrogels (alginate, agarose, MHA and puramatrix). [66, 67] In both of these studies the chondrocytes were superior to NP and BMSC cells in terms of total GAG and collagen production. Agarose was also found to be a more conducive medium towards the production of cartilaginous ECM, which correlated with an increase of close to 170 kPa in compressive modulus compared to 50 kPa for the other hydrogel after 56 days in culture. In addition, Zeiter *et al*. found that TGF-β1 added to the culture media improved the behaviour of BMSCs, regardless of the hydrogel, to levels comparable to chondrocytes and NP cells. Another study by Mauck *et al*. examined chondrocytes and BMSCs in agarose for long-term culture (70 days) with and without TGF-β1. [68] TGF-β1 supplementation was shown to improve both cell types, with significant ECM and modulus increases over time, but was more pronounced for the chondrocytes. In addition to the cell types examined, Mauck *et al*. also explored the effect of cell density on developing a structure/function relationship in agarose hydrogels. [69] Lower seeding densities of articular chondrocytes at 20 x 10^6 cells/mL displayed a greater response to dynamic stimulation (10 % strain at 1 Hz for 3 times daily, 1 h on 1 h off loading protocol) than a higher 60 x 10^6 cell/mL density after 28 days in culture. However, increases in aggregate modulus up to 70 kPa and close to 1.5 % w/v (wet) GAG and collagen accumulation in hydrogels, with lower seeding densities and dynamic stimulation, were comparable to the higher seeding density and statically cultured hydrogels. Ultimately, the ability to enhance the hydrogel stiffness by adjusting the culture conditions such as seeding density and static vs. dynamic stimulation was

demonstrated in these studies. Overall, chondrocytes were shown to be superior at producing a cartilaginous matrix in multiple hydrogel environments and were therefore chosen for study with our system for NP tissue engineering. Chondrocytes were considered a viable option for the NP tissue since NP tissue is a variant of the cartilaginous soft tissue present in the body.

2.4 Current Tissue Engineering Approaches for Nucleus Pulposus Repair

2.4.1 Hydrogel Scaffold Approach

A common approach for a regenerative cell-based repair strategy for load bearing soft tissues is to use a hydrogel to encapsulate a cell source that can actively synthesize a similar extracellular matrix profile to that of the host tissue. [70-73] Hydrogel prepolymer concentrations can be adjusted to mimic the water content (80 – 90 %) of the native nucleus pulposus tissue. The prepolymer concentration can also be increased and/or functionalization with cross-linking groups to increase the hydrogel modulus to approach values of the native load bearing soft tissue. The wide versatility of physical properties and hospitable environment for cells make a hydrogel system an ideal approach for a cell-based scaffold to repair and regenerate NP tissue. Chou *et al*. used methacrylic anhydride to functionalize alginate with low degree of methacrylation between 2.5 to 7.5 % based on the repeating sugar unit. [74] Hydrogels were made from each degree of methacrylation with prepolymer concentrations of 2 and 3 % w/v. The equilibrium modulus increased with degree of methacrylation and prepolymer % w/v but did not change over a 2 week culture with encapsulated bovine caudal NP cells. The 3 % w/v hydrogels with 7.5 % methacrylation appeared to swell from their original mold dimension and swelling increased as the degree of methacrylation decreased. However, the cell viability was found to zero after 3 days in culture for the 7.5 % methacrylated alginate hydrogels regardless of % w/v. With a lower degree of methacrylation between 2.5 and 5 %, initial cell viability was maintained between 80 –

100 %, but decreased over the 2 week culture. Cells appeared well distributed throughout the hydrogel and stained for chondroitin sulfate localized around the cells after 14 days. [74] The NP cells demonstrated a declining viability with time and the localized GAG that was produced did not have any effect on the already low equilibrium modulus of the alginate hydrogels. In a study by Collin *et al*., an injectable solution of collagen II and hyaluronic acid was stabilized with the addition of a star-poly(ethylene glycol) ether tetrasuccinimidyl glutarate (4S-StarPEG) cross-linker. [75] The 4S-StarPEG stabilized mixtures produced collagen II hydrogels with storage moduli under 1 kPa, which could support NP cells between 90 – 100 % viability over a 14 day culture period. During the 14 day culture period, gene expression for collagen II and aggrecan decreased and collagen I remained constant relative to the day 0 values. A portion of the NP cells originally seeded within the hydrogels were observed to proliferate on the outer surface of the hydrogels, and exhibited a fibroblast-like phenotype. The NP cells that remained within the hydrogels over the 14 day culture period maintained a rounded chondrocyte-like phenotype. A preliminary study with bovine adipose derived stem cells (ADSC) with the collagen II and 4S-StarPEG hydrogels also demonstrated high cell viabilities around 80 %. [75]

The poor activity of the NP cells in the previous hydrogel studies may be attributed to the senescent nature of adult NP cells once the notochordal population disappears. [47] For this reason other studies have examined different cell sources and materials to try and improve the cellular response over that of NP specific cells. In a study by Moss *et al*., a co-culture of human annulus fibrosis and nucleus pulposus cells (IVD cells) were encapsulated in a thiol modified hyaluronan and elastin-like polypeptide with a poly(ethylene glycol)-diacrylate cross-linker. [76] The IVD cell mixture was able to maintain an NP phenotype along with 70 % viability after 3 weeks in culture. However, mechanical properties of these cellular hydrogels still exhibited low moduli in the 10 kPa range. In an environment such as the IVD where loading can reach up to 2 – 3 MPa in the NP alone, the previously studied hydrogels do not have the load bearing abilities that would be

required in a functioning motion segment of the spine. Therefore, in addition to improving the encapsulated cellular response, the mechanical properties of the hydrogel need to be improved to support immediate loads in the body. This is particularly true in a degenerative disc environment where the constrictive abilities of the annulus fibrous may be compromised prior to the NP repair.

However, the studies of NP repair using hydrogels are fairly limited and may require techniques and methods that have been applied to alternative load bearing soft tissues such as articular cartilage due to the similarities in tissue composition and cell phenotype. The photo-cross-linking reaction is one such method that enables the rapid production of hydrogels with a wide range of mechanical properties by the modification of prepolymer properties (e.g. prepolymer concentration, degree of methacrylation, molecular weight, blending with multiple components and biodegradability). Moreover, the photo-cross-linking reaction is commonly applied to cartilage tissue engineering studies in a variety of hydrogel systems and has demonstrated little adverse effects on the encapsulated cells. [77-79] Therefore, in addition to the NP studies reviewed above, photo-cross-linkable hydrogel studies in the field of cartilage tissue engineering that may also be applicable to the repair of the NP have also been examined.

2.4.1.1 Glycol Chitosan

Chitosan is a popular hydrogel material since it is easily isolated from crustacean shells and has a molecular structure similar to glycosaminoglycans found in the body. [37, 80] The addition of glycol moieties allows chitosan to be water-soluble at neutral pH and can be modified using a simple reaction with glycidyl methacrylate under basic conditions to functionalize it to be photo-cross-linkable (Figure 2.2). [81] Even though it has promising properties for use as a biomaterial, few studies have examined its use for cell encapsulation and load bearing soft tissue work. A study by Park *et al*. used the modified glycol chitosan (MGC) to form 2 % w/v MGC hydrogels and MGC blends with 1 % w/v hyaluronic acid (HA) (75, 350 and 980 kDa). [82] Hydrogels with 5

– 25 kPa compressive moduli were formed by using visible light in the 400-500 nm spectrum at 300mW/cm^2 and riboflavin as a photo-initiator, and were used to encapsulate auricular rabbit ear chondrocytes (2 x 10^6 cells/mL). All hydrogels demonstrated high cell viability (greater than 80 % cell viability) and proliferation after 21 days in culture. Overall, blends with MGC and HA improved cell behavior, but it was unclear whether the cellular response was due to the presence of HA or from the possible loss of HA, since HA was not covalently linked to the MGC. MGC has the potential to produce the mechanical properties required for a functional LBST scaffold by adjusting the prepolymer concentration and degree of functional groups available for cross-linking. [81] However, more studies are required to assess the behavior of cell types common to cartilaginous soft tissues in MGC hydrogels modified to have mechanical properties approaching that of native load bearing soft tissues (LBST).

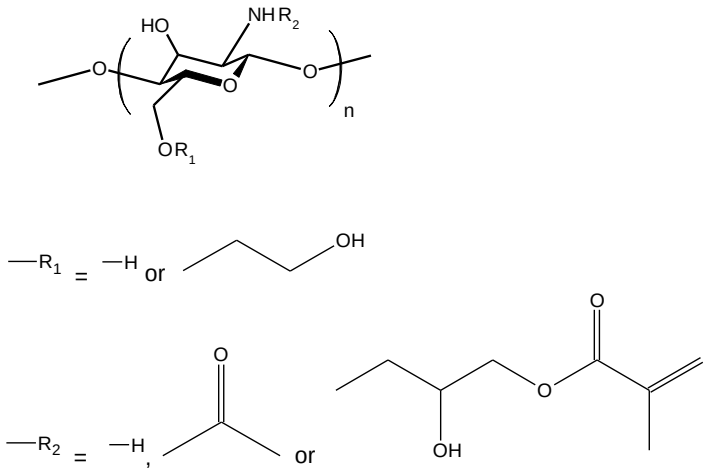

Figure 2.2: Structures of glycol chitosan composed of β(1→4) linkages and random glucosamine (R_2 = H) and *N*-acetylglucosamine ($R_2 = C_2H_3O$). Glycol groups ($R_1 = C_2H_5O$) allow chitosan to be soluble at neutral pH. Methacrylation of the primary amines was accomplished with the ring-opening reaction with glycidyl methacrylate ($R_2 = C_7H_{11}O_3$)

2.4.1.2 Chondroitin Sulfate

Chondroitin sulfate is a sulfated GAG component of proteoglycans found in hyaline cartilage, which is responsible for maintaining the structural and hydrodynamic properties of native load bearing soft tissues (Figure 2.3 (A)). Wang *et al*. demonstrated that chondroitin sulfate could be methacrylated with methacrylic anhydride (MA) (Figure 2.3 (B)) and the degree of substitution (calculated on repeating dimer unit) could be controlled by four main factors: reaction time, reaction temperature, MA concentration and NaOH concentration. [83] All factors, except temperature, increased the degree of methacrylation. The molecular weight of chondroitin sulfate, which is generally found in the body at less than 50 kg/mol and considered low molecular weight in comparison to other natural polysaccharides found in the body, would be beneficial for producing higher modulus hydrogels due to a higher network density. [84, 85] However, there seems to be a limited number of studies that have examined chondroitin sulfate by itself to produce hydrogels for cell encapsulation. Chondroitin sulfate does not have a strong affinity for the cell membrane receptors for the type of cells found in LBSTs, but does seem to have a strong proliferative effect when added to other hydrogel systems for blending. Other studies have incorporated molecules such as aggrecan, and the polysaccharides it is composed of, with chondroitin sulfate to improve the modulus, swelling and proliferative abilities of poly(ethylene glycol) diacrylate or dimethacrylate (PEGD) hydrogels. Varghese *et al*. encapsulated goat bone marrow derived mesenchymal stem cells (BMSC) in a 50:50 mixture of 20 % w/v 3400 g/mol PEGD and 20 % w/v 24000 g/mol methacrylated chondroitin sulfate (MCS). [86] Compared to a 10 % w/v PEGD hydrogel, the addition of MCS increased relative gene expression for chondrocyte markers and also demonstrated increased accumulation of collagen and GAG. MCS niches were found to be degradable within the blended hydrogel, which resulted in large cellular outgrowths to occur on the surface of the hydrogels after 42 days in culture. Multiple studies by Ingavle *et al*. have also used MCS to increase the bioactivity of an agarose hydrogel stabilized with PEGD with initial compressive moduli around 150 kPa. [87,88] Slight deceases in the compressive moduli of

cellular hydrogels were observed over a 6 week culture period, however a strong migratory effect of the encapsulated chondrocytes resulting in large structures being formed on the outer edge of the hydrogels. Therefore, natural prepolymers such as chondroitin sulfate, which can influence large changes in swelling and modulus of a hydrogel by itself or as a blend, requires further study in the field of LBST engineering.

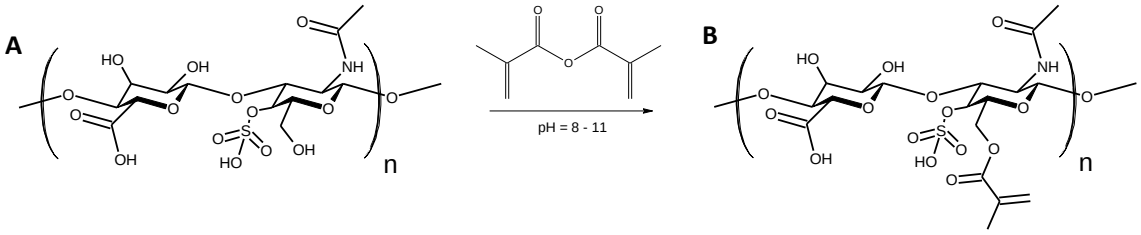

Figure 2.3: A) Repeating dimer structure of chondroitin 4 sulfate composed of alternating β(1→3) and β(1→4) glycosidic linkages of glucuronic acid and *N*-acetylgalactosamine units (sulfate in 4 or 6 position) and B) Representative chondroitin-4-sulfate after esterification reaction with methacrylic anhydride on the alcohol group of *N*-acetylgalactosamine.

2.4.1.3 Hyaluronic Acid

Hyaluronic acid (HA) is another natural polysaccharide which makes up a large part of cartilaginous LBSTs (Figure 2.4 (A)). Similar to chondroitin sulfate, HA it is responsible for maintaining the structural and hydrodynamic properties of hyaline cartilage with the exception that it is non-sulfated. One major advantage of HA is that it has a high affinity for the cell membrane receptor CD44 which is present on many cell types, including those found in cartilaginous LBSTs. The affinity of CD44 to HA is vital for the assembly of *de novo* tissue surrounding the cells in cartilage and also for the uptake and degradation of the HA molecule *in vivo*. [89, 90]

A study by Smeds *et al.* [91] was the first to modify HA with methacrylic anhydride; a synthesis which was later shown to be very unpredictable in terms of achieving a consistent final

degree of methacrylation (Figure 2.4 (B)). [92] Glycidyl methacrylate (GMA) has also been commonly used to modify HA, but has two possible reaction pathways with the free hydroxyl groups: a short-term, reversible, transesterification and a long-term, stable, ring opening polymerization. Therefore, 15 day reaction times are generally used to favour the more stable ring opening polymerization reaction. [93, 94] Bencherif *et al*. examined 5 % w/v hyaluronic acid with degree of methacrylation ranging from 10 – 90 % and was able to produce hydrogels with shear moduli between 20 – 60 kPa. This work demonstrated the ability to produce highly modified MHA hydrogels with compressive modulus that could be as high 200 kPa, however, no relevant cell culture work was conducted with these gels.

In another study by Chung *et al*. auricular chondrocytes (swine, 40 x 10^6 cells/mL) were examined in HA hydrogels modified with methacrylic anhydride (6-12 % methacrylation) for 3 different MWs (50, 350, 1100 kDa) between 2 – 20 % w/v. [95] The highest hydrogel compressive modulus of 100 kPa was obtained with the 50 kDa MHA prepolymer at 20 % w/v and 12 % methacrylation. However, cell viability which was tested using 3T3 fibroblasts, dropped from 96 to 20 % moving from the lowest prepolymer concentration and degree of methacrylation to the highest conditions. Therefore, the higher prepolymer concentration required to produce higher modulus hydrogels may be toxic to the encapsulated cells due to the heightened concentration of methacrylate groups and should be a consideration when selecting which hydrogel parameters to use. In a different study by Chung *et al*. 2 % w/v, methacrylated hyaluronic acid (MHA) hydrogels were used to encapsulate auricular and articular chondrocytes and were subsequently implanted subcutaneously in mice for development *in vivo*. The initial hydrogel moduli were close to 10 kPa, which did not change for the hydrogels with articular chondrocytes, but reached a level of 100 kPa in the hydrogels containing auricular chondrocytes after 12 weeks in culture. [65]

Larger increases in moduli of 1 % w/v MHA hydrogels were demonstrated by Erickson *et al*. by seeding the hydrogel with a high density of BMSCs and utilizing a dynamic culture

environment. [96] Under these culture conditions, the MHA hydrogels reached an equilibrium modulus in excess of 1 MPa. However, characterization of the BMSC phenotype was not conducted after the 9 week culture. Therefore, the BMSC and the type of tissue accumulated in the MHA hydrogel may not have been cartilaginous in nature. Regardless, the ability to increase the initial modulus of hydrogels through cell mediated processes such as ECM accumulation has been demonstrated in the literature. However, the length of time to obtain these physiologically relevant modulus values restricts their use for immediate load bearing repair of cartilaginous soft tissues such as the nucleus pulposus and articular cartilage. Therefore, there is still a need for a scaffold that can function as load bearing soft tissue immediately after implantation at the defect site and regenerate tissue gradually with time.

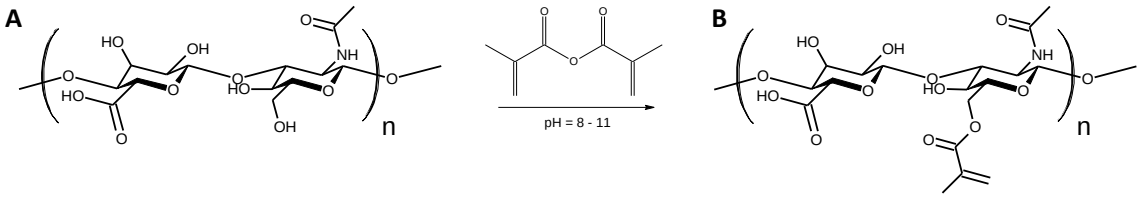

Figure 2.4: A) Repeating dimer structure of hyaluronic acid with alternating β(1→3) glucuronic acid and β(1→4) *N*-acetylglucosamine units B) after esterification reaction with methacrylic anhydride on the 4 possible hydroxyl groups (showing representative reaction with alcohol group on *N*-acetylglucosamine unit).

2.4.2 Biodegradable Elastomeric Scaffold Approach

Biodegradable elastomeric scaffolds are crucial at imparting mechanical properties to tissue engineering NP scaffolds. A variety of elastomeric biomaterials have been used for scaffold-based approaches for the repair of cartilaginous load bearing soft tissues. [37, 97-102] For elastomeric prepolymers to remain flowable, and therefore injectable at room-temperature, lower molecular weights are required. Once cross-linked, low molecular weight prepolymers form stiff

and resilient elastomers suitable for the replacement of the NP. However, elastomeric prepolymers are hydrophobic, which make them incompatible for encapsulating cells. To accommodate cells, elastomers are usually made with a porous structure (first step), which reduces the overall scaffold stiffness but allows for cells to be seeded after cross-linking (second step). [103] This multi-step process of forming the cellular elastomeric scaffolds requires the scaffolds to be pre-formed outside the body before implantation. [104] In a study by Gerecht *et al.*, neuroblastoma and human embryonic stem cells were encapsulated within a poly(glycerol-co-sebacate) acrylate (PGSA) elastomer using a glycerol cell carrier phase. [105] Although this elastomeric approach has the potential to be injectable in the presence of cells, the modulus (~ 50 kPa) of these scaffolds was not substantially better than a hydrogel based approach. Therefore, to date there are no injectable cellular based elastomeric scaffolds with sufficient overall mechanical properties to act as a stand-alone NP replacement.

2.4.2.1 Star-Copolymers Composed of ε–Caprolactone, D,L-Lactide and Trimethylene Carbonate

Synthetic aliphatic polyesters such as ε–caprolactone (CL), D,L-lactide (DLLA) and trimethylene carbonate (TMC) can be used to form biodegradable elastomers. Due to the elastic and resilient nature of these aliphatic polyesters, they have potential for use as scaffolding for load bearing soft tissues. [106-108] For an injectable approach, the polyester prepolymers need to be able to flow at room temperature operating conditions and to be cross-linkable to form the elastomer. Flow-able elastomeric based prepolymers can be made by keeping the molecular weights low enough (< 8 kg/mol). In addition, copolymers can be synthesized to enhance the capability for flow. For example, the DLLA and TMC monomers are solid at room temperature and. blending either monomer with the liquid CL monomer during the polymerization reaction can enable the formation of random copolymers, which are flowable at room temperature provided the molecular weight is kept low enough (< 10 kDa). [107, 109] Low molecular weight *star-*

shaped copolymers can also be utilized to increase the cross-linking density of the final elastomer and thereby reduce the possibility of crystallization. Modification of the terminal groups with vinyl moieties enable cross-linking of the *star*-shaped copolymers, which can be used to form the elastomer through a photo-initiated cross-linking reaction. [107, 109]

Chapanian *et al.* used flow-able tri-acrylated *star*-poly(ε-caprolactone-co-D,L-lactide) (DLLA:CL) prepolymers of 50:50 ratio and 7800 g/mol to form photo-cross-linkable elastomers with an average tensile modulus of 5.4 ± 2.1 MPa (Figure 2.5 (A)). [110] These DLLA:CL elastomers were shown to have an increased water uptake by 8 weeks *in vitro* and showed a delayed response in the loss of modulus by around 10 weeks. After 10 weeks, accelerated mass loss and decreases in moduli were observed, and by 20 weeks almost no scaffold remained. A similar tri-acrylated *star*-poly(ε -caprolactone-co-trimethylene carbonate) (TMC:CL) prepolymer of 50:50 ratio and 7800 g/mol was used to form photo-cross-linked elastomers with an average tensile modulus of 0.83 ± 0.14 MPa (Figure 2.5 (B)). The TMC:CL elastomers did not display significant changes in physical properties during a 30 week *in vitro* degradation study and *in vivo* degradation was mediated by foreign body giant cells and the generation of reactive oxidative species at the surface of the polymers. [107] In another study by Pego *et al.*, TMC:CL based co-polymers were found to have no change in mechanical properties with respect to *in vitro* degradation for up to a year. [111]

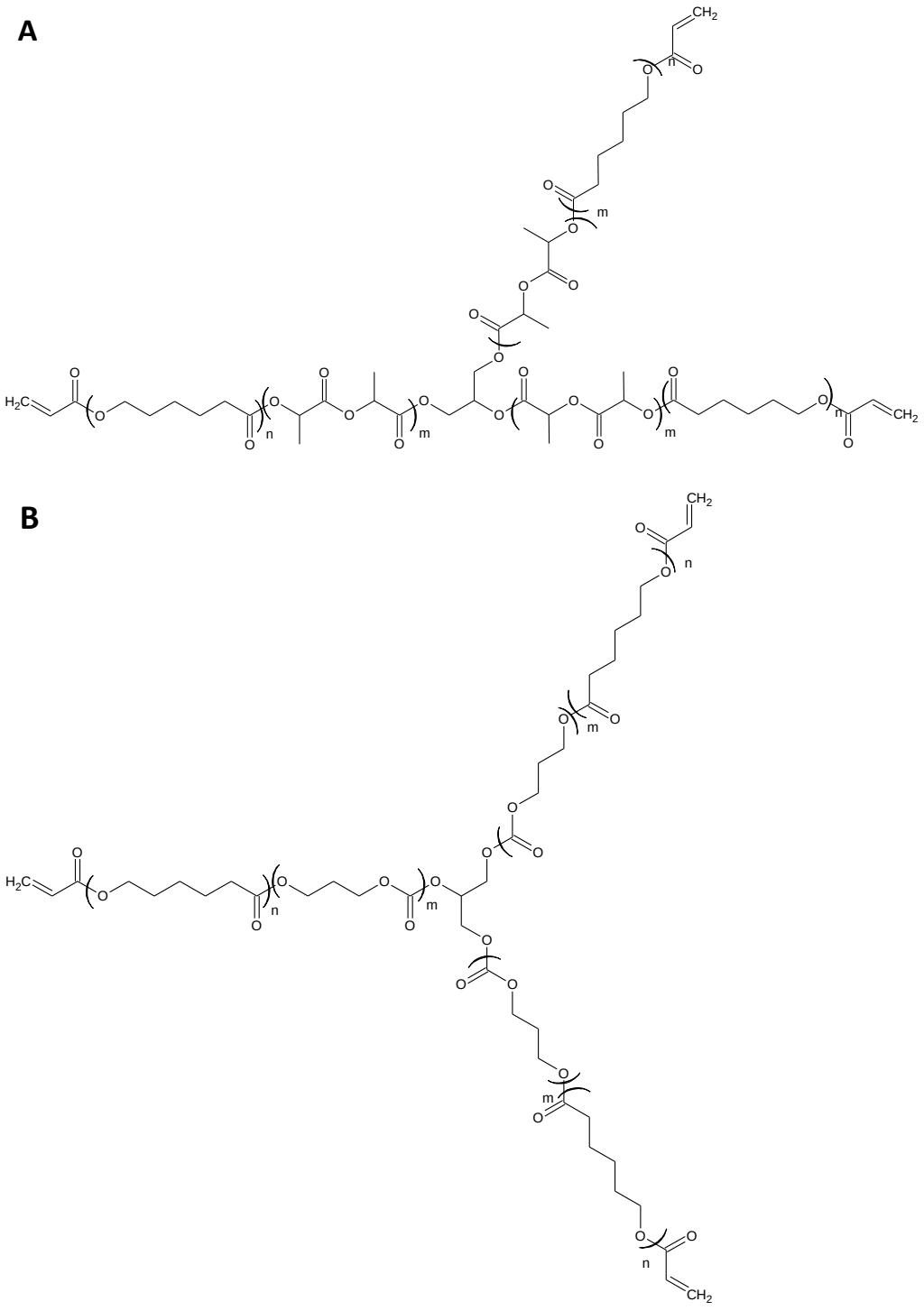

Figure 2.5: A) Structure of tri-acrylated *star* poly(ε-caprolactone-co-D,L-lactide), random repeating units of m = D,L-lactide and n = ε-caprolactone and B) structure of tri-acrylated *star* poly(ε-caprolactone-co-trimethylene carbonate) with random repeating units of m = trimethylene carbonate and n = ε-caprolactone

The homopolymers formed from the DLLA monomer are more brittle than those formed from the TMC monomers. Therefore, the DLLA monomer produced a stiffer co-polymer when blended with the CL monomer that degraded more rapidly via bulk hydrolysis than the enzymatically degraded TMC:CL based co-polymers. [107, 110] These studies have demonstrated the ability to form high modulus elastomeric scaffolds, which are tunable in terms of their mechanical and degradation properties. Alone these elastomers may not be suitable for a cell-based regenerative scaffold, but they have the potential to form a stiff, yet degradable platform to grow cells in or on. A solution to enhancing cell viability, while maintaining the beneficial properties of the elastomers outlined above may be to form a composite scaffold with the previously mentioned cell-laden hydrogel approach.

2.4.3 Composite Scaffold Approach

As shown in the previous sections, single-phase scaffold systems are often very good in one aspect (cell encapsulation or mechanical properties) of a scaffold design appropriate for load bearing soft tissue repair. Composite scaffolds are often used to impart multiple phases or segments that complement one another into a single scaffold. However, traditional composite scaffold designs are constructed in a step-wise fashion. [112-114] Therefore, current composite scaffold fabrication processes are not amenable for an injectable system. Peng *et al*. [117-117] were able to form an interpenetrating network (IPN) from a 4 % w/v HydroThane™ elastomer and 7.5 % w/v methacrylated gelatin hydrogel mixture. The mixtures were dissolved in dimethyl sulfoxide (DMSO) and vortexed before photo-cross-linking to form the IPNs. The IPN scaffolds were then freeze-dried and characterized in a dry state or after rehydration in serum containing media. Scaffold morphology and overall mechanical properties were shown to be controllable based on the degree of methacrylation (9 or 18 %), molecular weight and maturation of the gelatin solution. However, no biomaterial characterization or cell culture work was conducted on

these scaffolds. The methods used to form the IPN, such as vortexing and lyophilization would not have allowed for the encapsulation of viable cells in an *in situ* repair approach. Therefore, a modified version of this two-phase composite scaffold design as a biodegradable cell carrier with functional mechanical properties may be well suited for use as a regenerative NP replacement.

Chapter 3

Scope

3.1 Proposed Composite Scaffold Design

The scope of this study was to design, test and improve an injectable composite scaffold for functional load bearing nucleus pulposus replacement and regeneration. To fulfill the design criteria outlined in § 2.1, a cell suspension in an aqueous hydrogel prepolymer phase will be combined with a low molecular weight polyester copolymer phase to form an immiscible suspension with co-continuous morphology (Figure 3.1). A single photo-initiated reaction will be employed to cross-link both phases at once. The two continuous phases can then contribute individually to the overall scaffold properties; the hydrogel phase for the distribution and maintenance of the encapsulated cells and the elastomeric phase for the overall load bearing properties of the scaffold. Augmenting the material composition of each phase can be used to obtain different mechanical properties, degradation profiles and cellular responses. Given that the entire scaffold can be formed containing a viable cell population with a single photo-initiated reaction, it allows for scaffold delivery through an injectable device. The composite scaffold could then be used to initially replace the NP by minimally invasive surgery, cross-linked *in situ* to restore joint biomechanics and, over time, orchestrate the simultaneous degradation of the elastomer phase and accumulation of ECM from the hydrogel phase. Although, out of the scope of this project, the ultimate goal of the composite scaffold would be the eventual regeneration of sufficient *de novo* tissue to functionally take over the NP space.

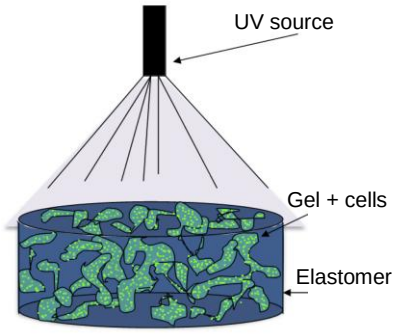

Figure 3.1: Proposed co-continuous scaffold design composed of a cell containing hydrogel phase interconnected with a mechanically load bearing elastomer phase.

3.2 Objectives

Currently there are no regenerative repair strategies available for lower back pain caused by a damaged or degenerated nucleus pulposus (NP). The current non-regenerative repair methods are invasive in that they replace the entire disc space, which limits the natural biomechanics and can cause further damage at the repair site and in adjacent discs in the long term. Recent trends in the literature regarding NP replacements show that a regenerative scaffold approach is feasible, especially if DDD is detected early enough before it affects the annulus fibrosus and adjacent vertebral bodies. [118] However, there is a lack of NP replacements with suitable mechanical properties that can be formed *in situ* and support viable cells. Therefore, injectable high modulus cell-based NP repair scaffolds would add a valuable niche to the field of cartilaginous load bearing soft tissue repair and regeneration. Scaffolding based around a cell encapsulating hydrogel system will be investigated for improving mechanical properties and cartilaginous tissue production. The specific aims of this research are listed below in the 4 main objectives.

3.2.1 Objective 1: Co-continuous Hydrogel and Elastomer Scaffold Design

The primary objective is to develop a hydrogel and elastomer composite scaffold for cellular regeneration and load bearing duties of the cartilaginous soft tissue in the intervertebral disc. To improve the stiffness of the hydrogel beyond its own capabilities, an immiscible elastomer phase will be blended with the hydrogel to form a composite morphology. In order for the elastomer phase to improve the overall mechanical properties of the composite scaffold, a continuous phase will be required. However, a continuous hydrogel phase will also be required to support viable cells in the centre of the scaffolds. Therefore, the preliminary objectives are to select elastomer and hydrogel prepolymers that are flow-able at room temperature, photo-cross-linkable and biodegradable. Once the materials are chosen, the next step will be to determine the blending conditions that form a co-continuous hydrogel and elastomer morphology and characterize the resulting mechanical properties. The final step of this preliminary study will be to determine if cells can be incorporated into the prepolymer mixture and endure the scaffold manufacturing process and photo-cross-linking reaction. Cell behavior within the scaffold and mechanical properties of the scaffold during culture (general ECM characterization, cell viability and modulus) will be characterized during a 2 week *in vitro* static culture.

3.2.2 Objective 2: Improvement to Elastomer Phase

The stability of the elastomer phase will be vital for the overall mechanical performance of the co-continuous scaffolds. The co-continuous scaffold design allows for improvements to be made by using different materials for either phase if any issues arise during the mechanical testing and cell culture characterization studies. Therefore, multiple elastomer prepolymers will be investigated for formation of a co-continuous morphology, resultant mechanical properties, degradation behaviour and its effect on the encapsulated cells. Long-term stability of the structural elastomer phase and behavior of the encapsulated cells will be investigated during a 2

month culture period. In addition, the injectability of the two-phase prepolymer mixtures and fatigue resistance of the co-continuous scaffolds will be tested to determine if our approach has the potential to be used for a minimally invasive repair of the nucleus pulposus.

3.2.3 Objective 3: Improvement to Hydrogel Phase

Once the elastomer phase degrades, the main structural component of the composite scaffold will be lost. Therefore, high mechanical properties are necessary in the cellular hydrogel phase, both initially and with time, as the actual elastomer degradation times *in vivo* may vary considerably. Therefore, alternative prepolymers that can improve hydrogel mechanical properties through cell mediated processes (ECM accumulation, proliferation and maintenance of cell phenotype) will be investigated. Identification of particular prepolymer parameters that need to be adjusted to improve initial hydrogel mechanical properties, while still supporting a high percent of viable and active cells, will be determined in this chapter.

3.2.4 Objective 4: Optimization of Cell behavior

Hydrogels identified with high moduli, low swelling after cross-linking, and promising preliminary cellular responses will be investigated over a long-term (1 month) static *in vitro* culture. The hydrogel environments responsible for improving cell behavior (chondrocyte phenotype) will be identified and related to the changes in hydrogel mechanical properties with time. The main objective will be to find a high modulus hydrogel that permit cell mediated processes to maintain or improve the overall mechanical properties and act as the regenerative phase in the co-continuous scaffolds.

Chapter 4

A Photocurable Hydrogel-Elastomer Composite Scaffold with Co-continuous Morphology for Cell Encapsulation

4.1 Completed Objectives

Chapter 4 was published in Macromolecular Biosciences in 2011 (DOI: 10.1002/mabi.201100179) where all experiments were designed and conducted by myself and I am the first author of the study. [119] The results presented in Chapter 4 fulfilled the requirements of Objective 1 (§ 3.2.1), which were to design a composite scaffold with a co-continuous morphology to provide a high modulus (1 MPa target), maintain cell viability during scaffold formation and have the potential to be injectable. This preliminary study utilized a 6 % w/v *N*-methacrylate glycol chitosan (MGC) hydrogel phase to transport and distribute primary bovine chondrocytes within the elastomer phase. The elastomer phase prepared from 50:50 molar ratios of an acrylated *star*-poly(ε-caprolactone-co-D,L-lactide) at either 4.8 or 9.3 kg/mol (4.8K or 9.3K ASCP) provided the main mechanical properties to the two-phase scaffold. A co-continuous morphology of both phases was obtained with a 30 % v/v loading of the 6 % w/v MGC solution in the 9.3K ASCP and confirmed using micro-CT scanning. The encapsulated chondrocytes displayed increases in metabolic activity and accumulated extracellular matrix over a 14 day culture period. A significant decrease in the mechanical properties of the cellular scaffolds occurred over the 14 day culture period, but still remained at a level similar to values reported for load bearing soft tissues *in vivo*.

4.2 Introduction

Avascular soft tissues within load bearing joints, such as the nucleus pulposus, articular cartilage and meniscus, possess limited self-repair abilities when damaged from a physical injury

or disease.[3, 120-123] Therefore, any damage sustained to these tissues often worsens with time and leads to abnormal joint loading, which ultimately results in excessive joint pain and reduced joint mobility.[121] This abnormal loading caused by the damaged tissue can potentially further compromise the structural integrity of the entire joint as well as other surrounding tissues thereby accelerating joint degeneration. Surgical intervention is the current standard of care, with the most extreme cases often requiring complete joint replacement (e.g. total hip, knee, or intervertebral disc replacement). [124, 125] The prosthetics used for joint replacement often have a limited lifetime, based mainly on the durability of the metallic/polymer materials used for their construction.[124]

The field of tissue engineering may be able to provide an alternative solution to a permanent prosthetic device by focusing mainly on the damaged load bearing soft tissues. [38] A biodegradable repair scaffold could be formulated to match the mechanical properties of the damaged native tissue. The degradation rate of the scaffold could also be adjusted to match the infiltration of *de novo* tissue. Moreover, the scaffold could be designed to be injectable and *in situ* curable to allow for a minimally invasive surgery. Previous work involving injectable scaffold delivery systems have focused on one of two main methodologies: 1) hydrogel cell encapsulation, to deliver cells to the site of injury and regenerate native tissue over time, [71, 72, 126] and 2) elastomer prosthetics that can mimic the mechanical properties of the native tissue. [37, 99-101] However, the disadvantages of these approaches are that hydrogel scaffolds have limited mechanical properties and elastomer scaffolds have poor cell encapsulation abilities.

The aim of this research was to combine a hydrophilic cell encapsulating hydrogel with the mechanical properties of a hydrophobic elastomer to form a co-continuous two-phase cell delivery device for the repair and/or replacement of load bearing soft tissues. The novelty of the approach was in the ability to incorporate viable cells throughout the entire scaffold during the fabrication process, which will have a significant impact on the usefulness of this cell delivery

system as an injectable and *in situ* curable device. The cell encapsulating hydrogel phase was composed of *N*-methacrylate glycol chitosan (MGC), a chitosan derivative that is water-soluble under neutral pH conditions and which has been demonstrated to be cytocompatible with chondrocytes and fibroblasts. [81, 127] Moreover, chitosan is structurally similar to glycosaminoglycans found in articular cartilage and the nucleus pulposus. [37, 80] The load-bearing elastomer phase was made up of terminally acrylated *star*-poly(ε-caprolactone-*co*-D,L-lactide) (ASCP) containing a 50:50 molar ratio of D,L-lactide to ε-caprolactone. In addition to being immiscible with the MGC phase, the ASCP was chosen for its proven biodegradability, biocompatibility and controllable physical properties (e.g. molecular weight, degree of cross-linking). [109, 110] The starting materials for both phases had photocurable functional groups to allow for a single method of cross-linking. Therefore, focus was initially placed on the ability to form a co-continuous scaffold morphology, followed by the encapsulation of primary bovine chondrocytes in this two-phase scaffold to investigate the effect on cell viability and extracellular matrix accumulation over a 14 day culture period.

4.3 Materials and Methods

4.3.1 Materials

The water soluble glycol chitosan was obtained from Wako Chemicals (Richmond, VA). D,L-lactide and ε-caprolactone were purchased from Purac Biochem (Gorinchem, NL) and Lancaster Synthesis (Morecambe, UK), respectively. The MTT assay kit for measuring cellular metabolic activity was provided by Invitrogen Canada Inc. (Burlington, ON). Dimethyl sulfoxide-D6 and deuterium oxide for ^{1}H NMR were obtained from Cambridge Isotope Labs (Andover, MA). All other reagents were received from Sigma-Aldrich Canada Inc. (Oakville, ON).

4.3.2 Scaffold Components and Manufacturing

Two different molecular weight prepolymers of 50:50 (mol:mol) terminally acrylated *star*-poly(ε-caprolactone-*co*-D,L-lactide) (ASCP) were synthesized as described previously. [109] Briefly, a star copolymer (SCP) was first prepared through glycerol initiated ring-opening polymerization of the lactone monomers catalyzed with stannous (II) ethylhexanoate. Monomer to initiator ratios were varied to produce targeted molecular weights of 4000 and 8000 g/mol. The termini of the SCP were acrylated by reacting the terminal hydroxyl groups with a molar equivalent amount of acryloyl chloride. The reaction was catalyzed with dimethylaminopyridine and triethylamine was added in an equimolar amount to the terminal hydroxyl groups on the SCP to scavenge the HCl formed. A water washing step was required to reduce the cytotoxicity of the ASCP prior to its use in the scaffold. Water washing of the ASCP was conducted with mechanical mixing in an excess of water at approximately 60 ºC until the pH of the wash water was close to neutral. The wet ASCP was vacuumed-dried at room temperature, which was indicated by a change in the ASCP appearance from opaque to clear. The copolymer composition, degree of acrylation and number average molecular weight (MW) of the ASCP samples (10 mg/mL in dimethyl sulfoxide-D6) were determined from ^{1}H NMR analysis on a Bruker Avance 400 MHz spectrometer.

N-methacrylate glycol chitosan (MGC) was also prepared according to previously published work. [81] Briefly, *N*-methacrylation of the primary amines on the repeating residual units of glycol chitosan were produced by reaction with 0.1 times molar excess of glycidyl methacrylate at pH 9 for 24 hours.

The degree of *N*-methacrylation of the MGC sample (20 mg/mL in deuterium oxide) was confirmed by ^{1}H NMR analysis, and is reported as the number of *N*-methacrylated residues per 100 residues in the glycol chitosan chain. ^{1}H NMR spectra of the MGC were collected at 90 ºC on

a Bruker Avance-600 Ultrashield spectrometer equipped with a 5 mm TBI S3 probe with Z gradient and variable temperature capability.

Various volume fractions of a 6 % w/v solution of MGC in F12 culture media and each molecular weight ASCP were used to manufacture the scaffolds. Dimethylsulfoxide (DMSO) at 1 % v/v of the final scaffold volume was added as a co-solvent along with 0.1 % w/v of Irgacure 2959 photoinitiator dissolved in 1 X PBS to the aqueous MGC phase. Acellular and cellular scaffolds were manufactured by mechanically mixing all of the components for 2 – 3 minutes at 50 rpm using a 3 mm diameter screw type impeller within a 6 mm diameter Teflon mold. Depending on the study, the mixture was transferred to another mold of predetermined shape for cross-linking. A 50 Watt metal halide lamp (EXFO, Mississauga, Ontario) filtered between 320 – 390 nm was used to photo-cross-link the scaffolds for 180 seconds at an intensity of 15 mW/cm^2.

4.3.3 Scaffold Characterization

4.3.3.1 Cross-linking efficiency

The sol content of acellular MGC hydrogels (n = 4) as well as acellular high molecular weight ASCP scaffolds containing 30 % v/v MGC/F12 (n = 3) were extracted with water. The sol content of elastomer-only samples (n = 4) were extracted with tetrahydrofuran (THF). Briefly, samples (10 x 10 x 1 mm) were divided into two halves and both initial wet weights were recorded. The first half of the sample was lyophilized immediately to obtain a dry to wet weight ratio. The second half of the sample was soaked in excess solvent for 24 hours with multiple solvent changes (3 times) to remove any extractable components. After the sol extraction, the second half of the sample was lyophilized to obtain the sol dry weight (m_{sol}). The initial dry weight (m_{int}) of the second half was predicted from the initial wet weight of the second half multiplied by the dry/wet ratio obtain from the first half of the sample. The sol fraction was calculated from the difference of m_{int} and m_{sol}, which was then divided by m_{int}.

ATR-FTIR spectra before and after cross-linking were collected on a Nicolet 6700 FT-IR spectrometer equipped with a smart orbit ATR diamond stage. The cross-linking efficiency was calculated according to the disappearance of the absorption band for the $–CH=CH_2$ at 810 cm^{-1} in reference to the $–CH_3$ absorption band at 2862 cm^{-1} before and after cross-linking (Equation 4.1). [128] In Equation 4.1, A represents the absorption band at either 810 or 2862 cm^{-1} and the subscripts x and o represent the cross-linked and uncross-linked spectra, respectively.

Equation 4.1: $$\boldsymbol{Conversion}\ (\%) = \left[1 - \left(A_{810,x}/A_{2862,x}\right)/\left(A_{810,o}/A_{2862,o}\right)\right] \boldsymbol{x\ 100}$$

4.3.3.2 Mechanical Property Measurement

Acellular scaffolds with varying volume fractions of the 6 % w/v MGC/F12 culture media solution, were prepared with both ASCP molecular weights. These scaffolds were used for non-destructive mechanical property assessment using a double indentation method. [129, 130] Unconfined square samples 10 x 10 x 1 mm in size were tested using two flat ended indenters of 2 and 4 mm diameter (n = 2, each tested on both sides) using a micromechanical tester (TA.TX*plus*™, TextueTechnologies Corp. Scarsdale, NY) equipped with a 50 kg load cell. Indentations were conducted at room temperature and a displacement rate of 0.1 mm/s for 2 s. The resulting load-displacement data from the indentations were collected at a frequency of 200 Hz. Load-displacement slopes (determined from a linear regression of the collected load-displacement data) from each indentation (2 and 4 mm) were used to calculate Poisson's ratio and instantaneous modulus for each of the scaffolds according to the procedure proposed by Hayes *et al.* [131] The double indentation method, which assumes a linear elastic and isotropic material, was deemed valid for these viscoelastic scaffolds when tested with infinitesimal indenter deformations. [129]

4.3.3.3 Determination of Scaffold Structure by Trypan Blue Staining

After the non-destructive mechanical testing, the same scaffolds were sectioned by hand through the middle using a # 21 scalpel blade. The cut surfaces were stained with trypan blue for 5 minutes and then rinsed in water before imaging. Images of the stained scaffolds were taken using a Wilovert Hund light microscope (Helmut Hund GmbH, Wetzlar, DE) and modified in Photosnap Essentials SE (Nero 8, Karlsbad, DE) to black and white for better contrast and easier comparison between the different scaffold phases (MGC and ASCP).

4.3.3.4 Cell Isolation and Encapsulation

Primary chondrocytes were isolated from articular cartilage of bovine metacarpal-phalangeal joints, as described previously. [132] The isolated cells were suspended in the 6 % w/v MGC/F12 culture media solution at a concentration of 4×10^7 cells/mL. 30 % v/v of this MGC/F12 culture media cell suspension was mixed into the high molecular weight ASCP according to the scaffold manufacturing protocol outlined above. Aliquots (40 μL) of this mixture were loaded into a cylindrical mold (5 mm dia.) possessing two adjustable parallel plungers (2.5 mm height). The cylindrical mold was attached in-line to a gear reduced shaft mixer (Stir-Pak Dual-Shaft Mixer, Cole-Parmer Canada Inc. Montreal, QC). The mold was rotated at 10 rpm while being exposed to UV light for 180 seconds (Figure A.1). The resulting scaffolds were removed from the mold, and cultured in 5% FBS/F12 culture media in an incubator maintained at 37 °C with an atmosphere supplemented with 5 % CO_2 for up to 14 days with media changed every other day. Media was supplemented with 1X antibiotics/antimycotics and 100 μg/mL ascorbic acid.

4.3.3.5 Determination of Scaffold Structure by Micro-CT X-ray Tomography

High resolution Micro-CT (μCT) images of the acellular scaffolds (5 mm dia. x 2.5 mm in height) were taken on an MicroXCT-400 scanner (Xradia, Pleasanton, CA) and reconstructed and modified in ImageVis3D software (Center for Integrative Biomedical Computing, University of Utah). The density of the MGC regions was increased using 150 mg/mL K_2HPO_4, as a CT calibration agent. [133] Due to the length of time required to perform the high resolution scans (10 – 12 hours) multiple samples (n = 2) were stacked in a humidity controlled container to prevent sample dehydration and shrinkage.

4.3.3.6 Equilibrium Modulus Determination

Stress relaxation measurements were conducted on both the acellular and cellular two-phase scaffolds to determine scaffold equilibrium modulus (n = 5 – 6). Testing was performed on a micromechanical tester (MACH-1™, Biomomentum Inc. Laval, QC) equipped with a 1 kg load cell housed in a standard incubator maintained at 37 °C, as described previously. [132] Briefly, unconfined samples (5 mm diameter x 2.5 mm in height) were immersed in a F12 culture media bath and stress relaxation tests were conducted at 2 % strain increments, to a total strain of 20 %. Step strains were applied at a rate of 6 %/s. At each step, the resulting force decay was recorded until equilibrium was reached. Equilibrium was defined as a change in force of less than 0.2 g/min. The equilibrium modulus was obtained from the slope of the equilibrium stress-stain curve between 10 – 20 % strains (linear region) (Figure A.2).

4.3.3.7 Viable Cell Tracking

The chondrocytes were pre-stained with PKH26 cell tracker prior to seeding within the two-phase scaffolds (n = 2). Scaffolds were manufactured as described previously using the cylindrical mold (5 mm dia. x 2.5 mm height). Scaffolds were removed from culture, cut by hand

using a # 21 scalpel blade and imaged along all cut surfaces (n = 8, 512 x 512 pixel images) to determine cell distribution and viability over the 14 day culture period. Fluorescent images were taken on a FluoView FV1000 laser scanning confocal microscope (inverted) using the 10 X objective and FV10-ASW software (Olympus America Inc. Center Valley, PA). The fluorescent images were converted to binary in ImageJ software version 1.44 (NIH, Bethesda, MD) and the cells counted using the analyze particle feature (2 – 30 pixel size and 0 – 1 circularity).

4.3.3.8 MTT Cell Viability Assay

Cell viability within the cultured cellular two-phase scaffolds was determined using the MTT assay, according to the manufacture's specifications (4 h incubation with the MTT solution at 37 °C). Acellular two-phase scaffolds were also tested to ensure background readings were minimal. 600 μL of DMSO was used to solubilize the formazan crystals that were formed within the cells after the incubation period. To facilitate solubilization, the scaffolds (n = 5 – 6) were crushed within microcentrifuge tubes using a metal rod. The MTT suspensions were then centrifuged at 10,000 g for 10 minutes. The supernatant was removed, added to a 96 well plate in 200 μL aliquots, and read at 500 nm (max absorption).

4.3.3.9 Biochemical Assays

Assays for DNA, sulfated GAG and collagen contents were performed on acellular (background) and cellular two-phase scaffolds (n = 5 – 6). Prior to culture, the wet masses of the scaffolds were recorded. Upon harvest from culture, scaffolds were re-weighed wet and then snap frozen in liquid nitrogen, and stored at -85 ºC until analysed. All samples were then lyophilized and once dry weighed again before being individually crushed and digested in papain buffer (80 μg/mL in 20 mM ammonium acetate, 1 mM ethylenediaminetetraactic acid and 2 mM dithiothreitol all in Type 1 water) for 3 days at 65 ºC. The supernatant was collected and stored at

-20 ºC until needed. DNA content was measured using the Hoechst 33258 dye binding assay. [134] Briefly, aliquots of the papain digest were diluted with 1X PBS (1:2 dilution) and calibrated against standard curves prepared from calf thymus DNA. Hoechst dye was added to the samples (in triplicate) in 96 well black plates and measured using a Synergy HT multi-mode microplate reader (BioTek, Winooski, VT) at 350 nm excitation and 450 nm emission. Sulphated GAG content in the papain digest was measured using the dimethylmethylene blue (DMMB) absorbance assay. [135] Undiluted aliquot of the papain digest were calibrated against a bovine chondroitin sulfate standard curve. Samples (in triplicate) were read at 525 nm absorbance. Collagen content was determined from a hydroxyproline (OH-pro) assay under the assumption that OH-pro accounted for 10% of the total collagen mass. [136] OH-pro was measured using a chloramine T and Ehrlich's reagent assay. [137] Briefly, an aliquot of the papain digest was hydrolyzed in 6 N HCl at 110 ºC for 18 hours. Afterwards the samples were neutralized with an equal volume of 5.7 N NaOH and adjusted with water to a final 1:5 dilution volume. Hydrolyzed samples (in triplicate) were correlated against L-hydroxylproline standards and read at 560 nm absorbance.

The initial wet (m_{wi}) and cultured wet (m_{wc}) and dry weights (m_{dc}) of the co-continuous scaffolds that were used for the biochemical assays (n = 5 – 6) were taken to determine the total water content (%) (Equation 4.2) and change in wet mass (%) (Equation 4.3) during culture.

Equation 4.2: $$\boldsymbol{Water\ Content}\ (\%) = (\boldsymbol{m_{wc}} - \boldsymbol{m_{dc}})/\boldsymbol{m_{wc}}$$

Equation 4.3: $$\Delta\ \boldsymbol{Wet\ Mass}\ (\%) = (\boldsymbol{m_{wc}} - \boldsymbol{m_{wi}})/\boldsymbol{m_{wi}}$$

4.3.3.10 MGC and GAG Complexation Assay

A GAG complexation assay was conducted to determine the amount of GAG that was bound to the MGC hydrogel during culture, thereby potentially affecting the GAG assay results. To find the maximum GAG complexation limit for the acellular MGC (6 % w/v in F12) hydrogels, samples (21.7 ± 0.5 mg) were first soaked in 5 % FBS/F12 culture media for 24 hours at 4 ºC to account for any competitive protein binding that may have occurred. After aspiration of the culture media, MGC hydrogel samples were incubated in 100 μL of various chondroitin sulfate standards ranging from 10 to 1600 μg/mL for 24 hours at 4 ºC. A DMMB absorbance assay was conducted on the supernatant, as described previously, to analyze the amount of free GAG (n = 3). The maximum GAG complexation limit, calculated on a per mass basis of MGC hydrogel sample was determined from the intersection point for complete GAG complexation (zero slope) and incomplete GAG complexation (increasing slope). It was assumed that the GAG assay could only detect GAG above the maximum complexation limit (free GAG). Therefore, only the significantly different DMMB assay results (from all other time points) were taken into account and thereby increased by the maximum GAG complexation value. To confirm that the bound GAG could not be released back into solution, a papain digestion was also carried out on the MGC hydrogel samples followed by the DMMB absorbance assay where no free GAG was detected.

4.3.3.11 MGC-only Scaffolds

As the two-phase scaffolds could not be effectively sectioned for histological assessment (due to the presence of, and the significant background staining of, the elastomer), MGC hydrogel-only cellular scaffolds were produced for this purpose. MGC cell suspensions were cross-linked in the same molds (5 mm dia. x 2.5 mm height) without the ASCP and cultured for up to 7 days. At selected time points, the MGC hydrogel-only constructs were removed from

culture and tested to determine the equilibrium modulus as previous explained. The samples were fixed in 4 % paraformaldehyde for 24 hours, and stored in 70 % ethanol. The fixed scaffolds were then paraffin-embedded and sections of 10 μm thickness were cut. The sections were de-waxed using toluene and rehydrated in a series of graded ethanol solutions with a final water soak. The de-waxed sections were stained in a 0.1 % w/v safranin-O solution for 5 minutes and then dehydrated back to toluene. The stained sections were covered with Permount mounting media before placing a cover slip over the sample. All sections were viewed under light microscopy.

4.3.4 Statistical Analyses

All results were expressed as the mean ± standard error of the mean (SEM) and analyzed using statistical software (SigmaStat 1.0, SPSS Science, Chicago, IL). Physical, biochemical and mechanical characterization results were analyzed using a one-way ANOVA and the Fisher's LSD post-hoc test. Significance was assigned at p-values of less than 0.05.

4.4 Results

4.4.1 Initial Acellular Scaffold Characterization

The ^{1}H NMR spectra of the individual pre-polymers (Figure A.3) were used to determine the degree of substitution, monomer molar ratio and MW as previously described for the ASCP and MGC and listed in Table 4.1. [81, 109] The two ASCP pre-polymers had 87 % of the end groups acrylated and final monomer compositions very close to the feed ratios. Water washing the ASCP did not appear to have any adverse effects on the final product, other than a slight increase in the targeted MW. The lower MW ASCP components were likely water soluble and removed during the water washing steps. The degree of *N*-methacrylation of the MGC was determined to be 5 %. Hydrogels prepared with the 6 % w/v MGC in F12 solution will be referred to as MGC.

Elastomers prepared with the 4.8KASCP will be referred to as 4.8KELAST, while those prepared with the 9.3KASCP will be referred to as 9.3KELAST.

Table 4.1: ASCP and MGC properties from ^{1}H NMR analysis

Polymer	DLLA:CL Monomer Feed Ratio (molar)	Actual DLLA:CL Monomer Ratio (molar)	Degree (%) of Functionalization	M_n (kg/mol) [targeted M_n]
4.8KASCP	50:50	52:48	87	4.8 [4]
9.3KASCP	50:50	53:47	87	9.3 [8]
MGC	N/A	N/A	5	93

Sol content and mechanical property measurement results for the photo-cross-linked scaffolds are summarized in Table 4.2. The individually cross-linked pre-polymers as well as a representative MGC loaded elastomer two-phase scaffold were all highly cross-linked with a minimal amount of extractable components, based on the low sol values obtained. The MGC-only scaffold had the highest amount of sol extracted at 5.4 ± 1.5 % w/w. In terms of mechanical properties, as the MGC loading increased, in both the 4.8KELAST and 9.3KELAST scaffolds, there was a corresponding increase in Poisson's ratio along with a simultaneous drop in elastic modulus. This change in property occurred between 10 and 20 % v/v MGC loading for the 4.8KELAST scaffolds, and between 30 and 40 % v/v MGC loading for the 9.3KELAST scaffolds.

Table 4.2: Acellular material and two-phase scaffold characterization. 4.8K and 9.3K data sets were compared separately and MGC-only data was included for each comparison. (*) Significant from all other modulus values, significant between the (‡) and (†) groups, but not within each group ($p < 0.05$).

Scaffold	Poisson Ratio	Modulus [kPa]	Sol Fraction [%]
4.8KELAST-only	$0.23^{‡}$	$4190 \pm 380^{*}$	0.5 ± 0.2
10 % v/v MGC-4.8KELAST	$0.25^{‡}$	$2103 \pm 15^{*}$	-
20 % v/v MGC-4.8KELAST	$0.50^{†}$	$395 \pm 37^{†}$	-
30 % v/v MGC-4.8KELAST	$0.45^{†}$	$357 \pm 28^{†}$	-
60 % v/v MGC-4.8KELAST	$0.50^{†}$	$194 \pm 19^{†}$	-
9.3KELAST-only	$0.24^{‡}$	$1619 \pm 69^{*}$	1.5 ± 0.3
30 % v/v MGC-9.3KELAST	$0.24^{‡}$	$610 \pm 29^{*}$	1.9 ± 0.5
40 % v/v MGC-9.3KELAST	$0.45^{†}$	$203 \pm 2^{†}$	-
60 % v/v MGC-9.3KELAST	$0.48^{†}$	$108 \pm 5^{†}$	-
MGC-only	$0.30^{‡}$	$124 \pm 10^{†}$	5.4 ± 1.5

4.4.2 Co-continuous Morphology

The MGC regions of these scaffolds were also stained with trypan blue and viewed under light microscopy (Figure 4.1) to assess the structure of the hydrogel and elastomer phases within the scaffold. From these images it was evident a co-continuous scaffold (Figure 4.1 (A and C)) was formed and that the higher MGC loading (30 % v/v) in the 9.3KELAST scaffolds resulted in more interconnected pathways throughout the scaffold compared to the 10 % v/v MGC-4.8KELAST scaffold.

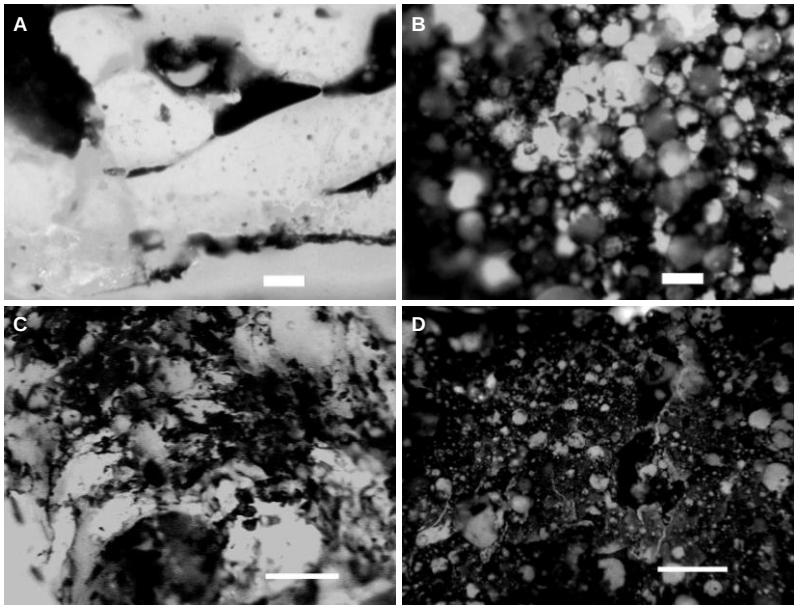

Figure 4.1: Trypan blue stained images to determine the range of MGC loading where phase transition occurred within the scaffolds, (A, B) 10 and 20 % v/v MGC in 4.8KELAST and (C, D) 30 and 40 % v/v MGC in 9.3KELAST. Images were converted to black and white; black for MGC regions and white for elastomer regions. The scale bars represent 100 μm.

The elastic modulus values of the 10 % v/v MGC-4.8KELAST scaffolds (2103 ± 15 kPa) were significantly higher than those for the 30 % v/v MGC-9.3KELAST scaffolds (610 ± 29 kPa). However, both of these values were significantly higher (17-fold and 5-fold higher, respectively) than that of the MGC-only scaffold (124 ± 10 kPa). Based on these results, the 30 % v/v MGC-9.3KELAST scaffold was chosen for the remainder of the study, due to the higher MGC loading that could be achieved while maintaining a continuous elastomer phase, and because it possessed mechanical properties within the range of most load bearing soft tissues. For example, typical confined modulus values reported for bovine load bearing soft tissues are 0.31 ± 0.04 MPa for nucleus pulposus, [42] 0.79 ± 0.36 MPa for articular cartilage, [138] 0.41 ± 0.09 MPa for meniscus.[42]

To ensure the formation of a co-continuous network between the hydrogel and elastomer phases, acellular 30 % v/v MGC-9.3KELAST scaffolds were imaged by μCT. A 3D reconstruction from the μCT scans of the 30 % v/v MGC-9.3KELAST scaffolds (Figure 4.2) revealed a continuous MGC region was present throughout the majority of the scaffold (indicated in blue). The unlabelled 9.3KELAST region, shown as the black void spaces between the blue MGC regions, also appeared to be continuous throughout the scaffold.

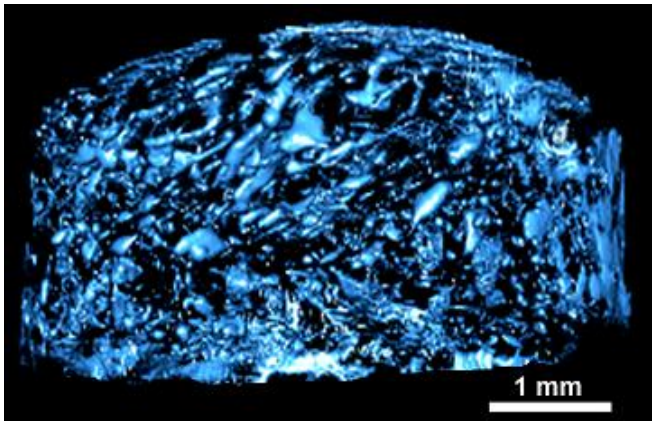

Figure 4.2: Confirmation of co-continuous morphology in an acellular 30 % v/v MGC-9.3KELAST scaffold. ImageVis3D reconstruction; blue for MGC phase and black for 9.3KELAST phase. The scale bar represents 1 mm.

4.4.3 Physical Assessment of Cellular Co-continuous Scaffolds

Cellular and acellular scaffolds of the 30 % v/v MGC-9.3KELAST scaffolds were then created and cultured for a 14 day period. Scaffolds were harvested at 1, 3, 7 and 14 days to assess the changes in mechanical properties, cell viability and accumulation of extracellular matrix within the scaffolds. Over the 14 day culture period there was no significant change in the average water content of the co-continuous scaffolds (Figure 4.3 (A)). The average wet mass of the co-continuous scaffolds appeared to decrease over the 14 day culture period. For the cellular

scaffolds, there was a slight, but significant, decrease in wet weight from the initial day 1 time point (Figure 4.3 (B)).

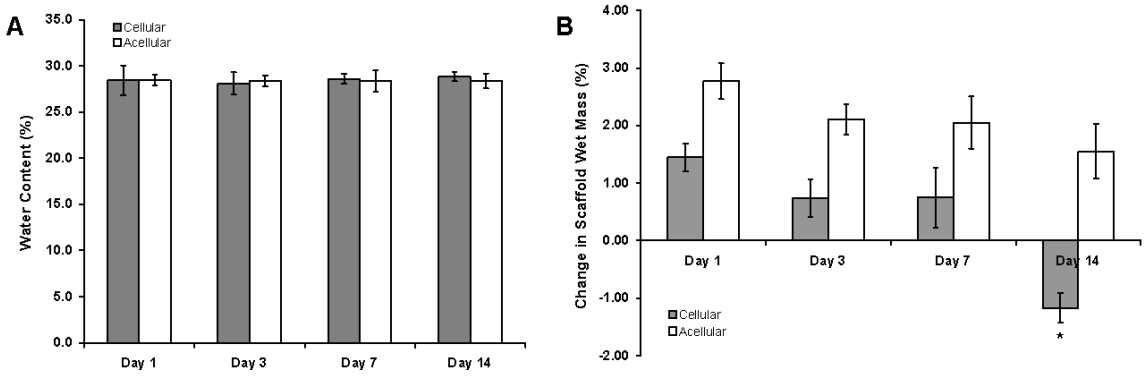

Figure 4.3: Change in properties of 30 % v/v MGC-9.3KELAST scaffolds during culture (A) water content (%) and (B) wet mass before and after culture (%). (*) Significant from day 1 values ($p < 0.05$).

As the equilibrium modulus of the acellular scaffolds remained fairly constant throughout the entire 14 day culture period (Figure 4.4), the acellular modulus was used as a baseline to assess cellular activity in the cell-encapsulated scaffolds. With increasing time in culture, dramatic changes in scaffold mechanical properties were observed. At day 1, the equilibrium modulus of the cellular scaffolds experienced an almost 6-fold decrease (123 ± 7 kPa) compared to the day 1 acellular scaffolds (697 ± 146 kPa). By day 3, the cellular scaffold equilibrium modulus (1015 ± 123 kPa) had increased to a value higher than that of the acellular scaffolds (764 ± 81 kPa). Beyond day 3, the equilibrium modulus of the cellular scaffolds remained above their acellular scaffold counterparts. However, a significant decrease in the cellular scaffold's equilibrium modulus was observed between day 3 and day 14.

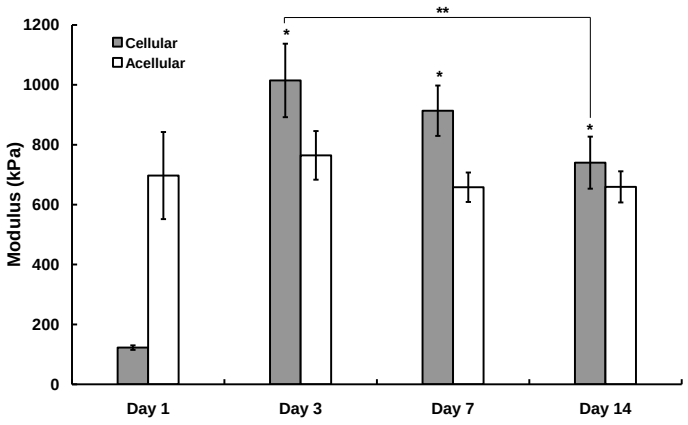

Figure 4.4: Equilibrium modulus data for acellular and cellular 30% v/v MGC-9.3KELAST scaffolds cultured for up to 14 days in static culture. (*) Significant from day 1 modulus data ($p < 0.05$), (**) significant within group ($p < 0.05$)

A shorter term culture was performed on the MGC-only scaffolds for up to 7 days. There did not appear to be any significant influence of the cells to the equilibrium modulus values for either the cellular or acellular scaffolds (Figure 4.5).

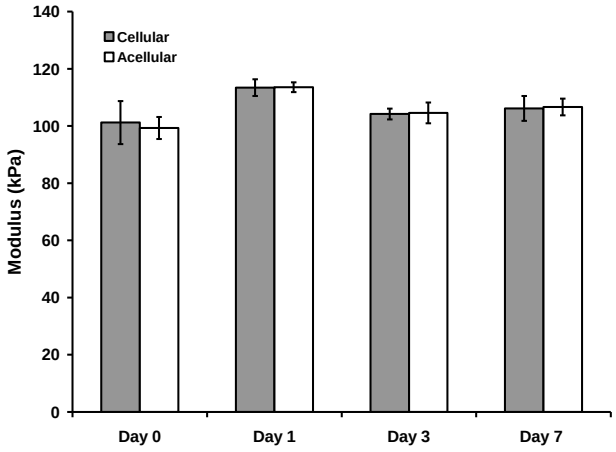

Figure 4.5: Equilibrium modulus values for MGC-only scaffolds cultured for a shorter 7 day period to determine the effect of cells on MGC phase and if the MGC phase contribute to the overall mechanical properties of the co-continuous scaffolds.

In addition, the MGC 9.3K ASCP and co-continuous scaffolds were characterized using ATR-FTIR to determine the cross-linking efficiency. From the ATR-FTIR spectra for the cellular 30 % v/v MGC-9.3KELAST scaffold there was 94 % conversion of the $–CH=CH_2$ band after cross-linking (Figure 4.6). The 9.3KELAST alone and acellular 30 % v/v MGC-9.3KELAST co-continuous scaffolds both had conversions of 95 and 94 %, respectively (Figure A.4). The ATR-FTIR analysis indicated that the elastomer phase was being cross-linked efficiently. No obvious changes in the MGC phase could be determined from the ATR-FTIR spectra before and after photo-cross-linking (Figure A.4). Therefore, only the sol fraction data was used to assess the cross-linking degree of the MGC phase.

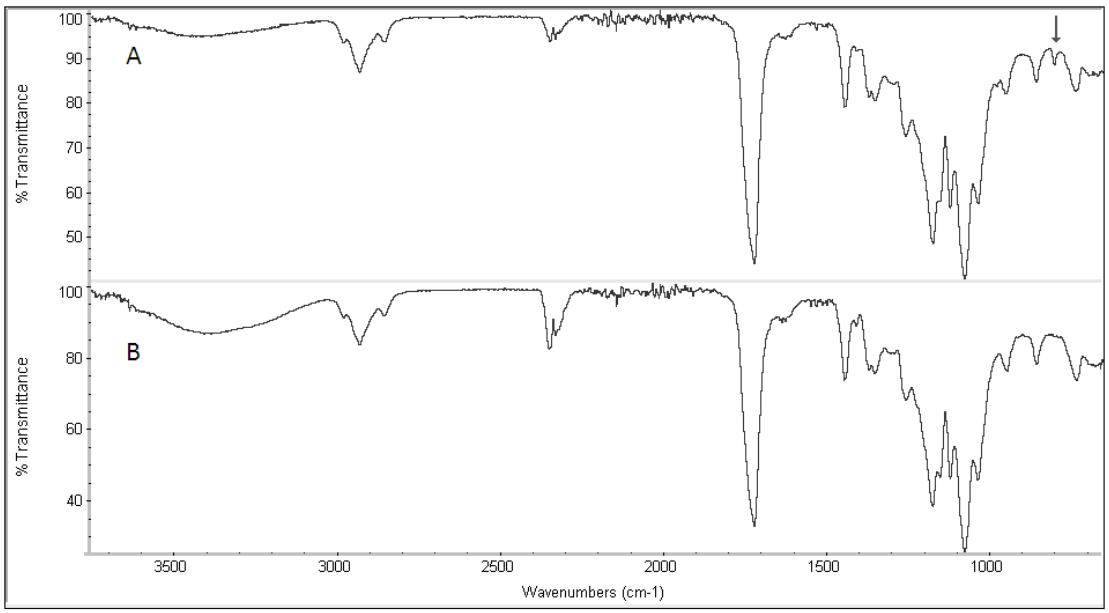

Figure 4.6: Transmission ATR-FTIR spectra of the cellular 30 % v/v MGC and 9.3KASCP scaffold mixture before (A) and after (B) photo-cross-linking to show the disappearance of the $–CH=CH_2$ absorption band at 810 cm^{-1} (arrow).

4.4.4 Cell localization within Co-continuous Scaffolds

To ensure cells were evenly distributed throughout the scaffold, cell membranes were pre-stained with PKH26 and tracked over the 14 day culture period. PKH26 cell tracking was also used to assess potential changes in scaffold cellularity throughout the culture period. PKH26 cell tracking images (Figure 4.7) indicated that the chondrocytes were well distributed within the scaffold and remained distributed throughout the 14 day culture period. Cellularity of the scaffolds (counted from the PKH26 confocal images) significantly increased from 145 ± 18 cells/image to 278 ± 15 cells/image between day 1 and day 14, respectively. However, no significant changes in scaffold cellularity were observed between day 3 and day 14 of culture.

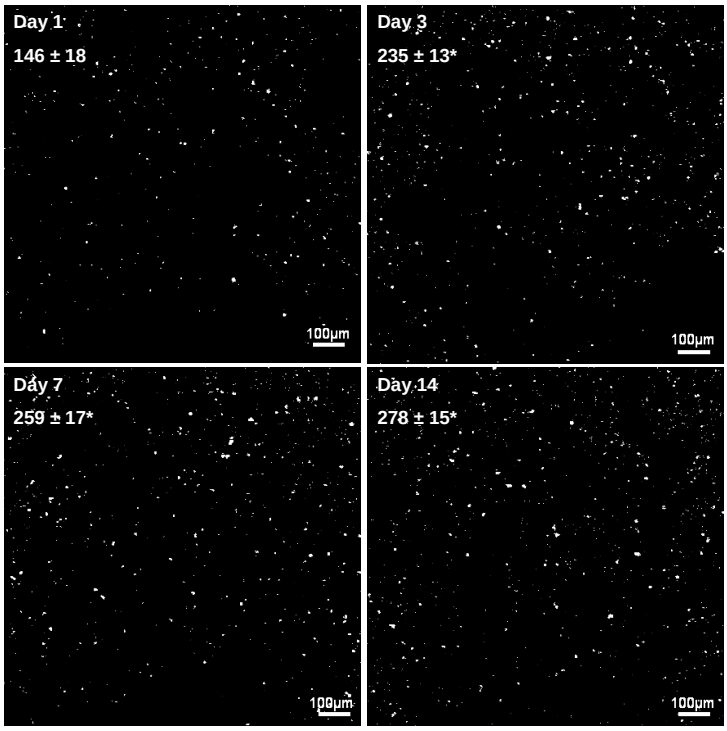

Figure 4.7: Confocal images of PKH26 labeled cells within the 30 % v/v MGC-9.3KELAST scaffolds after 1, 3, 7 and 14 days in culture. PKH26 labeled cells are shown as white to enhance contrast for the images. Text insert: Showing time in culture and average cell counts (n = 8) ± SEM. (*) Significant from day 1 value ($p < 0.05$). Scale bar represents 100 µm.

4.4.5 Cell Viability within Co-continuous Scaffolds

The MTT assay was used to monitor the viability of the chondrocytes within the 30 % v/v MGC-9.3KELAST scaffolds over the culture period (Figure 4.8). Over the 14 day culture period, there was an increasing trend in the cell viability within the scaffolds. Specifically, the metabolic activity of the cells increased significantly after day 3 and appeared to remain constant with increasing time in culture. DNA content was also used to measure the relative change in cell numbers over the entire culture period to reinforce the semi-qualitative cell counts from the PKH26 images. DNA content results displayed similar trends with significant increases observed after day 3 in culture (Figure 4.8).

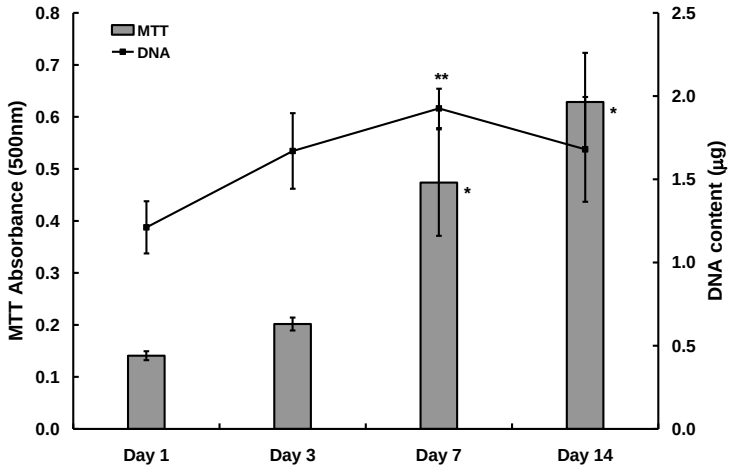

Figure 4.8: MTT metabolic activity assay and DNA content for cellular 30 % v/v MGC-9.3KELAST scaffolds over the 14 day culture period. (*) Significantly higher than day 1 and day 3 MTT values ($p < 0.05$), (**) significantly higher than day 1 DNA value ($p < 0.05$).

4.4.6 ECM Accumulation within Co-continuous Scaffolds

To determine whether the encapsulated chondrocytes within the 30 % v/v MGC-9.3KELAST scaffolds could accumulate extracellular matrix, biochemical markers for sulfated GAG and collagen production were measured throughout the culture period and normalized to

DNA content (Figure 4.9). A significant decrease from the day 1 normalized GAG values was observed only for the day 7 time point. An increase in the normalized collagen content was observed at day 3 and appeared to decrease throughout the rest of the culture period.

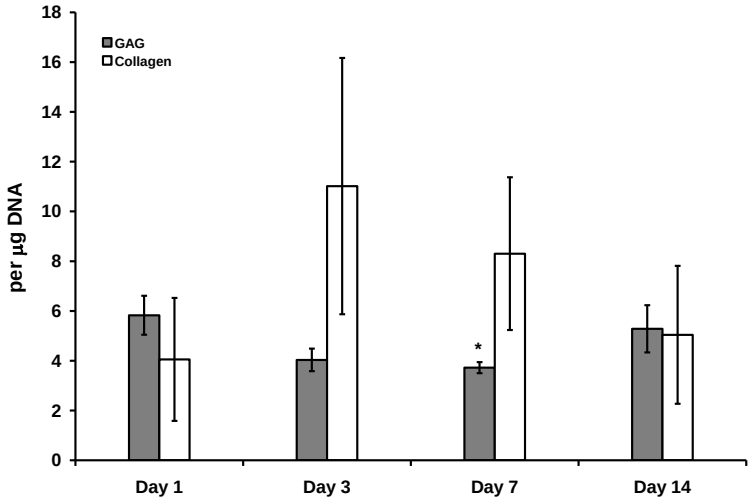

Figure 4.9: GAG and collagen normalized to DNA accumulation within the cellular 30 % v/v MGC-9.3KELAST scaffolds. (*) Significant from day 1 data ($p < 0.05$).

As the MGC electrostatically complexed GAG, additional studies were conducted to gain a better understanding of GAG accumulation within the MGC hydrogel. Due to problems with sectioning the two-phase scaffolds and the significant background staining of the elastomer, GAG accumulation was assessed by safranin-O staining in histological sections of the MGC-only scaffolds (containing the same cellular density as the 30 % v/v MGC-9.3KELAST scaffolds). Immediately after encapsulation there appeared to be safranin-O staining only within or on the chondrocytes (Figure 4.10 (Day 0)), which was then lost after 24 hours of culture (Figure 4.10 (Day 1)). By day 3 of culture, intracellular safranin-O staining returned along with the presence of GAG staining throughout the MGC matrix (Figure 4.10 (Day 3)). Both intracellular, and

especially MGC matrix, safranin-O staining, was further enhanced by day 7 of culture (Figure 4.10 (Day 7)).

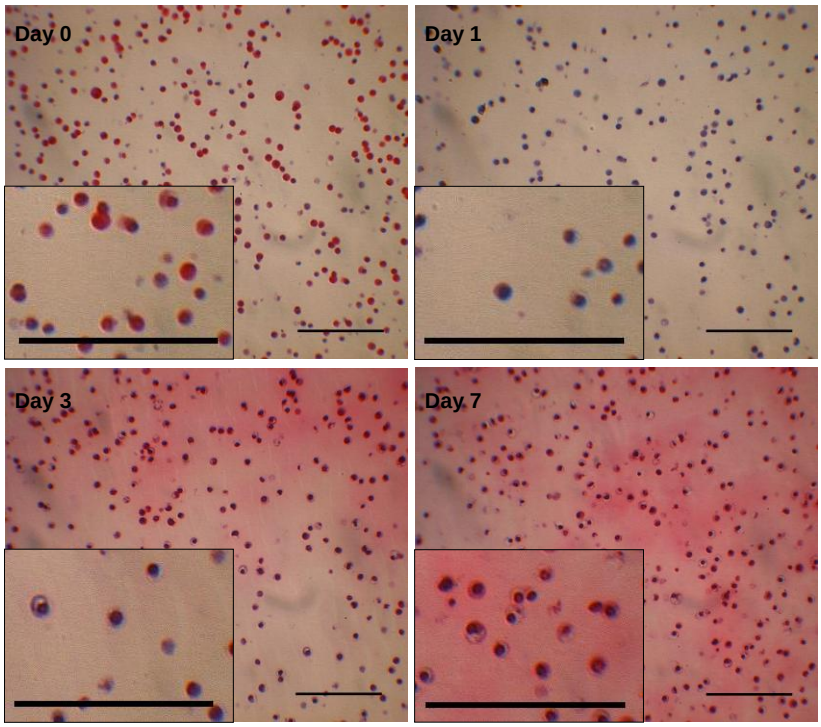

Figure 4.10: Safranin-O staining for the cellular MGC-only scaffolds after 0, 1, 3, and 7 days in culture. Insert: Higher magnified area around the scale bar. Scale bars represent 100 μm.

4.5 Discussion

In this study, we report on the design and characterization of a two-phase scaffold for the encapsulation and delivery of cells to aid in the repair of load bearing soft tissues. The two-phase scaffold design was constructed from a hydrogel and elastomer phase. Interconnectivity within each of the two phases was a design parameter necessary to impart elastomeric mechanical properties to the scaffold while at the same time to allow for a viable cell population within the hydrogel phase. The hydrogel phase was chosen to encapsulate the chondrocytes to provide a 3D

environment required to maintain cellular phenotype *in vitro*. [126] The initial acellular scaffold characterization was conducted to determine if a co-continuous two-phase morphology could be attained within the constraints of the scaffold system. Once it was established that a suitable co-continuous scaffold was formed, cells were incorporated into the scaffold fabrication procedure. The cellular co-continuous scaffolds were then cultured for a two week time period. During this culture period the behaviour of the cells and the overall mechanical properties of the scaffold were analysed.

Relatively few studies have investigated the use of an injectable biphasic scaffold for tissue engineering. A recent study by Peng *et al.* demonstrated the feasibility of a photocurable gelatin hydrogel and HydroThane™ elastomer composite to form an interpenetrating network (IPN) for wound healing applications. [117] The IPN in the elastomer phase allowed the biphasic scaffold to have controllable physical properties (mechanical and swelling) between each of the individual scaffold components. However, the ability to encapsulate and culture viable cells within the biphasic scaffold was not investigated.

Several studies have been conducted to predict the two-phase morphology and physical properties of immiscible binary polymer systems based on the viscosity ratio and the interfacial tension between the two phases and the shear rate of mixing. [139-144] However, the use of theoretical mixing rules to accurately predict the two phase morphology within a given system is not currently available due to the many variables and complex nature of most immiscible polymer blends.

In the current study, the mixing shear rate was kept constant and only the MGC solution content and ASCP molecular weight were changed. It was apparent (Figure A.5 (C and D)) that an increase in MGC content in the scaffold resulted in the occurrence of a co-continuous morphology around the phase inversion limit of the mixture. A coarsening or ripening effect of the co-continuous morphology was also observed after allowing the 30% v/v MGC-9.3KELAST

scaffold mixture to rest for 1 hour at 37 ºC before cross-linking (Figure A.6). These observations are analogous to immiscible binary polymer emulsions previously reported in the literature. [140, 145]

The effect of the two-phase morphology on the mechanical properties of the scaffolds was observed in the mechanical properties of the acellular scaffolds (Table 4.2). While the addition of the MGC phase reduced the moduli of the elastomer-only scaffolds, the two-phase scaffold stiffness remained significantly higher than the MGC-only scaffold, provided the MGC loading was low enough that a continuous elastomeric phase was formed. For MGC loading above the phase inversion limit, a discontinuous elastomeric phase was formed and the moduli of the scaffold decreased and approached that of the MGC-only scaffold. An associated increase in Poisson's ratio for the two-phase scaffolds was also attributed to the elastomeric phase inversion. Another interesting observation was that an increased molecular weight of ASCP (from 4.8K to 9.3K) increased the MGC content at which phase inversion, or a co-continuous morphology, was observed. This effect was attributed to an increase in viscosity of the polymer with increased molecular weight, [146] resulting in a greater resistance to breakup of the stretched ASCP phase during mixing, ultimately leading to a change in the phase inversion limit. [140, 147]

The higher MGC content of the 9.3KELAST co-continuous scaffold (Figure 4.1 (C) and Figure 4.2) produced a higher degree of MGC phase interconnectivity than in the 4.8KELAST co-continuous scaffolds (Figure 4.1 (A)). A higher degree of MGC phase interconnectivity would allow for a more evenly distributed cell population throughout the entire scaffold. The higher MGC loading also allowed for more cells to be encapsulated within the scaffold (at a constant cellular density), which may be advantageous in initiating chondrogenesis and accelerating cartilaginous-like tissue formation *in vitro*. [148] The higher degree of MGC interconnectivity would also offer multiple routes for nutrient transport to the centre of the scaffold. Based on these reasons, the 30% v/v MGC-9.3KELAST scaffold was chosen for further study.

Mechanical property measurements of the cellular 30% v/v MGC-9.3KELAST scaffolds revealed that initially there was a large decrease in equilibrium modulus compared to the acellular co-continuous scaffolds. Additional work determined that the lower day 1 modulus values could not be attributed to ECM accumulation within the MGC phase alone (Figure 4.5) or from delayed cross-linking of the elastomer phase in the presence of cells (Figure 4.6). In addition, there were no observable changes in the cellular or acellular co-continuous scaffolds' water content and only a slight change in wet mass during culture (Figure 4.3). Therefore, aside from the addition of cells to the co-continuous scaffolds, the actual cause for the change in modulus is unknown. One possibility for these changes in modulus was that the cells caused a disruption at the interface between the MGC and 9.3KELAST phases. We also postulate that only with increasing time in culture could the cells synthesized and accumulate ECM to re-establish the interfacial region and thereby restore the load transfer between the hydrogel and elastomer phases. This notion is potentially confirmed by the observation that the modulus of the cellular scaffolds was restored to normal (acellular) levels after three days in culture. However, additional experiments will need to be conducted in order to substantiate this explanation.

A fluorescent PKH26 cell membrane tracker was used to localize and monitor the distribution of the cells within the MGC hydrogel regions of the 30 % v/v MGC-9.3KELAST scaffold. It should be noted that the PKH26 stain was not used as a direct measure for cell viability, it was assumed that images of intact cell membranes were indicative of viable cells. PKH26 confocal images confirmed that the cells remained evenly distributed throughout the entire scaffold and that the cellularity of the scaffolds increased during the culture period investigated. These results suggest that the majority of the MGC regions of the scaffolds were interconnected; otherwise, a decreasing cell population and/or uneven distribution patterns would have been observed due to decreased nutrient availability. The MTT assay supported this reasoning as increased cell metabolic activity of the encapsulated chondrocytes was observed

with time in culture. Combining the PKH26 and MTT results, it was evident that cells throughout the scaffold were able to maintain a viable and increasingly active cell population over the 14 day culture period. Similarly, the DNA content of the scaffolds was also measured and used as an indication of cellularity. A comparison of the PKH26 cell counts and DNA content indicated that there appeared to be a general trend of increasing scaffold cellularity throughout the 14 day culture period.

The chondrocytes within the co-continuous scaffolds synthesized extracellular matrix components, specifically sulfated GAGs and collagen, throughout the culture period. However, due to the possibility of GAG complexation to the MGC, it was reasoned that the initial readings from the GAG assay were artificially low. Previous work by Roughley *et al.*, had demonstrated that positively charged chitosan hydrogels can retain a significant amount of negatively charged GAG molecules. [149] Therefore, an experiment was conducted to determine the maximum GAG complexation within the MGC hydrogel (Figure A.7). The results of this study demonstrated that a considerable amount of GAG (1.68 ± 0.04 μg GAG/mg MGC hydrogel) was bound to the MGC hydrogel. Based on the amount of MGC within the 30% v/v MGC-9.3KELAST scaffolds (15.1 ± 0.7 mg) the maximum amount of GAG that could be bound to the MGC hydrogel was approximately 25.5 ± 1.7 μg. Therefore, the total amount of GAG within the co-continuous scaffold was not being read by the DMMB dye assay. In an attempt to visualize GAG accumulation within the MGC phase, cellular MGC-only scaffolds were cultured and stained with safranin-O for GAG. Although the MGC-only scaffolds did not directly determine what was occurring within the co-continuous scaffolds it demonstrated the possibility of increasing GAG accumulation with time (Figure 4.10). Further studies will be required to better characterize the ECM being synthesized and accumulated within the co-continuous scaffolds.

The 30 % v/v MGC-9.3KELAST scaffolds also accumulated collagen throughout the 14 day culture period. Although the amount of accumulation was not significantly different between

the various time points, there was a trend in collagen content that was similar to the equilibrium modulus data for the co-continuous cellular scaffolds. The loss of collagen that was observed between day 3 and 14 may be related to a variety of factors; therefore, longer-term studies are required to determine the fate of the collagen within the scaffolds.

4.6 Conclusion

The ability to integrate the benefits of traditional hydrogel and elastomer scaffolds together into a single two-phase scaffold design has been demonstrated. The 30 % v/v MGC-9.3KELAST was determined to be a suitable two-phase scaffold composition, based on the highest MGC loading to form a co-continuous morphology and its mechanical properties approximating those of soft tissues. Cell culture experiments conducted with the 30 % v/v MGC-9.3KELAST scaffolds demonstrated that the chondrocytes remained viable throughout the entire manufacturing process and were able to proliferate and accumulate matrix components over 14 days in culture. Collagen accumulated within the 30 % v/v MGC-9.3KELAST scaffolds; however, no significant differences in the levels of accumulation were detected throughout the culture period. While a significant amount of GAG was ionically complexed to the MGC, histological staining demonstrated that the encapsulated cells were able to produce an increasing amount of GAG within the MGC phase over time. Cellular 30 % v/v MGC-9.3KELAST scaffolds possessed moduli higher than the acellular scaffolds and were within the range of load bearing soft tissues. Future work will examine the long-term cellular behavior within the two-phase scaffolds and the feasibility of this scaffold as an injectable and *in situ* cross-linkable cell delivery system.

Chapter 5

Injectable, High Modulus and Fatigue Resistant, Composite Scaffold for Load-Bearing Soft Tissue Regeneration

5.1 Completed Objectives

In the paper for this chapter, all of the experiments were designed and completed by myself and published in Biomacromolecules 2013 (DOI: 10.1021/bm4010595) where I am the first author. [150] The work completed in Chapter 5 met the requirements for Objective 2 (§ 3.2.2), which included longer term mechanical characterization of the previous MGC and poly(ε-caprolactone-co-D,L-lactide) (5446DLLACL) ASCP scaffolds to monitor the effects of 5446DLLACL degradation. For the purpose of this study, the mechanical properties of the 5446DLLACL based scaffolds were found to drop quickly within the first month of culture, which was not compensated by sufficient accumulation of functional tissue in the hydrogel phase in order to maintain a high modulus. The rapid degradation of the elastomer phase was attributed to auto-catalyzed hydrolysis of the D,L-lactide monomer and a highly porous structure of the 5446DLLACL phase. To overcome these shortcomings, a poly(ε-caprolactone-co-trimethylene carbonate) (7030TMCCL) ASCP, which was less susceptible to hydrolysis, was studied to produce the same co-continuous morphology. In addition to the long-term culture, the injectability of the prepolymer mixture and the interconnectivity of the hydrogel phase and fatigue resistance of the cross-linked scaffolds were examined. The two-phase mixtures could be injected before cross-linking with no alteration to the co-continuous morphology. Based on complete aqueous based dye diffusion to the centre of the co-continuous scaffolds, the hydrogel phase was shown to be fully interconnected. The 7030TMCCL based scaffolds did not degrade during the 2 month culture, and displayed better resistance to cyclic loading and higher accumulation of cartilaginous tissue in the MGC hydrogel phase compared to the 5446DLLACL

based scaffolds. Overall, this work highlighted the possibility of using different elastomer phases to create co-continuous scaffolds with different mechanical properties and degradation profiles. The base design of these scaffolds was confirmed to be suitable for a minimally invasive injectable repair strategy for cartilaginous load bearing soft tissues such as the nucleus pulposus.

5.2 Introduction

Cartilaginous load-bearing soft tissues (LBST), such as the articular cartilage and nucleus pulposus, can be affected by degenerative joint diseases. [151-154] These diseases are progressive in nature and there are no effective early stage treatments currently available. Therefore, the affected joints are treated palliatively until functionality has been lost and joint instability [153, 155, 156] and debilitating pain [154, 157-159] become major concerns for the patient. At this stage of degeneration, the only effective treatments are invasive surgeries that replace the entire joint with artificial prostheses or fuse the joint together with non-articulating hardware. [160-163] Thus, early stage, preventative treatments are required to alter the degenerative course of these diseases. One such promising solution is a regenerative cell-seeded scaffold to replace the damaged tissue at an early stage in the degenerative disease process. [164-166]

Load-bearing soft tissues are found in physically demanding environments in the body, usually under heavy repetitive loading [41, 167] and with low levels of nutrients available. [11, 168] This environment results in a very limited ability for self-repair once damage occurs, leading to a progressive loss of tissue over time. Regeneration of LBSTs requires a scaffold that can replace or fill the void of the damaged tissue, share some of the mechanical requirements of the joint, and eventually produce functional tissue. [38, 169-171] In addition, it would be a distinct advantage if a cell-seeded scaffold could be injected and cross-linked *in situ*, to allow for a minimally invasive surgery. Current strategies for these tissues typically involve the use of either hydrogel [172, 173] or elastomeric [97, 98, 174] scaffolds as the cell carrying phase. For load-bearing applications, an

elastomeric scaffold would be beneficial due to the high strains (10 – 20%) and repetitive loading environment that the native tissues are subjected to *in vivo*. [175] However, regenerative elastomeric scaffolds are generally designed to be porous for cell infiltration, which drastically reduces their overall mechanical properties. [99, 176] Moreover, most porous elastomeric scaffolds are pre-formed before implantation due to the multi-step fabrication process required, which restricts their ability to be created via injectable delivery systems. [104] Hydrogels have also been considered, based on their ability to form 3-D environments to support cell viability and function. [73 81] However, hydrogels for cell encapsulation generally lack the appropriate mechanical properties for use as a load-bearing soft tissue scaffold.

One approach to overcome the limitations of these scaffold materials would be to create a composite scaffold that can be readily formed *in situ* following injection. By combining a photo-cross-linkable elastomer and hydrogel to produce a co-continuous, two-phase composite morphology, the beneficial properties of both materials are provided within a single scaffold design. The feasibility of such an approach was demonstrated in our previous work, wherein chondrocytes were encapsulated within a co-continuous scaffold comprised of photo-cross-linked, biodegradable acrylated *star*-poly(ε-caprolactone-co-D,L-lactide) as the elastomer phase and *N*-methacrylated glycol chitosan as the hydrogel phase. [119]

In the current study, we continued to investigate the suitability of acrylated star-poly(ε-caprolactone-co-D,L-lactide) and compared its performance to acrylated star-poly(ε-caprolactone-co-trimethylene carbonate). The weight fraction of acrylated star-copolymer in the formulation was first optimized for each acrylated star-copolymer to ensure the two phases (hydrogel and elastomer) in the resulting cross-linked scaffold were fully interconnected. The force of injection was then measured to ensure the formulations could be injected at a reasonable force while still resulting in a co-continuous morphology. Fatigue testing on both scaffold materials was conducted to determine the influence of repeated loading at high physiological

strains on the overall mechanical properties of the scaffolds. Finally, the effect of elastomer degradation on scaffold mechanical properties and behaviour of articular chondrocytes encapsulated within the two co-continuous scaffolds was assessed using long-term static culture.

5.3 Methods and Materials

5.3.1 Pre-scaffold characterization

5.3.1.1 Materials

Glycol chitosan (number average molecular weight, M_n = 93 kg/mol, $Đ$ = 1.2) was obtained from Wako Chemicals (Richmond, VA, USA). Trimethylene carbonate monomer was purchased from Boehringer Ingelheim (Ingelheim, Germany). D,L-lactide monomer was purchased from Purac Biochem (Gorinchem, The Netherlands). The ε-caprolactone monomer was purchased from Lancaster Synthesis (Morecambe, United Kingdom). Collagen type I antibody (rabbit anti-bovine, BD-T40113R) was supplied from CedarLane Labs (Burlington, ON, Canada). Collagen type II (mouse anti-bovine II-II6B3) and aggrecan (mouse anti-bovine 1C6s) primary antibodies were obtained from the Iowa Hybridoma Bank (University of Iowa). All other materials were obtained from Sigma-Aldrich (Oakville, ON, Canada) and were used as received unless otherwise noted.

5.3.1.2 Polymer Synthesis

The star-copolymers with terminal acrylate functionality were synthesized as described previously. [107, 119] Briefly, the star-copolymers (SCP) were first prepared with monomer feed ratios of 50:50 for ε-caprolactone and D,L-lactide and 70:30, 50:50 and 30:70 for ε-caprolactone and trimethylene carbonate through a glycerol initiated ring-opening polymerization of the monomers catalyzed with stannous 2-ethylhexanoate. The monomer to initiator ratio was set to

produce a targeted number average molecular weight of 8 kg/mol for each SCP. After polymerization, the terminal hydroxyl groups of the SCP were acrylated by reaction with an equimolar amount of acryloyl chloride to the SCP terminal hydroxyl groups, catalyzed with dimethylaminopyridine, in anhydrous dichloromethane. An equimolar amount of triethylamine (TEA) to the SCP terminal hydroxyl groups was added to scavenge the HCl formed. The acrylated star-copolymers (ASCP) were purified by first dissolving in ethyl acetate to precipitate TEA-HCl; the crystals were subsequently removed by filtration. After removal of the excess ethyl acetate by evaporation under vacuum, the ASCP were precipitated in cold methanol (-20 ˚C). Following this precipitation step and methanol removal under vacuum, the resultant ASCP were washed with an excess of Type I water under mechanical mixing at 60 ˚C until the pH of the wash water was neutral (5 washes). The wet ASCP was vacuum-dried at room temperature prior to use.

N-Methacrylated glycol chitosan (MGC) was prepared according to previously published work. [81] Briefly, glycol chitosan dissolved in Type I water was reacted with 100 X molar excess glycidyl methacrylate at pH 9 for 24 h. The MGC solution was purified by overnight dialysis, then lyophilized for storage.

5.3.1.3 Polymer Characterization

^{1}H NMR spectra of the ASCPs were collected from 1 mL samples (20 mg/mL in DMSO-d_6 at room temperature) on a Bruker Avance-400 MHz spectrometer. The copolymer composition, degree of acrylation and number average molecular weight of the ASCP samples were determined from ^{1}H NMR analysis as previously described. [119] Briefly, end group analysis was used to determine the degree of acrylation from the ratio of the averaged area under the peaks for protons arising from the acrylate group (between δ = 6.4 – 5.9 ppm) and those of the unreacted OH groups (δ = 5.5 ppm for DLLACL and δ = 5 ppm for TMCCL). Number average

molecular weight and monomer ratios were also calculated using the area under the characteristic proton peaks for the DLLA, TMC and CL residues with peaks centered at δ = 5.1 (methine), 4.1 (methylene) and 4.0 ppm (methylene), respectively. [107, 109]

^{1}H NMR spectra of the MGC were collected from 1 mL samples (dissolved to 20 mg/mL in deuterium oxide and heated to 90 ˚C to help with peak separation) on a Bruker Avance-600 MHz Ultrashield spectrometer. The degree of *N*-methacrylation of glycol chitosan (GC) was confirmed by ^{1}H NMR analysis, and was reported as the number of *N*-methacrylated residues per 100 residues in the GC chain as previously described. [81] Briefly, the ratio of the integration of the vinyl protons on the *N*-methacrylate group (average of δ = 6.2 and 5.9 ppm) over the integration of protons assigned to the C1 protons of the acetylated and de-acetylated glycol chitosan residues (δ = 5.05 and 5.1 ppm) was used to calculate the degree of substitution.

The glass transition temperature (T_g) of the ASCPs was measured with a Mettler Toledo DSC 1 Star System. Thermal data were taken from the 2nd heating cycle to ensure a common thermal history. The cycles used were as follows: (1^{st}) -100 ˚C to 20 ˚C, (2^{nd}) 20 ˚C to -100 ˚C, and (3rd) -100 ˚C to 20 ˚C (data taken). A 10 ˚C/min heating rate with a 1 min hold time at each set point was utilized.

Cross-linking efficiency was assessed through measurement of the sol content of specific scaffolds. The sol content was determined by measuring the change in dry mass of samples soaked multiple times in Type I water. [119]

5.3.2 Acellular Scaffold Characterization

5.3.2.1 Injectability and Rheology Measurements of ASCP/MGC Mixtures

The zero shear rate viscosity of the two-phase mixtures and various MGC % w/v solutions were measured on an AR 2000 TA instruments rheometer. Samples (~ 200 μL) were loaded onto the rheometer base and a 20 mm stainless steel flat plate was used with a 200 μm gap

to characterize the samples maintained at 25 ˚C. To prevent moisture evaporation the samples were contained during testing. Data was captured between shear rates of 0.1 and 10 s^{-1}, collecting 20 points per decade. Zero shear viscosity was determined from the average of the initial plateau region in the viscosity versus shear rate plots.

To assess the injectability of the mixtures prior to cross-linking, samples were mixed within a 3 mL syringe (P-system, MEDMIX, Switzerland). Injectability was measured using a TA XTplus texture analyzer with a 5 kg load cell and texture exponent 32 software. The syringe was secured vertically into a custom clamp to fit within the texture analyzer (Figure A.8). A 15 mm/min crosshead speed was used to measure the injection force of the mixtures with various 3.8 cm long needles (16, 18 and 20 Ga) attached to the syringe. The plateau region of the injection profile, taken as the maximum injection force, was recorded for each needle gauge (n = 3). The maximum injection force was correlated to the inner radius of the different needles and the increase in pressure was determined and compared to theoretical values calculated from the Poiseuille equation (Equation 5.1):

Equation 5.1: $$\boldsymbol{P_{gauge} = 8\eta LQ/\pi r^4}$$

Where, η = viscosity of the mixture, L = length of needle, Q = volumetric flow rate, r = needle radius and P_{gauge} = pressure difference. In using Equation 5.1 it was assumed that the two-phase mixtures behaved as a Newtonian fluid under the test conditions. [176]

5.3.2.2 Co-continuous Scaffold Fabrication

N-Methacrylated glycol chitosan (MGC) was dissolved in F12 culture medium at varying weight percentages for at least 24 h prior to use to ensure the MGC was completely dissolved. Mass fractions of the various MGC solutions were used to produce co-continuous morphologies

by co-mixing with the acrylated star-copolymers (ASCP). The photoinitiator, Irgacure 2959, dissolved in 1X PBS, was used at 0.1 % w/v of the total mixture mass. Acellular and cellular scaffolds were individually manufactured by mechanically mixing all of the components for 2 min with a spatula to produce a homogeneous and opaque mixture. The mixture was transferred to a 3.2 mm dia. Teflon ring with a height of 3.5 mm. The ends of the ring were capped with a microscope cover slip and the entire mold assembly was held in a clamp so as to leave the ends visually unobstructed. Cross-linking of the scaffolds was induced by exposure to 320 – 390 nm UV light at an intensity of 50 mW/cm^2 for 60 s on both sides using a 2 leg quartz fibre light guide (3 mm diameter).

5.3.2.3 Assessment of Hydrogel Interconnectivity in Co-continuous Scaffolds

The extent of diffusion of a water-soluble dye, toluidine blue, within the MGC hydrogel was used to determine the interconnectivity of the MGC phase. It was assumed that the toluidine blue dye (M_w 270 g/mol) would reflect the diffusion behavior of nutrients and waste products within the MGC phase. For these experiments, intact co-continuous scaffolds were incubated in 1 mL of an aqueous 1 % w/v toluidine dye solution at room temperature. Fully intact scaffolds were removed at various time points and cut in half axially down the centre and the cut surfaces were imaged with a Zeiss Discovery V12 stereomicroscope equipped with an AxioCam ICc1 camera and CL1500 co-axial light source. From the cut surfaces the depth of dye penetration was assessed visually to determine an approximate time for complete dye diffusion into the centre of the scaffolds.

5.3.2.4 Assessment of Co-continuous Scaffold Mechanical Properties

Stress relaxation and dynamic compression measurements were conducted on the co-continuous scaffolds to determine the equilibrium modulus and hysteresis values (n = 6). Testing

was performed on a micro-mechanical tester (MACH-1, Biomomentum Inc. Laval, QC) equipped with a 1 kg load cell and housed in a 37 ˚C incubator. Unconfined scaffold samples (3.2 mm dia. x 3.5 mm height) were immersed in a F12 culture media bath with a solid base and moving upper platen (1 cm dia. each). Stress relaxation tests were conducted at 2 % strain increments, to a total strain of 20 %. Step strains were applied at a rate of 6 %/s. At each step, the resulting force decay was recorded until equilibrium was reached. Equilibrium was defined as a change in force of less than 0.2 g/min. The equilibrium modulus was obtained from the slope of the linear region of the stress-stain curve (10 – 20 % strain). Dynamic compression testing was conducted on the acellular and cellular scaffolds for 20 cycles at 20 % strain and 1 Hz. The average of the last 5 cycles was used to calculate the areas under the loading and un-loading curves. The average difference between the loading and unloading curves was presented as the hysteresis in percentage.

5.3.2.5 Fatigue Testing

Acellular co-continuous scaffolds (n = 6) were manufactured using the same ring mold (3.2 mm dia. x 3.5 mm height). After photo-cross-linking the scaffolds were loaded into a multi-well fatigue tester attached to a Bose Enduratec ELF3200 dynamic mechanical analyzer (DMA) (Figure A.10). A non-restrictive outer ring (height = 1 mm) was placed along the bottom of the wells to minimize sample movement during testing. Sample wells were filled with 1 X pH 7.4 PBS at room temperature. The upper platen lid was mounted to the DMA through a centre pin and set-screw and the gap was adjusted using a spacer of the same height as the samples. Once the gap was set the spacers were removed allowing the upper platen lid to be actuated freely against the fixed bottom well plate. Plastic wrap along the outer edges was used to prevent media evaporation from the wells. Samples were tested at 20 and 30 % amplitude for 100K, 500K and 1M cycles at 3 Hz frequency, with media topped up daily. Samples were weighed and dimensions

taken before and after each fatigue measurement. Samples were analyzed post-fatigue using the same mechanical testing protocols described above for equilibrium modulus and hysteresis.

5.3.3 Cellular Scaffold Characterization

5.3.3.1 Influence of UV Intensity and MGC Concentration on Cell Viability

Primary chondrocytes were isolated from the articular cartilage of bovine metacarpal-phalangeal joints, as described previously. [119] The isolated cells were suspended in a 6 % w/v MGC solution at a concentration of 4 x 10^7 cells/mL. The effect of UV intensity was then assessed on the cells in the MGC solution at intensities of 10, 50 and 250 mW/cm^2 for 60 s of exposure on both sides using a 2 leg quartz fibre light guide (3mm diameter). The encapsulated chondrocytes were cultured under static conditions for 24 h following UV exposure. Cell viability was also examined at 0 and 7 days for various 4, 6 and 8 % w/v MGC solutions with 4 x 10^7 cells/mL and cross-linked at 50 mW/cm^2 and 60 s. The MTT assay was used to measure metabolic activity of the chondrocytes under the various conditions. A standard curve of MTT absorbance as a function of cell number (100k, 400k, 700k and 1M cells) was also performed to determine the number of active cells after photo-cross-linking within the MGC hydrogels, which could then be converted to a % ratio of the number of cells originally seeded in the scaffolds. The number of cells initially seeded in the scaffolds was calculated based on the cell density and the volume of MGC hydrogel. The non-attached chondrocytes used to produce the standard curve were not exposed to UV and were incubated under the same conditions for the MTT assay. For the MTT assay, 10 μL of the MTT solution (5 mg/mL in 1 X PBS) was added per 100 μL of culture media (1 mL) surrounding the MGC hydrogels and incubated at 37 ˚C for 4 h. The hydrogels were removed from solution and crushed in 600 μL of DMSO or in the case of the standards the cells were spun down at 700 g's for 7 minutes and 95 % of the media was aspirated

before adding 600 μL of DMSO. The MTT solutions were removed and read at 540 nm (180 μL/well in a 96 well plate).

5.3.3.2 Long-Term Static Culture of Co-continuous Scaffolds

Primary chondrocytes were suspended in the MGC solution at a concentration of 4 x 10^7 cells/mL. Either 25 or 30 % w/w of this MGC/F12 culture media cell suspension was mixed into the 5446DLLACL or 7030TMCCL ASCP, respectively, as described earlier in the scaffold preparation section. The mixtures were loaded into the cylindrical molds (3.2 dia. x 3.5 mm height) and exposed to UV light as described above. The resulting scaffolds were removed from the mold, and cultured in medium supplemented with 10 % v/v FBS, 100 mg/mL ascorbic acid, 1 X antibiotic/antimycotic and in an incubator maintained at 37 ˚C with an atmosphere supplemented with 5 % CO_2 and 95 % relative humidity for up to 56 days with the medium changed every other day. Scaffolds were analyzed post-culture at 0, 7, 21, 35 and 56 days using the same mechanical testing protocols described above for equilibrium modulus and hysteresis.

5.3.3.3 Biochemical Assays (DNA, GAG and Collagen)

Assays for DNA, sulfated glycosaminoglycan (GAG) and collagen contents were performed on acellular and cellular scaffolds (n = 5 – 6) at days 0, 7, 21, 35 and 56. Prior to culture, the wet weights of the scaffolds were recorded. Upon harvest from culture, scaffolds were weighed again and stored at -85 ˚C until analyzed. The frozen samples were thawed, individually crushed, and digested by papain (80 mg /mL in 0.020 M ammonium acetate, 10^{-3} M ethylene diamine tetraacetic acid and 2 x 10^{-3} M dithiothreitol all in type-1 water) for 3 days at 65 ˚C. The supernatant was collected and stored at -20 ˚C until required. DNA content was measured using the Hoechst 33258 dye-binding assay. [134] In addition, the DNA content for a number of chondrocytes (100k, 400k, 700k and 1M) was determined and used to calculate an average DNA

(mass) per chondrocyte, which could then be used to approximate the number of cells in the initial co-continuous scaffolds after photo-cross-linking. Sulfated GAG content in the papain digest was measured using the dimethylmethylene blue (DMMB) absorbance assay. [135] Collagen content was determined from a hydroxyproline (OH-pro) assay under the assumption that OH-pro accounted for 10 % of the total collagen mass. [136] OH-pro was measured using a chloramine T and Ehrlich's reagent assay after hydrolysis in 6 N HCl at 110 ˚C for 18 h. [178]

To determine the amount of GAG that was bound to the MGC hydrogel during culture, a GAG complexation assay was conducted as previously described. [119] Acellular MGC (8 % w/v in F12) hydrogel samples were soaked in 10 % FBS/F12 culture media for 24 h at 4 ˚C to account for any competitive protein binding that may have occurred. After aspiration of the culture media, MGC hydrogel samples were incubated in 100 μL of various chondroitin sulfate standards ranging from 10 to 1600 mg/mL for 24 h at 4 ˚C. A DMMB absorbance assay was conducted on the supernatant to analyze the amount of free GAG (n = 3). The maximum GAG complexation limit, calculated on a per mass basis of MGC hydrogel sample was determined from the intersection point for complete GAG complexation (zero slope) and incomplete GAG complexation (increasing slope). Due to the unknown amount of GAG complexation in the actual cellular co-continuous scaffolds only time points from the GAG assay that were significantly greater than the baseline values (time 0 scaffolds) were adjusted and presented in the results section.

5.3.3.4 Histology and Immunohistochemistry

The two-phase morphology made conventional paraffin embedding and sectioning of the scaffolds difficult. Therefore, scaffolds were first fixed in 4 % w/v paraformaldehyde for 24 h. Fixed samples of the cellular scaffolds from days 0, 7, 21, 35 and 56 were cut by hand to ~ 500 μm using a single sided razor blade. Free-floating sections of the co-continuous scaffolds were

stained with safranin-O for sulfated GAG within the MGC hydrogel phase. A 0.01 % aqueous solution of safranin-O was used to stain the sections for 5 min. Samples were rinsed in reverse osmosis water 3 times for 5 min each. The wet sections were then imaged with a Zeiss Discovery V12 stereomicroscope equipped with an AxioCam ICc1 camera and CL1500 bi-axial light source.

To identify load-bearing soft tissue-specific proteins, sections of the co-continuous scaffold were immunostained with antibodies for collagen type I, collagen type II and aggrecan. All staining was performed on the free-floating sections within 1.5 mL eppendorf tubes using 100 μL of solution for each step. Collagen type I antibody (Rabbit anti-bovine, BD-T40113R) was used at a 1:100 dilution. Collagen type II (II-II6B3) and aggrecan (1C6s) primary antibodies were used at a lower dilution of 1:10 due to the lower concentration of antibody in the bioreactor supernatant. The sections were first removed from the 70 % v/v ethanol and soaked in water for 2 rinses, 5 min each. For the aggrecan antibody the samples were pre-treated with a 10 mM dithiothreitol reducing solution for 2 h at 37 ˚C, 40mM iodoacetamide alkylating solution for 1 h at 37 ˚C, and 0.25 U/mL chondroitinase ABC antigen retrieval solution for 1 h at 37 ˚C. For the collagen antibodies the sections were pre-treated for 30 min at 37 ˚C with a 0.05 % trypsin solution for antigen retrieval. All sections were then blocked for 30 min with their respective host sera of the secondary antibody, 1.5 % v/v horse serum (S-2000, Vector Labs, Burlington, Ontario) for collagen type II and aggrecan and 1.5 % v/v goat serum (S-1000, Vector Labs) for collagen type I. Next, the sections were rinsed with 1X PBS and the appropriate primary antibodies were added for overnight incubation in a humid chamber at 4 ˚C. The following day the required Texas red conjugated secondary antibodies were added at 1:100 dilution in a 2 % w/v BSA solution for 2 h. Goat anti-rabbit secondary antibody (TI-1000, Vector Labs) was used for collagen type I and horse anti-mouse secondary antibody (TI-2000, Vector Labs) was used for both collagen type II and aggrecan. In between all steps the sections were rinsed with 1X PBS.

Negative controls were prepared by substituting the primary antibody with additional blocking using the appropriate host sera. Acellular controls were run in parallel using both primary and secondary antibodies to determine non-specific staining due to the polymers. After staining, sections were submerged in Vectashield® mounting media containing DAPI (H-1200, Vector Labs). The sections were analyzed on a Zeiss Imager M1 fluorescent microscope equipped with an AxioCam Mrm camera and Axiovision Rel. 4.7 software.

5.3.4 Statistical Analyses

All results are expressed as the mean ± the standard error of the mean (SEM) and analyzed using statistical software (SigmaStat 1.0, SPSS Science, Chicago, IL). Physical, biochemical, and mechanical characterization results as a function of time were analyzed using a one-way ANOVA and the Fisher's LSD post-hoc test. Paired t-tests (95 % confidence interval) were also conducted between cellular and acellular scaffolds during long-term culture and between the 5446DLLACL and 7030TMCCL cellular scaffolds for biochemistry results. Significance was assigned at p values of less than 0.05.

5.4 Results

5.4.1 Polymer Properties

The composition and physical properties of the acrylate star-copolymers (ASCP) used in this study are listed in Table 5.1. For each ASCP, the final monomer composition was very close to the feed monomer composition used in synthesizing the star-copolymer, and the degree of acrylation were greater than 75 %. The number average molecular weights (M_n) calculated from ^{1}H NMR spectra analysis for each ASCP were roughly consistent, ranging from 8 – 11 kg/mol. The M_n values for the ASCP were higher than the targeted value of 8 kg/mol, due to loss of low

molecular weight fractions during polymer purification. All the ASCP had low glass transition temperatures, ensuring that the elastomer phase formed after their cross-linking would be rubbery at physiologic temperature. The *N*-methacrylate glycol chitosan (MGC) had a degree of methacrylate substitution of 4 %.

Table 5.1: ASCP properties from NMR and DSC analysis

Polymer	Monomer Feed ratio (molar)	Actual Monomer Ratio (molar)	T_g (˚C)	Degree of Functionalization (%)	M_n (kg/mol) [Targeted M_n]
5446DLLACL	50:50	54:46	-18	81	10.9 [8]
7030TMCCL	75:25	70:30	-37	76	8.4 [8]
5149TMCCL	50:50	51:49	-50	82	10.5 [8]
2377TMCCL	25:75	23:77	-61	81	8.8 [8]

5.4.2 Scaffold Composition

5.4.2.1 Optimization of Co-continuous Morphology with Star-Poly(ε-Caprolactone-co-D,L-Lactide) Triacrylate

To better understand the role of the MGC solution in forming the co-continuous morphology in the scaffold, the zero shear rate viscosity of a variety of MGC concentrations (4, 6, 7, 8 and 10 % w/v MGC in F12 culture media) were measured (Figure 5.1 (A)). Increasing the solution weight percentage of MGC increased the solution viscosity, as was expected. The influence of the MGC solution concentration, and thus viscosity, on the mechanical properties of co-continuous scaffolds prepared with star-poly(ε-caprolactone-co-D,L-lactide) triacrylate using a constant MGC solution content of 25% w/w are shown in Figure 5.1 (B). The co-continuous scaffolds were mechanically tested at 1 %/s strain rates until failure or the limits of the load cell were reached. The 1 %/s loading curves demonstrated higher stress values for the co-continuous scaffolds when compared to the hydrogel-only scaffolds. The hydrogel-only scaffolds began to show signs of failure between strains of 35 – 40%, which were observed in the loading curves as

a sudden drop in stress. From the loading curves there appeared to be a region of co-continuous morphologies for scaffolds prepared with 6 – 8 % w/v MGC (viscosities of 3 – 11 Pa·s) that did not show significant signs of failure before 40 % strain and reached maximum stress levels of approximately 1 MPa. The co-continuous scaffolds prepared with 4 % w/v (1 Pa·s) and 10 % w/v (50 Pa·s) MGC solutions demonstrated noticeable signs of failure before 30 % strain but higher stress values than the hydrogel alone scaffolds.

To visualize the hydrogel phase it was stained with trypan blue (Figure 5.1 (C – G)). The lower 1 Pa·s MGC solution was not incorporated evenly throughout the 5446DLLACL elastomer as seen in the post failure test images (Figure 5.1 (C)). Increases of 1 % w/v MGC between 6 – 8 % (3 – 11 Pa·s) exhibited much finer and well-distributed MGC networks as the MGC solution viscosity increased (Figure 5.1 (D – E)). The highest viscosity (50 Pa·s) MGC solution resulted in the most dispersed MGC morphology, which displayed signs of possible phase inversion (Figure 5.1 (G)). Moreover, the higher viscosity MGC solutions (11 and 50 Pa·s) exhibited signs of failure in the post-tested images as marked by the red arrows in Figure 5.1 (F and G).

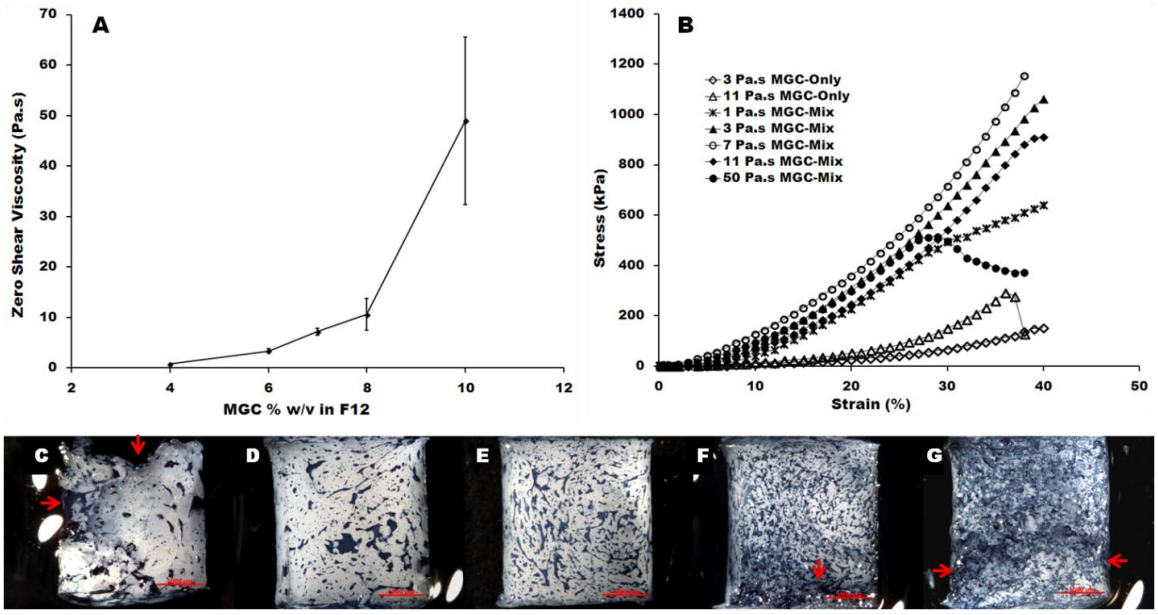

Figure 5.1: (A) Zero shear rate viscosity measurements with increasing MGC solution concentration (B) Effect of MGC solution viscosity on failure properties of DLLA:CL ASCP scaffolds all at 25 % w/w solution loading. (C-G) Images of 25 % w/w loaded scaffolds for 1, 3, 7, 11 and 50 Pa·s MGC solutions stained with trypan blue, respectively. Arrows (red) to indicate factures in scaffolds. 1000 μm scale bar.

5.4.2.2 Optimization of Co-continuous Morphology with Star-Poly(ε-Caprolactone-co-Trimethylene Carbonate) Triacrylate

Star-poly(trimethylene carbonate-co-ε-caprolactone) triacrylate with different TMC:CL molar ratios were investigated for producing co-continuous scaffold morphologies with a constant 25 % MGC loading (Figure 5.2 (A – D)). The objective was to achieve a similar co-continuous morphology in the cross-linked scaffold as obtained with the star-poly(ε-caprolactone-co-D,L-lactide) triacrylate (5446DLLACL ASCP).

The star-poly(trimethylene carbonate-co-ε-caprolactone) triacrylate which best approximated the consistency of the 5446DLLACL ASCP was composed of 70 mol% trimethylene carbonate (7030TMCCL). However, to form a co-continuous-like morphology with

this prepolymer, a higher MGC solution viscosity (8 % w/v) was required (Figure 5.2 (D)). Nevertheless, 20 h dye diffusion analyses revealed that the 25 % loading of the 8 % w/v MGC solution was not sufficient to form an interconnected MGC network (Figure 5.2 (E)). Alternatively, scaffolds formed with 30 and 35 % of the 8 %w/v MGC solution had complete dye diffusion to the scaffold centre after 20 h (Figure 5.2 (F and G), respectively). The increased MGC gel content in the scaffold also resulted in a reduction of scaffold modulus from 1476 to 972 kPa for MGC gel contents of 25 to 35 % w/w, respectively.

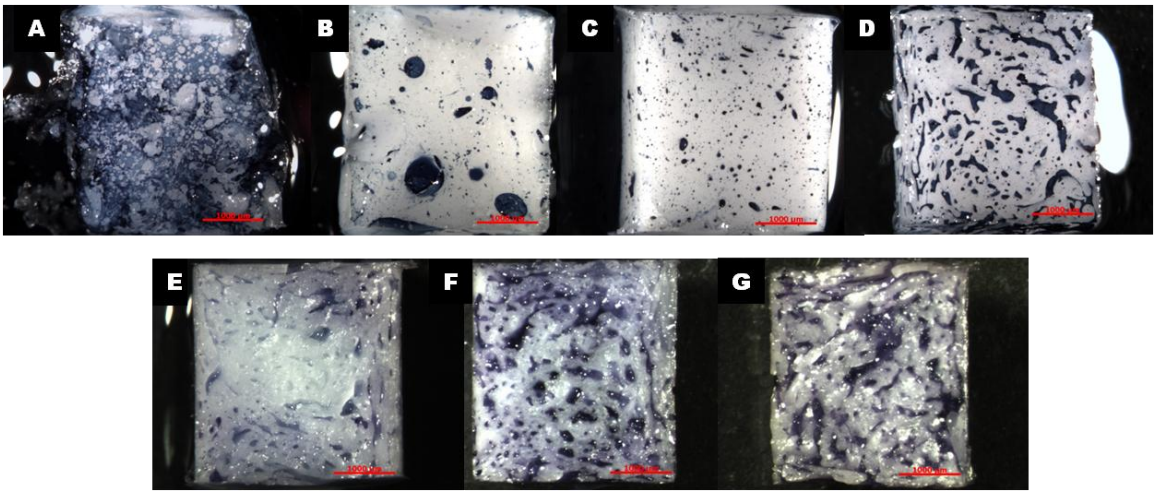

Figure 5.2: Effect of MGC loading and solution concentration on co-continuous morphology in the TMC:CL ASCP scaffolds. Scaffolds stained with trypan blue made using a 25 % w/w loading of a 6 % w/v MGC solution with different TMC:CL monomer ratios: (A) 23:77, (B) 51:49 and (C) 70:30. (D) Scaffold stained with trypan blue with a 25 % w/w loading of a 8 % w/v MGC solution in the 70:30 TMC:CL ASCP (modulus = 1472 kPa). (E-G) Different loadings of an 8 % w/v MGC solution in the 70:30 TMC:CL ASCP after 20 h dye diffusion in toluidine blue 1% solution to determine interconnected MGC network. (E) 25 % w/v MGC loading (modulus = 1476 kPa), (F) 30 % w/v MGC loading (modulus = 1168 kPa) and (G) 35 % w/v MGC loading (modulus = 972 kPa). Scale bar 1000 μm.

Two formulations were chosen for additional assessment: (i) a mixture of 25 % w/w of a 6 % w/v MGC solution in the 5446DLLACL ASCP (5446DLLACL), and (ii) a mixture of 30 % w/w of an 8 % w/v MGC solution in the 7030TMCCL ASCP (7030TMCCL). The porosity (volume) for both scaffolds was approximately 32 %, as calculated based on the difference in wet and dry mass of the co-continuous scaffolds and assuming densities of 1 g/mL for the MGC solutions and 1.26 g/mL [179] for the elastomers. These compositions yielded hydrogel-elastomer scaffolds displaying superior mechanical properties (moduli of 1580 ± 54 and 1156 ± 57 kPa, for 5446DLLACL and 7030TMCCL, respectively) over the hydrogels alone (moduli of 105 ± 4 and 181 ± 10 kPa for hydrogels prepared with 6 and 8 % w/v MGC solutions, respectively) while possessing a co-continuous morphology. Sol content measurements also confirmed that the individual hydrogel and elastomer components possessed a low water extractable component (2.3 ± 1.1 and 7.8 ± 2.3 % w/w sol, respectively).

5.4.3 Rheology and Injectability Assessment of the Two-Phase Scaffold Mixtures

To test the injectability of the MGC solution-in-ASCP mixtures, rheological measurements were performed. The 5446DLLACL and 7030TMCCL mixtures before cross-linking did not show any significant difference between their zero shear rate viscosities (908 ± 224 and 1027 ± 46 Pa.s, respectively). The injection profiles of the mixtures (Figure 5.3) indicated an initial linear increase in injection force until the mixture started to flow from the needle tip after which a constant pressure (maximum injection force) was attained.

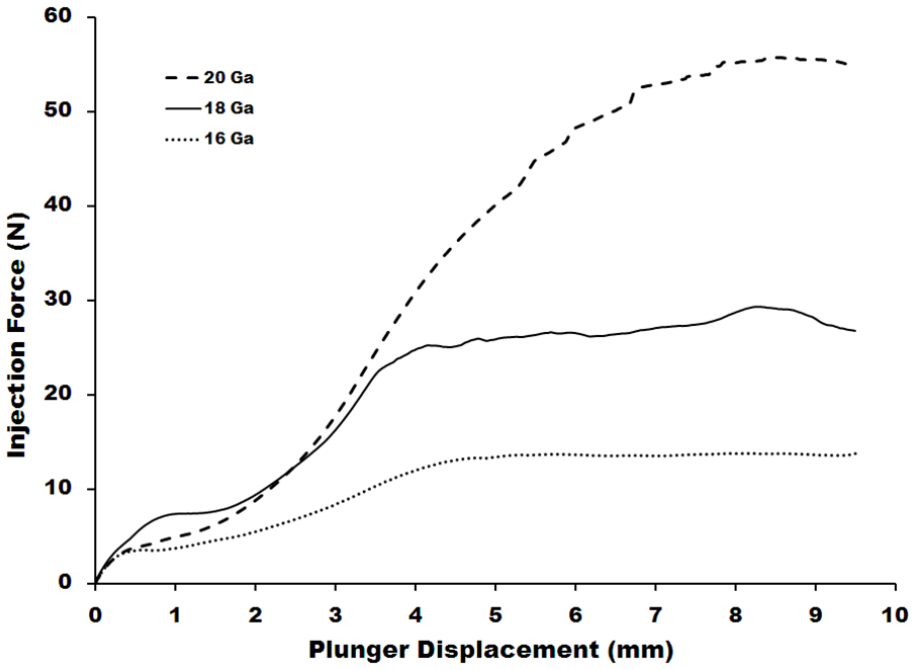

Figure 5.3: Typical injection force versus plunger displacement profile for 5446DLLACL mixtures through a 20, 18 and 16 Ga, 3.8 cm long needle. Mixture ejection from the needle tip occurred slightly before the maximum force was reached (plateau region), after which a steady mixture ejection rate was observed until finished.

Three different needle tips of 20, 18 and 16 Ga (0.584, 0.838 and 1.194 mm I.D.) all 3.8 cm in length were used to determine the influence of needle internal diameter on injection force (Figure 5.4). For the smallest diameter (20 Ga needle), the 5446DLLACL and 7030TMCCL mixtures had injection forces of 56.2 ± 2.1 N and 54.5 ± 0.03 N, respectively. In comparison, the force of injection for the larger (16 Ga) needles dropped to 13.2 ± 0.6 and 16.7 ± 1.1 N. No significant differences were observed between the 5446DLLACL and 7030TMCCL mixtures, in terms of zero shear viscosity and maximum injection force (Figure 5.4 (A)). Images of the post-injected and photo-cross-linked scaffolds for both of the mixtures also did not show any noticeable differences due to injection or needle size on the co-continuous morphologies (Figure 5.4 (B – E)). The ratio of pressure with respect to the needle diameters for both mixtures

calculated using the Poiseuille equation showed good agreement with the experimental results (Table 5.2).

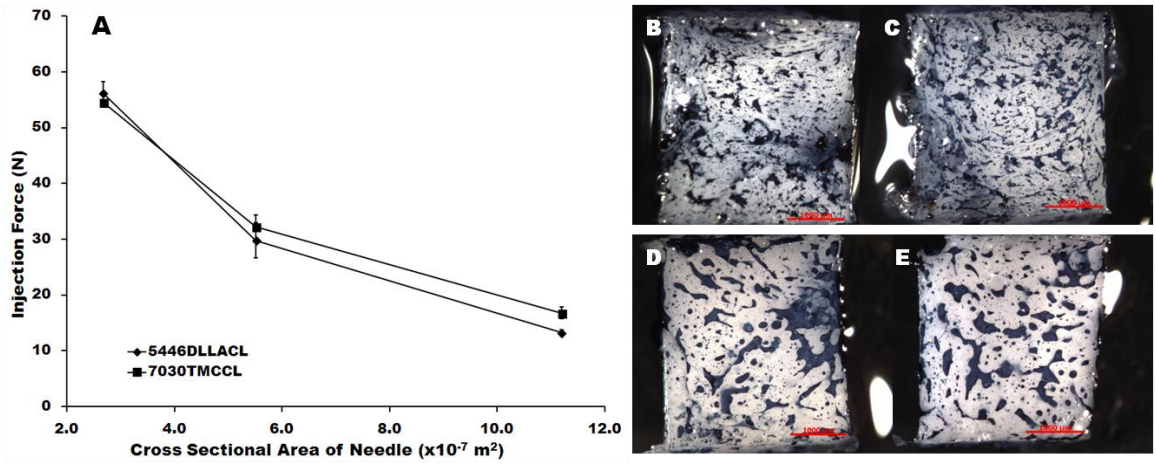

Figure 5.4: (A) Comparison of maximum injection force with various needle diameters for 5446DLLACL and 7030TMCCL mixtures. (B-E) Post-injection and photo-cross-linking morphology of scaffolds stained with trypan blue to highlight the MGC phase: (B) 5446DLLACL with 20 Ga needle, (C) 5446DLLACL with 16 Ga needle, (D) 7030TMCCL with 20 Ga needle, (E) 7030TMCCL with 16 Ga needle. Scale bar 1000 μm.

Table 5.2: Change in injection pressure with change in needle diameter for 5446DLLACL and 7030TMCCL mixtures.

	Pressure Ratio		
Needle Gauge Ratio	Poiseuille's Equation Prediction	Experimental DLLACL Values	Experimental TMCCL Values
18/16	4.1	4.6 ± 0.5	3.9 ± 0.4
20/18	4.3	3.9 ± 0.4	3.5 ± 0.2
20/16	17.5	17.8 ± 1.0	13.6 ± 0.9

5.4.4 Assessment of Diffusive Transport within the Interconnected Gel Phase

To ensure the co-continuous scaffolds were fully interconnected in the hydrogel phase, a time course study of diffusion of a water-soluble, blue dye from the scaffold surface to the

interior was conducted to visually assess the rate of diffusive transport into the centre of the 5446DLLACL and 7030TMCCL scaffolds (Figure 5.5). At the earlier time points (Figure 5.5 (A and E)) the dye had not had sufficient time to penetrate past the outer edges, which was indicated by the white centre area visible in the images. With time, the major dye front penetrated further into the centre of the scaffolds and complete penetration was achieved between 3 to 6 hours (Figure 5.5 (D and H)). The elastomeric phase of the 5446DLLACL scaffolds (Figure 5.5 (A – D)) appeared to possess microporosity as the dye front moved evenly throughout the entire scaffold (elastomer and hydrogel). In contrast, in the 7030TMCCL scaffolds, dye diffusion was limited to the MGC only phase (Figure 5.5 (E – I)) with minimal diffusion within the elastomer phase, which remained white in appearance. Diffusion times between 3 – 6 hours were required for the dye to reach the centre for both scaffold formulations.

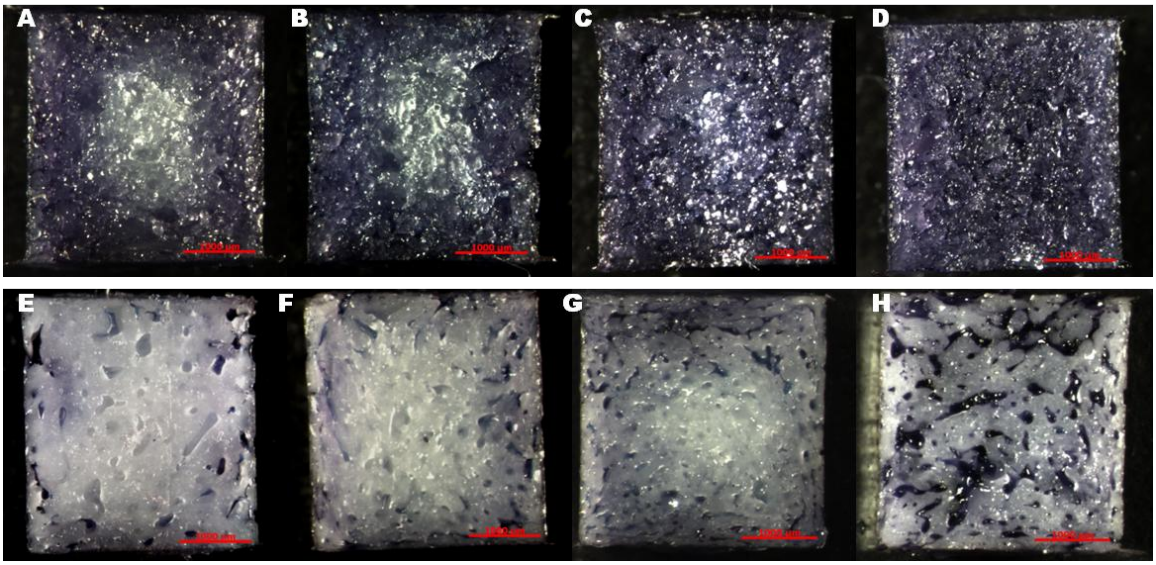

Figure 5.5: (A-D) The cut face of 5446DLLACL scaffolds after removal from toluidine dye solution at 0.5, 1, 3 and 6 h respectively. (E-H) The cut face of 7030TMCCL scaffolds after removal from toluidine dye solution at 0.5, 1, 3 and 6 h, respectively. Scale bar 1000 μm.

5.4.5 Physical Characterization of Acellular Scaffolds Post-Fatigue

The effect of high strain and cycle numbers on the mechanical properties of the scaffolds was investigated to ensure they could endure dynamic loading conditions and still retain the majority of their mechanical integrity (Figure 5.6). The initial modulus values for the 5446DLLACL scaffolds (1580 ± 54 kPa) were slightly higher than the 7030TMCCL scaffolds (1156 ± 57 kPa) (Figure 5.6 (A)). Initial hysteresis values were 9.8 ± 0.5 and 11.0 ± 0.5 %, respectively. Fatigue testing at 20 % strain amplitude had no significant effect on the initial modulus or hysteresis for both the 5446DLLACL and 7030TMCCL scaffolds, regardless of the number of cycles (Figure 5.6 (B)). After 1 x 10^6 cycles at 20 % strain amplitude, the 5446DLLACL scaffolds displayed an 11 % decrease in modulus and 26 % increase in hysteresis compared to a 3 % decrease in modulus and 13 % decrease in the hysteresis for the 7030TMCCL scaffolds. The largest change in mechanical properties between the two scaffolds was seen in the 5446DLLACL scaffolds after 1 x 10^6 cycles at 30 % strain amplitude with a 58 % decrease in modulus ($p < 0.05$) and a 221 % increase in hysteresis ($p < 0.05$). Although significant, the 7030TMCCL scaffolds displayed a small decrease of 17 % in equilibrium modulus and 14 % increase in hysteresis after the same 30 % strain amplitude and 1 x 10^6 cycles. No differences were detected between the different cycle numbers for each condition tested for either the equilibrium modulus or hysteresis data. In terms of the physical properties, only a change in volume for the 7030TMCCL scaffolds at 20 % amplitude and 1 x 10^5 cycles showed a significant difference from the other cycle numbers. No other changes in mass or volume were observed in the acellular scaffolds with respect to amplitude or cycle number (Table A.1).

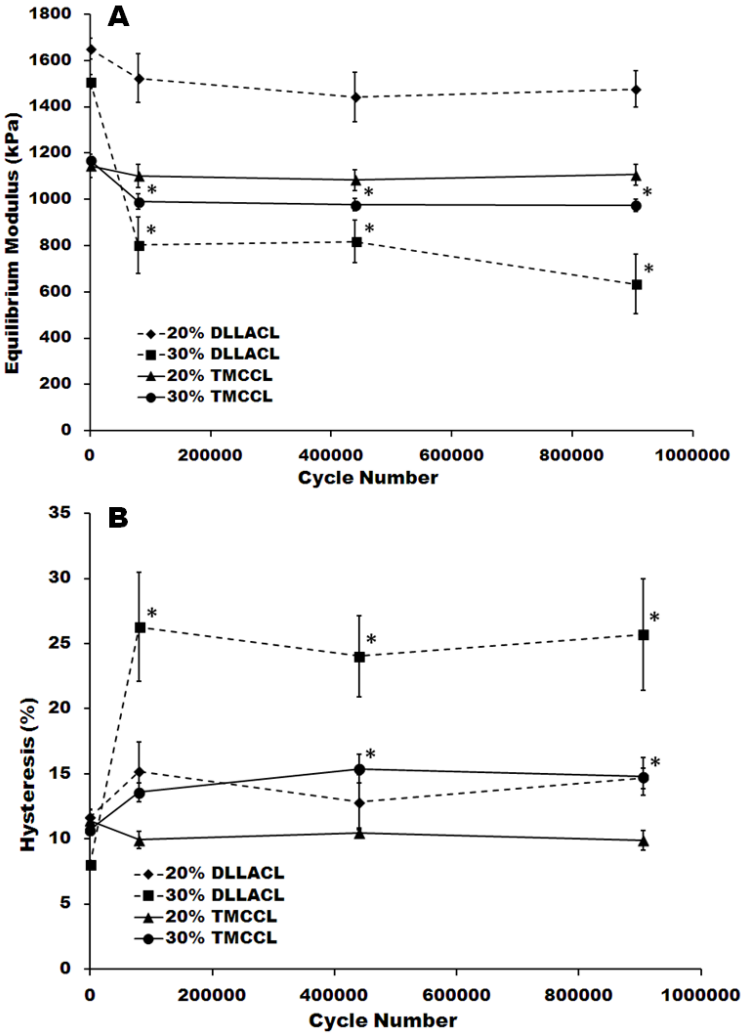

Figure 5.6: (A) Equilibrium modulus and (B) Hysteresis values for 5446DLLACL and 7030TMCCL scaffolds pre- and post-fatigue. Samples were fatigued at 3Hz in 1X pH 7.4 PBS at room temperature at either 20 or 30 % amplitude. (*) Significant from pre-fatigue values ($p < 0.05$).

5.4.6 Influence of Photo-Cross-Linking on Scaffold Cellularity

Due to the opaque nature of the two-phase mixtures, higher UV intensities (50 mW/cm^2) were required to obtain a uniformly cross-linked scaffold, as compared to the hydrogel alone scaffolds, which only required 10 mW/cm^2 to be fully cross-linked. Cellularity was reported as

the ratio of post UV cellular activity to the initial cell seeding density with respect to UV intensity and MGC concentration in the F12 medium for the encapsulated chondrocytes (Figure 5.7). A significant decrease in cellularity was only observed when an intensity of 250 mW/cm^2 was used to crosslink the 6 % w/v MGC hydrogel (Figure 5.7 (A)). The initial cellularities of the chondrocytes encapsulated at 50 mW/cm^2 within the 4, 6 and 8 % w/v MGC hydrogels were 65.1 ± 2.1, 72.2 ± 8.5 and 60.2 ± 8.9 %, respectively. The chondrocytes were able to increase their metabolic activity similarly by a factor of 2.5 over the 7 day culture period (Figure 5.7 (B)). Based on these results, all other studies were done with co-continuous scaffolds cross-linked at 50 mW/cm^2 for 60 s.

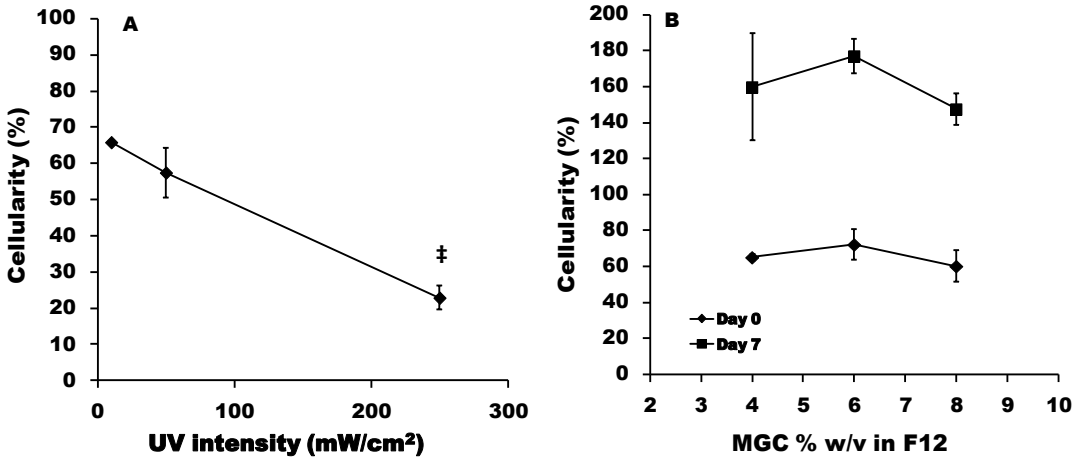

Figure 5.7: (A) Effect of UV intensity on cellularity 24 h following chondrocyte photo-encapsulation in hydrogels prepared with 6 % w/v MGC dissolved in F12. (‡) Significant from all other values ($p < 0.05$). B) Effect of MGC solution concentration on chondrocyte viability following photo-encapsulation at 50 mW/cm^2 UV intensity for 60 s after 1 and 7 days in culture. Viability was measured via the MTT assay.

5.4.7 Distribution of Chondrocytes in the Co-continuous Scaffolds During 2 Months Static Culture

Cells within the 5446DLLACL scaffolds initially appeared well distributed in the centre of the scaffolds; however a general loss of cells was observed over the culture period (Figure 5.8 (A – D)). The 7030TMCCL scaffolds also initially displayed cells distributed throughout the scaffolds, but did not show any observable signs of decrease in cell number with culture time (Figure 5.8 (E – H)).

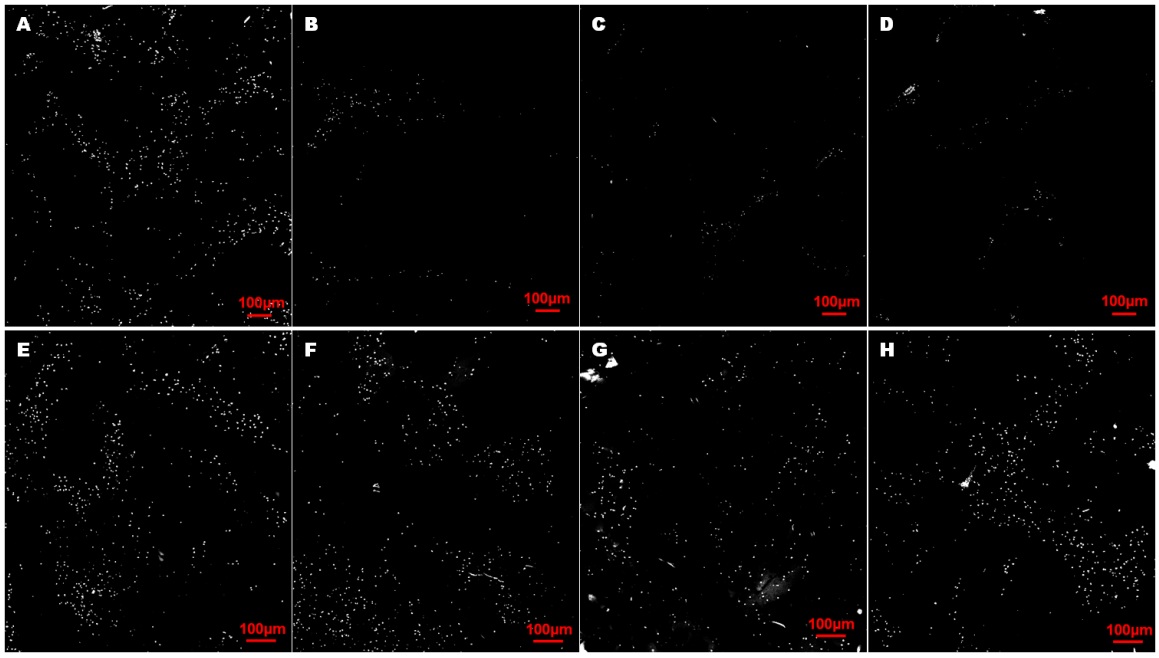

Figure 5.8: DAPI staining in 5446DLLACL scaffolds for days 7 (A), 21 (B), 35 (C) and 56 (D) and for 7030TMCCL scaffolds for days 7 (E), 21 (F), 35 (G) and 56 (H).

5.4.8 Biochemistry of Co-continuous Scaffolds During 2 Months Static Culture

The DNA content in the day 0, 7030TMCCL scaffolds, after photo-cross-linking was compared to the amount of cells initially seeded in the scaffolds. Based on an average of 5.6 ± 0.1

pg DNA/chondrocyte (Table A.2), we could account for 98% of the originally encapsulated cells after manufacture of the co-continuous scaffolds.

The long-term culture scaffolds were also analyzed for DNA, GAG and collagen accumulation (Figure 5.9 (A – C)). The maximum complexation limit of GAG to MGC occurred at a level of 1.14 μg GAG/mg MGC hydrogel. Therefore, only the GAG assay results that were significantly different from the day 0 time point were adjusted and plotted in Figure 5.9 (B). The cellular 7030TMCCL scaffolds demonstrated significant increases in DNA, GAG and collagen contents at day 56 (3.1 ± 0.1, 20.1 ± 1 and 35.5 ± 1.8 μg, respectively) compared to day 0. In contrast, at day 56, the 5446DLLACL cellular scaffolds displayed a significant decrease in DNA content (1.3 ± 0.1 μg), a small increase in GAG content (13.2 ± 0.6 μg), and no observable changes in collagen content (6.2 ± 3.4 μg).

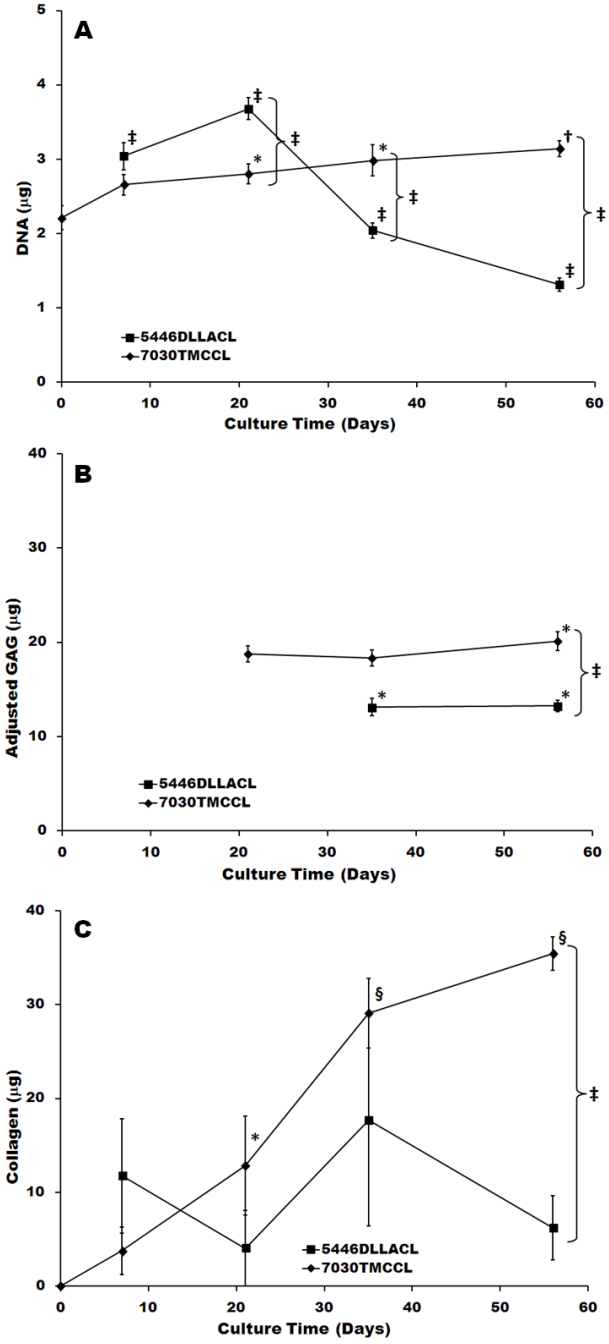

Figure 5.9: Biochemistry results for cellular 5446DLLACL and 7030TMCCL scaffolds for (A) DNA, (B) GAG and (C) collagen up to 56 days in static culture. Note that only the GAG values that were significantly greater than zero were adjusted to account for possible non-assayable GAG due to its complexation with MGC. (*) Significantly different from day 1 values, (‡) significantly different from all values, (†) significant difference between day 1 and 7, values (§) significant difference between day 1, 7, and 21 values ($p < 0.05$).

5.4.9 GAG Distribution in Co-continuous Scaffolds During 2 Months Static Culture

Safranin-O histology staining was performed on the 5446DLLACL and 7030TMCCL scaffolds to visualize the GAG accumulating within the MGC phase (Figure 5.10). Over time in the static culture, it appeared that GAGs were accumulating at the hydrogel/elastomer interface in the 5446DLLACL scaffolds (Figure 5.10 (A – C)). This accumulation pattern was much different within the 7030TMCCL scaffolds, which showed an even distribution of GAG staining throughout the MGC phase (Figure 5.10 (D – F)).

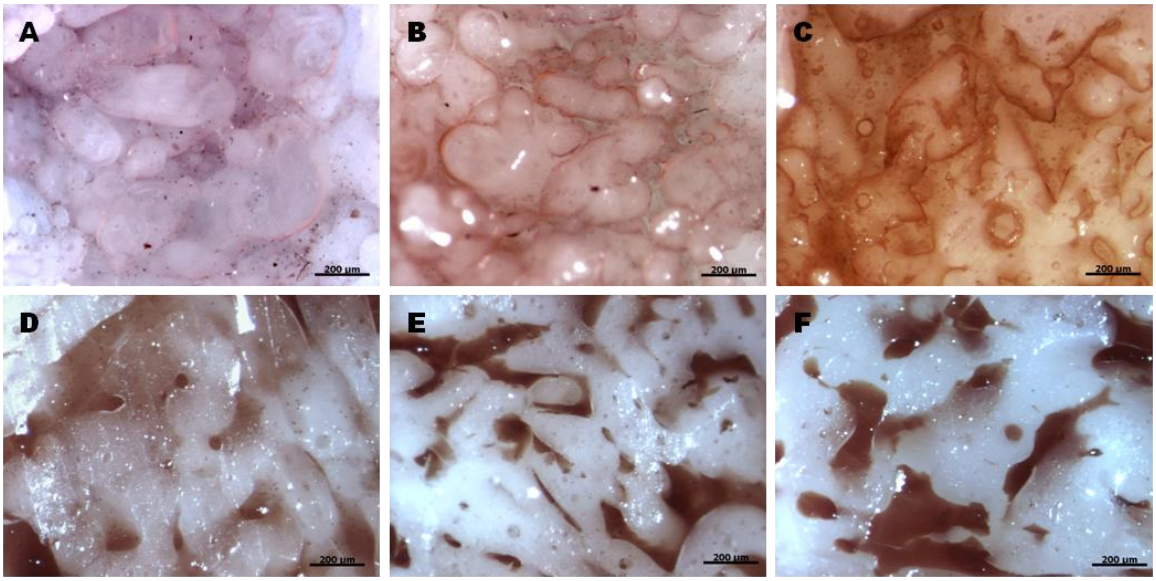

Figure 5.10: Safranin-O staining for GAGs of the 5446DLLACL scaffolds at day 7 (A), day 35 (B), and day 56 (C) and of the 7030TMCCL scaffolds at day 7 (D), day 35 (E) and day 56 (F). Differences in the safranin-O color were seen between the two scaffolds due to a higher background staining in the 5446DLLACL elastomer phase, which made white balancing difficult.

5.4.10 Mechanical Properties of Co-continuous Scaffolds During 2 Months Static Culture

Cellular and acellular scaffolds prepared from both 5446DLLACL and 7030TMCCL formulations were cultured for up to 56 days. Periodically harvested scaffolds were analyzed for changes in mass, volume, and mechanical properties. The 5446DLLACL scaffolds had initially high equilibrium modulus (1369 ± 45 kPa), but after 56 days in culture, the average modulus decreased to 439 ± 15 kPa (Figure 5.11 (A)). A 117 % increase in hysteresis was also observed after 56 days in culture from the initial values for the 5446DLLACL scaffolds (Figure 5.11 (B)). The modulus and hysteresis of the 7030TMCCL cellular scaffolds remained relatively constant for the entire 56 day culture period (Figure 5.11 (C and D), respectively). For the acellular scaffolds, the overall trends in modulus and hysteresis were similar to that of the cellular scaffolds. The physical properties of the scaffolds (mass and volume) were relatively unchanged until later times in culture. After 56 days, the 5446DLLACL scaffolds (cellular and acellular) exhibited 8 – 10 % increases in mass and volume ($p < 0.05$), whereas the 7030TMCCL scaffolds (cellular and acellular) exhibited relatively minor changes in mass or volume (± 2 %) (Table A.3).

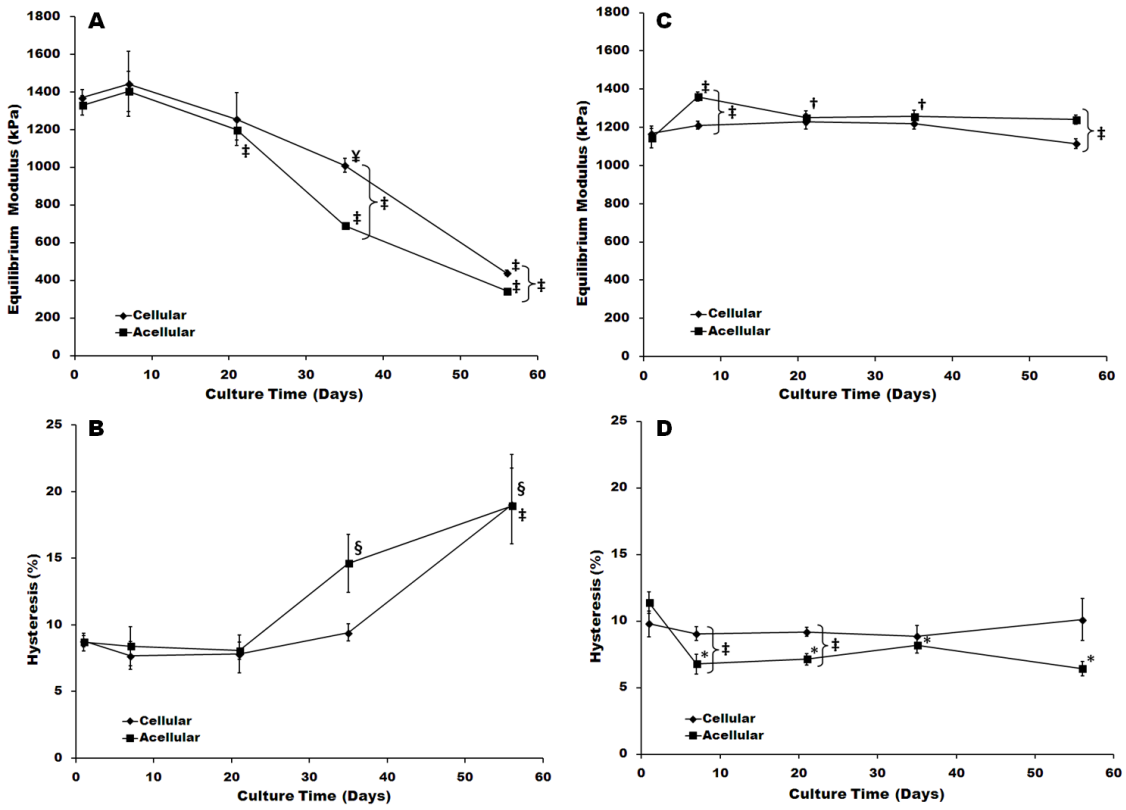

Figure 5.11: Long-term culture of cellular and acellular 5446DLLACL and 7030TMCCL scaffolds. (A) Equilibrium modulus data and (B) Hysteresis data for 5446DLLACL pre- and post-culture. (C) Equilibrium modulus data and (D) Hysteresis data for 7030TMCCL scaffolds pre- and post- culture. (*) Significant from day 1, (¥) significant from all values except day 21, (‡) significant from all values, (†) significant from days 1 and 7, (§) significant from days 1, 7, 21 ($p < 0.05$).

5.4.11 Immunohistochemistry of 7030TMCCL Scaffolds During 2 Months Static Culture

Due to the large drop in mechanical properties seen with the 5446DLLACL scaffolds no further characterization was conducted with these scaffolds. Additional immunohistochemistry (IHC) staining of the 7030TMCCL scaffolds was completed to visualize more specific markers characteristic of cartilaginous tissues, such as collagen II and aggrecan. IHC staining showed only a slight increase in staining for the negative cartilaginous marker, collagen I, over the entire 56

day culture period (Figure 5.12 (A – C)). By contrast, there was an increase in the presence of both positive markers, collagen type II and aggrecan, within the MGC phase, beginning in day 35 (Figure 5.12 (E) – collagen type II and Figure 5.12 (H) – aggrecan) and continuing to day 56 (Figure 5.12 (F) – collagen type II and Figure 5.12 (I) – aggrecan).

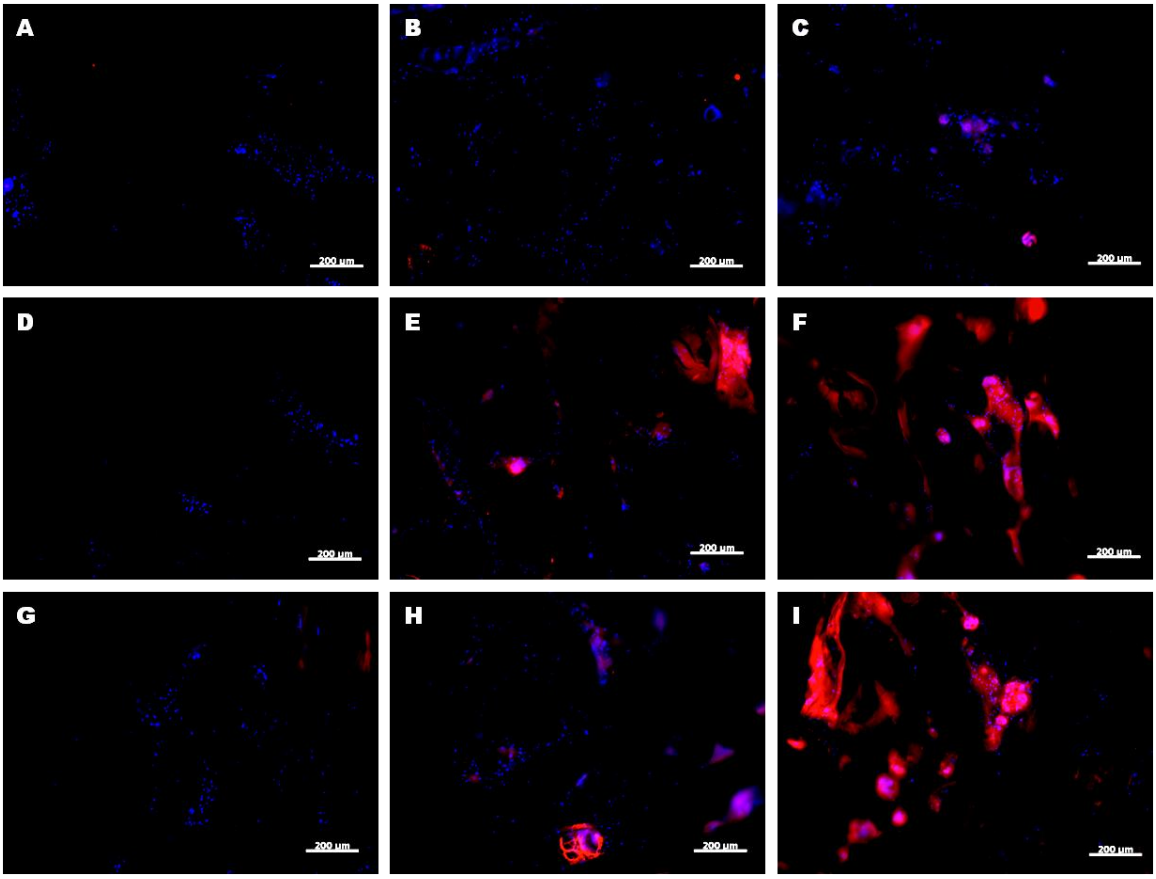

Figure 5.12: Immunohistochemistry staining (red) for collagen type I (A-C), collagen type II (D-F) and aggrecan (G-I) within the 7030TMCCL scaffolds at days 7 (A, D, G), 35 (B, E, H) and 56 (C, F, I). Counterstaining was done with DAPI (blue); the scale bar represents 200 µm.

5.5 Discussion

Both scaffold mixtures could be injected with reasonable force and without adverse effect to their final co-continuous morphology. The highest injection force (~ 60 N) was manageable by hand and is deemed acceptable as reported in other studies. [177, 180] The flow properties of the scaffold mixture allows it to be injected, conform to the geometry of the defect space and be formed *in situ*, making it potentially useful as a minimally invasive repair technique.

The injectable scaffolds had a high equilibrium modulus (1 – 2 MPa) and a fully interconnected hydrogel phase as indicated from the dye diffusion tests. The co-continuous scaffolds are suitable for load bearing soft tissue replacement where physiological loading and strain amplitudes can be high and thereby require a replacement scaffold with high modulus. For example, modulus values for cartilage are in the higher range of load bearing soft tissues at around 0.45 – 0.9 MPa. [181] Nucleus pulposus tissue on the other hand has been reported to have a confined compressive modulus of 0.31 ± 0.04 MPa. [42] In this study, the co-continuous scaffolds were tested in an unconfined state since it is possible to have limited support from the annulus in a degenerative disc repair scenario [182] and therefore any scaffold used in this application will likely require higher modulus values than healthy native tissue alone can provide. Previous studies by Peng *et al*. produced similar photo-cross-linked two-phase scaffolds from methacrylated gelatin hydrogel and a HydroThane™ elastomer, but with much lower modulus values (< 100 kPa). [117] Moreover, their scaffolds were initially freeze-dried and then rehydrated before testing, which may have altered their overall structure. In another study, Gerecht *et al*. formed a porous cell encapsulating elastomer using a 3-armed poly(glycerol-co-sebacate)-acrylate polymer mixed with 35 % w/v glycerol. [99] This elastomer, however, had a relatively low compressive modulus value of 80.2 ± 28 kPa and a low porosity of about 18 %, making it of limited utility for effective cell encapsulation for a load bearing application.

Fatigue properties of the photo-cross-linked co-continuous scaffolds were examined as the scaffolds should be able to withstand physiological loading regimens without significant signs of degradation in mechanical properties. [183-185] Physiological loadings for LBSTs have been reported at 15 – 20 % strain [175] and we investigated the co-continuous scaffolds at 20 and 30 % strain to ensure the effects on mechanical properties were well within the physiological range, but also below the strain limits of the hydrogel alone (~ 40% strain). A slightly higher than physiological (< 1 Hz), [13] loading frequency of 3 Hz was used to accommodate shorter testing times to ensure scaffold degradation had a minimal effect on the fatigue data. The largest change in modulus and hysteresis was seen in both scaffolds tested at the 30 % strain amplitude. The decrease in mechanical properties leveled off after the first 100K cycles for both scaffolds, which indicated that amplitude had a greater affect than cycle number on the scaffold properties. Non-significant changes in physical properties (mass and volume) also suggested that the damage remained internal and appeared to manifest as localized fractures. Comparing the two scaffold formulations, the 5446DLLACL scaffolds showed significantly greater effects of fatigue compared to the 7030TMCCL scaffolds. A possible explanation for the 5446DLLACL scaffolds being more susceptible to fatigue could be the micro-porous structure within the elastomer phase as observed from the diffusion experiments, which may have allowed for micro-fractures to form in the elastomer phase as well as in the hydrogel phase. Regardless of the differences, both scaffold formulations were able to perform at high strains for a large number of cycles and were still able to maintain mechanical properties that were superior to the hydrogel alone scaffolds.

Equally important as mechanical properties for the *in vivo* efficacy of the co-continuous scaffolds is their ability to support viable and active cells. The DNA analysis following photo-encapsulation in the 7030TMCCL scaffolds showed that 98 % of the initially seeded cellular DNA remained within the scaffold. The number of viable cells after photo-encapsulation, determined from the MTT assay (72.2 ± 8.5 and 60.2 ± 8.9 % for the 6 and 8 % w/v MGC

hydrogels, respectively) raised the possibility that the remaining viable cells, especially those in the centre of the scaffolds, may become nutrient deprived. [186] However, both scaffolds showed that the dye front required just over 3 h to reach the centre of the scaffolds in the static environment. The increase in viable cells (MTT and DNA assay) and matrix accumulation in the co-continuous scaffolds over the long-term static cultures indicated that the scaffold manufacturing and culture environments were able to preserve and support a good working number of cells in the scaffolds.

The 5446DLLACL scaffolds appeared to be more susceptible to elastomer degradation by hydrolysis, as they exhibited a significant drop in modulus at the early time frames, which was accompanied by an increase in scaffold volume and decrease in scaffold mass observed at the end of the 56 day culture. This result was likely due to a more rapid hydrolysis of lactoyl-lactoyl ester linkages along the polymer backbone as compared to the carbonate or caproyl linkages in the 7030TMCCL elastomer. [187-190] The hydrolysis rate within the 5446DLLACL elastomer phase may have also been enhanced due to its apparently micro-porous nature, which would have increased the surface area of the elastomer that would be in contact with the water. Acidic degradation product accumulation within the 5446DLLACL scaffolds could also explain the decreased cellularity and cellular activity as a function of time observed with these scaffolds. [191, 192] One interesting observation was the significantly higher modulus values of the cellular 5446DLLACL scaffolds at the day 35 and 56 time points compared to their acellular controls. It is possible that the cells were able to mediate some effect of the 5446DLLACL polymer degradation through the significant accumulation of GAG within the scaffolds as was indicated in the biochemistry results. The safranin-O staining of these scaffolds indicated that GAGs accumulated at the interfacial region between the hydrogel and elastomer, which became more obvious at the later time points (day 35 and 56). This increase in GAG accumulation at the hydrogel/elastomer interface may have helped suppressed the weakening of the overall scaffolds,

since the interfacial region would be vital for the overall integrity of the co-continuous scaffolds. In contrast, the scaffolds prepared with 7030TMCCL underwent hydrolysis at a much slower rate and maintained constant modulus and hysteresis values during the culture period. The slower degradation rate of the TMCCL scaffolds appeared to have a beneficial effect on the cells within the MGC hydrogel phase. Synthesized extracellular matrix (ECM) within the 7030TMCCL scaffolds appeared to be restricted solely within the MGC phase and was cartilaginous in nature as evidenced by the accumulation of type II collagen and aggrecan with no detectable staining for type I collagen. In addition, the histological analyses were consistent with the results of the biochemistry assays, which was especially important for the GAG assay since the MGC is known to complex with the GAG molecules. [149, 193] However, since the slower degrading TMCCL elastomer phase contributed the majority of the mechanical properties, the ECM accumulation in the MGC hydrogel did not contribute significantly to the overall mechanical properties.

It is not known whether the encapsulated chondrocytes will degrade the MGC hydrogels *in vivo*. However, previous work has shown that the physiological enzyme lysozyme can degrade MGC *in vitro* at a very slow rate with only 30 % mass after 5 month in culture. [81] Therefore, longer culture times and *in vivo* experiments are required to determine if the cells can degrade the MGC hydrogel and accumulate sufficient ECM to improve the mechanical properties of the 7030TMCCL scaffolds. This study was principally concerned with an examination of the influence of the elastomer phase on scaffold performance. Future work will examine the influence of the hydrogel phase on scaffold properties and cell response for specific load-bearing soft tissue applications.

5.6 Conclusions

Two different elastomers (5446DLLACL and 7030TMCCL) were investigated for use in a two-phase elastomer/hydrogel scaffold for load-bearing soft tissues. Scaffolds prepared from

each elastomer had similar co-continuous morphologies. The 7030TMCCL scaffolds were better suited as a load-bearing tissue engineering scaffold as they were able to maintain the majority of their initial mechanical properties during long-term fatigue testing as well as over a 56 day culture period *in vitro*. Chondrocytes encapsulated within the scaffold remained viable and were able to synthesize and accumulate cartilaginous ECM. The co-continuous scaffolds could also be created in conjunction with an injectable delivery system without a loss of morphology. Overall, co-continuous hydrogel-elastomer scaffolds show promise for load-bearing soft tissue repair.

Chapter 6

Methacrylated Glycol Chitosan and Methacrylated Hyaluronic Acid Blended with Methacrylated Chondroitin Sulfate to Improve Hydrogel Modulus and Chondrocyte Activity in Load Bearing Soft Tissue Constructs

6.1 Completed Objectives

The previous studies, which examined MGC as the hydrogel phase demonstrated an acceptable cellular response from the encapsulated chondrocytes. However, these studies were principally concerned with the formation of the co-continuous morphology. Therefore, the focus of the next objectives was placed on the hydrogel phase to optimize the response of the encapsulated chondrocytes. To fulfill Objective 3 (§ 3.2.3), Chapter 6 compared hyaluronic acid (MHA) and chondroitin sulfate (MCS) with MGC to determine their potential for modification and the initial chondrocyte viability within them. Chapter 6 will be submitted to Biomacromolecules where I will be the first author as all the experiments were designed and conducted by myself.

Photo-cross-linked hydrogels produced from methacrylated glycol chitosan (MGC), hyaluronic acid (MHA) and chondroitin sulfate (MCS) were examined for their potential use in load bearing soft tissue (LBST) repair constructs. The effect of the degree of prepolymer methacrylation (X, Y or Z; based on a repeating dimer unit) on the final hydrogel properties was investigated using solutions of 6 % w/v for MGC (6wtMGC-X, where X = 12, 26 or 58 %) and MHA (6wtMHA-Y, where Y = 14, 42 or 96 %) and 20 % w/v for MCS (20wtMCS-Z, where Z = 16, 26 or 45 %). The goal was to produce hydrogels with initial moduli approaching that of native LBST (200 ± 100 kPa), stable equilibrium swelling properties after cross-linking, initial cell viabilities greater than 70 % and high metabolic activity of the encapsulated chondrocytes.

Hydrogels of 6wtMGC-12 and 6wtMHA-42 had the lowest change in equilibrium mass after cross-linking and possessed equilibrium moduli within the targeted range. Photo-cross-linking mixtures of either the 6wtMGC-12 or 6wtMHA-42 with the 20wtMCS-45 prepolymer at 50 % mass fraction (5050 MGC12MCS45 and 5050 MHA42MCS45) yielded hydrogels with equilibrium moduli between 174.9 ± 4.2 and 247.4 ± 25.0 kPa while still maintaining a minimal change in mass following swelling to equilibrium. Photoencapsulated chondrocyte viability was greater than 70 % at 24 h for all the hydrogels formed. Chondrocytes photoencapsulated within the MHA based hydrogels, regardless of prepolymer methacrylation, displayed the highest metabolic activities compared to the other hydrogels. Overall, the wide range of polysaccharide hydrogel properties and the ability of the hydrogels to support active chondrocytes in culture demonstrated the hydrogels potential for use as a reparative load bearing soft tissue construct.

6.2 Introduction

Load bearing soft tissues (LBST), such as articular cartilage and the central tissue of the intervertebral disc, can be affected by progressive degeneration either slowly through the natural aging process or more rapidly from disease and injury. [121, 138, 194, 195] Current treatments only address the symptoms, such as pain, until damage to the LBST has progressed to the point where invasive surgeries are required to replace the entire joint with permanent hardware. [32] However, these non-regenerative options alter the natural joint biomechanics, which can lead to additional issues in the surrounding tissues and possible implant failure under normal operating conditions. [196, 197] Therefore, LBST in need of repair would benefit greatly from a cellular replacement scaffold that can be used as an earlier treatment option to maintain as much of the original joint architecture as possible, restore immediate load bearing abilities to the joint and regenerate functional tissue with time.

Hydrogels are an ideal medium within which to encapsulate cells and study their behavior in a 3-dimensional environment. Provided sufficient mechanical properties can be obtained, a cell-laden hydrogel would be suitable for use as a load bearing soft tissue scaffold. Equilibrium modulus values for human articular cartilage have been reported to be between 500 to 1000 kPa, depending on the age and health of the tissue. [138, 198] In addition, reported aggregate moduli for confined compression of the degenerated and healthy human nucleus pulposus tissue are between 440 ± 190 to 1010 ± 430 kPa, respectively. [199] Photo-cross-linkable polysaccharide hydrogels, modified with (meth)acrylated groups, have the proven ability of rapid gel formation, a wide range of physical properties (modulus, swelling and degradation) and high viability and activity of the encapsulated cells. [81, 200-202] However, the study of encapsulated cell behavior in photo-cross-linkable hydrogels with stiffnesses approaching these magnitudes has been hampered by poor cell viability, which may be attributed to the higher concentration of the reactive methacrylate groups. [203, 204] Therefore, it is common for LBST hydrogel studies to use the lowest prepolymer concentrations possible along with a minimum cross-link density to lessen any cytotoxic effects on the cells. Generally, these hydrogels have low moduli of around 10 kPa and a high degree of swelling with swelling ratios close to 40. [74, 203] A variety of load bearing soft tissue cell types and stem cells encapsulated in these low modulus hydrogels have been able to increase the hydrogel stiffness up to approximately 100 kPa, either through cell proliferation and/or the accumulation of extracellular matrix, but only after 4 – 12 weeks in culture. [65, 67, 68, 205, 206] The high swelling ratios of these low modulus hydrogels also indicated that a large amount of water absorption was occurring in order to reach their equilibrium state. Significant increases in the initial hydrogel dimensions would therefore be expected during swelling, which could also affect their usefulness as a defect filling device. These changes in dimension with swelling will also change the intended mechanical properties and initial cell densities of the hydrogels. [73, 207] In an *in situ* gelation situation, hydrogels will not have the opportunity to reach equilibrium before

implantation. Therefore, in the field of LBST repair, there is a need for cellular hydrogels with initial moduli closer to that of native LBST, which are also dimensionally stable after cross-linking. The higher modulus hydrogels will also be required to support chondrocyte-like cell behavior and regenerate *de novo* cartilage tissue over time.

The use of prepolymers synthesized from the major constituents of the native tissue under study is common practice in the field of tissue engineering. Typical natural polysaccharides used to form hydrogels for LBST studies are hyaluronic acid and chondroitin sulfate. [208, 209] Hyaluronic acid (HA) is a high molecular weight (> 1 x 10^3 kg/mol), anionic, non-sulfated polysaccharide common in load bearing connective soft tissues. [210] Chondroitin sulfate (CS) is a lower molecular weight (< 50 kg/mol) sulfated polysaccharide that forms aggregates with the protein aggrecan. In LBST, aggrecan is responsible for creating hydrostatic pressure, which in turn structurally supports the tissue. The cell membrane receptor CD44, which is present on most LBST cells, has been shown to have partial specificity to CS, but principally recognizes HA. [211] Knudson *et al*. reported that the HA specificity to CD44 facilitated the self-assembly and anchorage of the pericellular matrix around the chondrocyte membranes. [89] Chitosan is a cationic polysaccharide isolated from crustacean shells with a glycosaminoglycan-like structure, which can be modified with glycol moieties to provide solubility at neutral pH. The similarities in structure, molecular weight and ease of modification makes glycol chitosan a good comparison to the HA and CS. Furthermore, methacrylated glycol chitosan (MGC) has been used to produce photo-cross-linked hydrogels suitable for cell encapsulation and LBST studies. [81, 82]

The use of glycidyl methacrylate (GMA) to modify glycol chitosan through the primary amines is a well characterized, efficient and relatively short 24 h reaction. [81] However, the use of GMA to modify the hydroxyl groups on hyaluronic acid and chondroitin sulfate yields a hydrolytically labile ester bond. [93, 94, 212] Therefore, the long-term stability of the hydrogels physical properties may not be related to material degradation but to the hydrolytic stability of the

methacrylate group substitution. Methacrylic anhydride, originally reported by Smeds *et al*., is commonly used to methacrylate the hydroxyl groups on HA and CS. However, the reaction has been shown to be inconsistent and unpredictable in terms of the final degree of methacrylation. [91, 92] Therefore, initial work concentrated on improving the methacrylic anhydride reaction for both HA and CS modification to obtain predictable and controllable degrees of methacrylation using a simple protocol optimized for short reaction times. Greater control of the degree of methacrylation provides the ability to adjust hydrogel properties such as swelling and network stiffness. [83, 94]

To improve a hydrogels initial mechanical properties and encapsulated cellular activity, previous studies have looked to blending for a solution. For example, hydrogel stiffness has been increased by using a lower molecular weight polyethylene glycol copolymer to increase the cross-link density in higher molecular weight MCS or methacrylated alginate hydrogels. [84, 213] Studies have also used MCS to enhance chondrocyte or mesenchymal stem cell growth and ECM production within poly(ethylene glycol) based hydrogels. [85, 86, 214, 215] However, PEG based hydrogels are non-degradable and require additional modification to incorporate natural and degradable properties into the synthetic network. To prevent these issues with synthetic prepolymers, some groups have also examined all natural and degradable hydrogel blends. A study by Levett *et al*. used methacrylated gelatin as the main component blended with small amounts of MHA and/or MCS to encapsulate passaged chondrocytes and cultured the hydrogels for up to 8 weeks. [206] The gelatin based hydrogels all had initial modulus between 20 – 30 kPa, but only those containing MHA were able to produce sufficient ECM and demonstrate an increase in modulus, by up to 114 kPa, after 8 weeks in culture. Although the cellular benefits of blending with either MHA or MCS have been demonstrated, no studies to our knowledge have investigated MHA-MCS and MGC-MCS copolymer networks to produce hydrogels with initial

moduli approaching that of native LBSTs and the ability to maintain active chondrocytes in culture.

In this study, individual prepolymers of glycol chitosan, hyaluronic acid and chondroitin sulfate were examined over a range of solution concentrations and degrees of prepolymer methacrylation to obtain hydrogels with highest modulus and minimal swelling upon reaching equilibrium. Hydrogel modulus was further improved by blending and co-cross-linking the higher molecular weight (~ 100 kg/mol) MGC and MHA with the lower molecular weight (~ 50 kg/mol) MCS prepolymers at different mass ratios. Hydrogels that met the design criteria of high modulus and minimal swelling were found to have moduli in the range of 100 – 300 kPa, which for an initial modulus was higher than most hydrogels typically used for cell encapsulation and approached values close to native LBST. We attempt to demonstrate the benefits of these hydrogels for their potential use in a reparative load bearing soft tissue device.

6.3 Methods and Materials

6.3.1 Materials

Sodium hyaluronate (number averaged molecular weight, M_n = 116 kg/mol, dispersity index, $Đ$ = 1.3, 99.8 % purity) was obtained from Lifecore Biomedical (St. Paul, MN, USA) and used as received. Bovine chondroitin sulfate ($M_n \approx 50$ kg/mol, ≥ 90 % purity) was purchased from LKT Laboratories (St. Paul, MN, USA). Glycol chitosan (M_n = 93 kg/mol, $Đ$ = 1.2, 60 % purity) was obtained from Wako Chemicals (Richmond, VA, USA) and further purified by dialysis before use. All other materials were obtained from Sigma-Aldrich (Oakville, ON, Canada) and were used as received unless otherwise noted.

6.3.2 Polymer Synthesis

N-Methacrylated glycol chitosan (MGC) was prepared according to previously published work. [81] Briefly, glycol chitosan dissolved in Type I water at 2 % w/v was reacted with 0.1, 0.3 and 0.6 molar equivalents of glycidyl methacrylate to the repeating monomer unit of glycol chitosan. The solution was initially adjusted to pH 9 with 1 M NaOH and allowed to react at room temperature for 24 h with stirring. The MGC solution was purified by dialysis for 4 h in 50 kDa MWCO tubing with water and membranes changed twice. The purified products were lyophilized and stored at -20 ˚C.

Hyaluronic acid and chondroitin sulfate were methacrylated by dissolving at 2 % w/v in Type I water and reacting with up to a maximum of 10 molar equivalents of methacrylic anhydride to the repeating dimer units of the prepolymers to obtain 3 different degrees of methacrylation. The reactions were conducted at room temperature and maintained at an average pH of 9 for 1 h with stirring. A separate reaction with 10 molar equivalents of methacrylic anhydride to the repeating dimer units of hyaluronic acid and chondroitin sulfate was also conducted to monitor the pH with time. The non-pH controlled reactions were initially adjusted to pH 10 with 5 N NaOH and allowed to react under constant agitation at 4 ˚C for 24 h and removed periodically to monitor the pH. Once the methacrylation reactions were finished, the prepolymers were purified by precipitation in 100 % ethanol, then dissolved in Type I water and dialysed with 14 kDa MWCO tubing for 48 h with multiple water changes. After dialysis, the solutions were neutralized with 1 M NaOH before lyophilization and storage at -20 ˚C.

6.3.3 Polymer Characterization

^{1}H NMR spectra of the prepolymers were collected from 0.7 mL samples dissolved at 20 mg/mL in deuterium oxide and run on a Bruker Avance-400 MHz spectrometer. The mol % *N*-methacrylation of glycol chitosan (GC) was confirmed by ^{1}H NMR analysis. The ratio of the

integration of the peaks corresponding to the vinyl protons on the *N*-methacrylate group (average of δ = 6.2 and 5.9 ppm) over the integration of the peaks corresponding to the C1 proton (δ = 5.1 ppm), present in every residue, was used to calculate the number of *N*-methacrylated residues per 100 residues in the GC chain. [81] The molar degree of methacrylation based on a repeating dimer units for hyaluronic acid and chondroitin sulfate was also confirmed by ^{1}H NMR analysis using representative peak integrations following the method used by Van Vlierberghe *et al*. [216] For MHA and MCS, vinyl protons appear at δ = 6.1 and 5.7 ppm, while methyl protons from the N-acetyl groups and methacrylate group appear between δ = 2.0 and 1.8 ppm. The reported molar excess of GMA and degree of methacrylation for MGC has been doubled so as to be based on a dimer repeating unit and therefore comparable to the values for MHA and MCS.

The viscosity of the prepolymer solutions for a few select conditions was measured on an AR2000 rheometer (TA Instruments, Delaware, USA). The prepolymers were dissolved in water at 20 mg/mL and 200 μL were added to the test surface. A flat 20 mm stainless steel platen was used for testing and viscosity was measured from 0.01 to 10 rad/s shear rate. The plateau regions averaged at the low shear rate conditions (< 0.1 rad/s) were taken as the zero shear values (Pa·s). Cross-linking efficiency was assessed through measurement of the sol content for all hydrogels (n = 3). The sol content (% w/w) was determined by measuring the difference in dry mass of the as-made samples versus samples soaked multiple times in F12 culture media (also used to dissolve prepolymers) over the as-made dry mass. [150] Equilibrium water content (% w/w) was calculated as the difference in swollen wet mass and dried mass over the swollen wet mass. The mass swelling ratio (q) was determined from the ratio of swollen wet mass over the dried mass.

6.3.4 Hydrogel Manufacture and Cell Encapsulation

Primary chondrocytes from the articulating surfaces of bovine metacarpal joints were isolated as described previously. [150] The prepolymers were dissolved at varying concentrations in

Ham's F12 culture media containing Irgacure 2959 photo-initiator (0.1 % w/v final concentration) with manual mixing and if required a final centrifugation step (100 g for a few seconds) to remove entrapped bubbles. Cell-laden hydrogels were made by gentle mixing of a concentrated cell suspension and prepolymer solution, both in F12 culture medium, to obtain a final density of 4 x 10^7 cells/mL and the desired prepolymer concentration. Cylindrical molds were constructed from Teflon tubing cut with parallel ends (3.2 mm I.D. and 2.2 mm height). The mold was placed on a glass coverslip, solution was transferred by pipet to the mold in excess, then covered with another coverslip on the top and held in place with a clamp, leaving the top and bottom view of the prepolymer solution unobstructed. The clamp and mold assembly was then secured between two light guides placed 1 cm axially from each end of the mold (long-wave UV intensity at base of the mold = 10 mW/cm^2). Hydrogels were formed after 60 s exposure to the UV light, which was filtered to 320 – 390 nm. Hydrogels were immediately transferred to a 24 well culture plate containing 2 mL of F12 culture medium supplemented with 10 % fetal bovine serum (FBS) and 1X antibiotic/antimycotic. Acellular and cellular hydrogels were maintained in culture in an incubator maintained at 37 ˚C with an atmosphere supplemented with 5 % CO_2 and 95 % relative humidity. The medium was replaced with fresh medium every other day for up to 35 days in culture.

6.3.5 Cellular Characterization

Viability/cytotoxicity of the encapsulated chondrocytes was determined using Live/Dead™ staining (Life Technologies Inc., Burlington, Ontario, Canada). Live (2 µM Calcein AM) and Dead (4 µM ethidium homodimer-1) solutions were made in 1 X PBS following manufacturer guidelines. The chondrocytes were encapsulated in the hydrogels made with the lowest and highest degree of prepolymer methacrylation and cultured for 1 and 7 days. At each time point the hydrogels (n = 2) were removed and added to 1 mL of the staining solutions for 30

min before imaging. Fluorescent images were taken using an inverted FluoView FV1000 laser scanning confocal microscope with a 10 x objective and FITC/TRITC filter set. Cells were counted, using ImageJ software, for both live (green) and dead (red) channels and viability was calculated as the number of live cells over the total number of cells.

For the MTT assay, 100 μL of the MTT solution (5 mg/mL in 1X PBS) was added per 1 mL of culture medium surrounding the hydrogels and incubated at 37 ˚C for 4 h. After incubation, the hydrogels were transferred to a 1.5 mL micro-centrifuge tube with 600 μL of 100 % DMSO and crushed with a pestle to dissolve the resulting formazan crystals. The suspensions were centrifuged at 700 g for 7 minutes and the supernatant was added at 180 μL/well in a 96 well plate and read at 540 nm absorbance. The MTT assay was also used to calculate the number of cells remaining after photo-encapsulation in the selected single component and blended hydrogels following a previously reported protocol. [150] Briefly, a standard curve of MTT absorbance as a function of cell number (100k, 400k, 700k and 1M cells) was used to convert the measured absorbance to an approximate cell number. The original number of cells was calculated based on the volume of the hydrogel solution added to the cross-linking mold and the original cellular density of the prepolymer solution (4×10^7 cell/mL).

6.3.6 Mechanical Properties

Stress relaxation measurements were conducted in compression on both the acellular and cellular hydrogels to determine the equilibrium modulus values (n = 4 – 5). Testing was performed on a micro-mechanical tester (MACH-1, Biomomentum Inc. Laval, QC) equipped with a 1 kg load cell all housed in a 37 ˚C incubator. Unconfined scaffold samples (3.2 mm diameter x 2.2 mm height) were immersed in a Ham's F12 culture media bath with a solid base and moving upper platen (1 cm in diameter). Stress relaxation tests were conducted at 2 % strain increments, to a total strain of 20 %. Step strains were applied at a rate of 6 %/s. The resulting

force decay was recorded until equilibrium was reached, which was defined as a change in force of less than 0.2 g/min. The equilibrium modulus was obtained from the slope of the linear region of the decayed stress versus applied stain curve (10 – 20 % strain).

Hydrogels (n = 3 – 4) were also tested at constant strain rate to determine the failure stress and strain values. The same setup used for stress relaxation testing was used for failure analysis. Unconfined hydrogels of the same dimensions as above (3.2 mm diameter x 2.2 mm height) were fully submerged in Ham's F12 culture medium and a 1 %/s strain rate was applied until a sharp drop in load data was observed. The sharp drop in stress represented hydrogel failure due to fracture. Peak stress (kPa) and strain at failure (%) were reported at the point of hydrogel failure. The compressive modulus (kPa) was calculated using linear regression on the linear region of the stress strain curve between 10 – 20 % strains.

6.3.7 Statistical Analyses

All results are expressed as the mean ± the standard deviation and analyzed using statistical software (SigmaStat 1.0, SPSS Science, Chicago, IL). Mechanical and cellular characterization results were analyzed using a 2-way ANOVA and the Fisher's LSD post-hoc test. Significance was associated with p values of less than 0.05.

6.4 Results

6.4.1 Prepolymer Degree of Methacrylation

The addition of the methacrylic anhydride (MA) to the reaction mixture of hyaluronic acid (HA) and chondroitin sulfate (CS) resulted in a rapid decrease in pH, which both leveled off between pH 4 – 5 after 140 and 80 minutes, respectively (Figure 6.1). The rapid drop in pH of the reaction mixture was due to the formation of methacrylic acid as a byproduct from MA reacting

with the hydroxyl groups on the prepolymers and also from the reaction of MA with the excess water. The lower reaction pH reduced the nucleophilic ability of the hydroxyl groups on the HA and CS prepolymers to attack the anhydride bond of the MA molecule. Therefore, the shortened 1 h reaction was maintained under basic conditions (pH 8 – 10) to help catalyze the reaction between MA and the hydroxyl groups present on the HA and CS prepolymers.

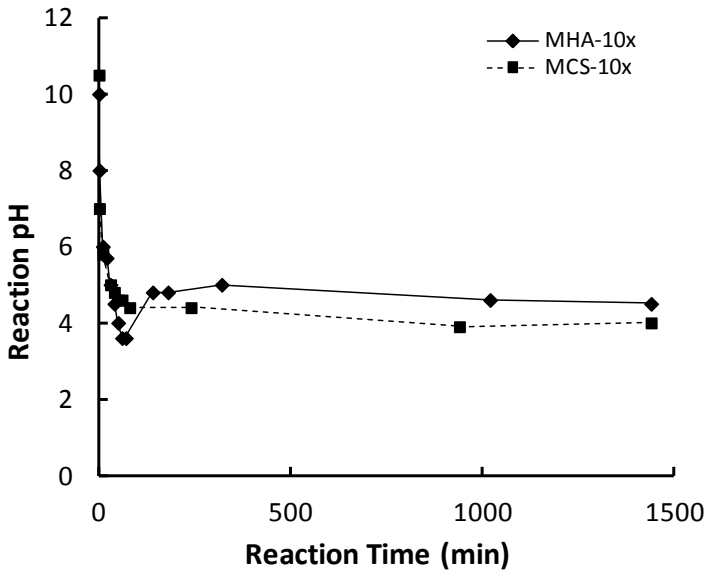

Figure 6.1: Monitoring pH of a representative reaction with hyaluronic acid or chondroitin sulfate with 10 molar equivalents of methacrylic anhydride to the repeating dimer units of the prepolymers. The reaction solution was initially adjusted to pH 10 after the addition of MA and allowed to react for a 24 hour period.

The molar feed ratio of methacrylating reagent to repeating units and final degree of methacrylation for the various prepolymers were calculated from the ^{1}H NMR spectra (Figure A.11) and results are presented in Figure 6.2. Methacrylation of glycol chitosan using glycidyl methacrylate (GMA) was more efficient than the methacrylation of hyaluronic acid or chondroitin sulfate using methacrylic anhydride (MA). However, both methods produced a wide range of degrees of methacrylation for each prepolymer. MGC prepolymers between 6 to 29 %

methacrylation were obtained for 0.1, 0.3 and 0.6 times molar feed ratios of GMA (both calculated per residue), but have been presented based on a repeating dimer basis (12, 26 and 58 %) to be comparable with MHA and MCS (Figure 6.2 (A)). MHA demonstrated the greatest range of % methacrylation of 14, 42 and 96 % for 1, 5 and 10 x molar excess MA (Figure 6.2 (B)). Comparatively, MCS prepolymers with 16, 26 and 45 % methacrylation were obtained using 5, 7.5 and 10 times molar feed ratios of MA (Figure 6.2 (B)). The lower degree of methacrylation of MCS may be related to the sulfate group on the repeating dimer units of chondroitin sulfate, which reduces the number of primary hydroxyl sites available for reaction with MA. [217]

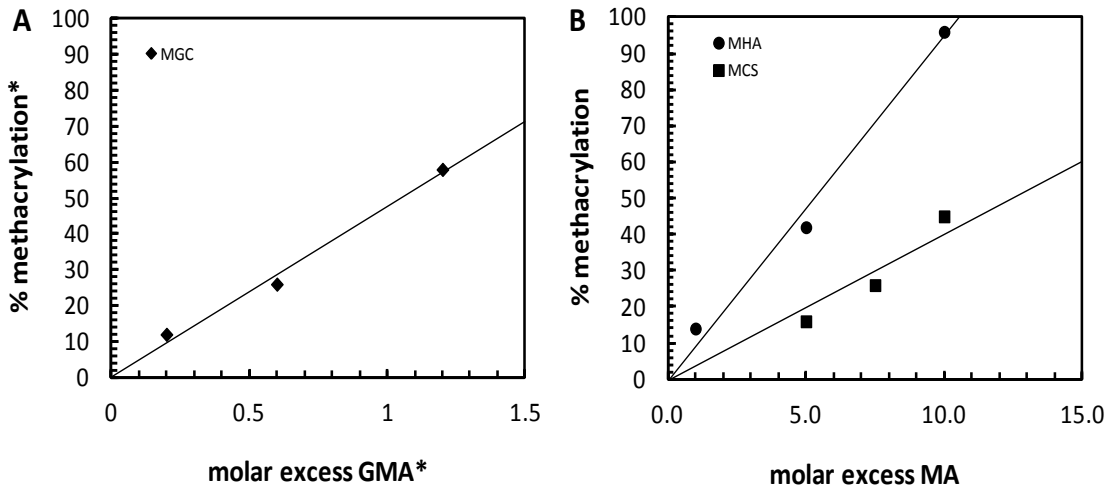

Figure 6.2: The degree of methacrylation expressed as a percent of dimer units for each prepolymer as a function of the molar feed ratio of the respective methacrylating agent. (A) GMA modified glycol chitosan and (B) MA modified hyaluronic acid and chondroitin sulfate. (*) Original molar excess of GMA and final degree of methacrylation for glycol chitosan was based on a monomer repeating unit but was converted to a dimer unit for comparison with MHA and MCS.

6.4.2 Effect of Prepolymer Concentration on Hydrogel Properties at Low Degree of Methacrylation

Prepolymers with the lowest degree of methacrylation were used to determine the lowest prepolymer concentrations that could produce hydrogels with equilibrium moduli greater than 100 kPa, as this modulus value was within the targeted range set out in the design criteria. A preliminary study was conducted with prepolymer concentrations of 4, 6 and 8 % w/v for MGC-12 and MHA-14 and 10, 20 and 30 % w/v for MCS-16. The hydrogels prepared with the lowest prepolymer solution concentrations (4 % w/v for MGC (4wtMGC-12) and MHA (4wtMHA-14)) had equilibrium modulus values below 100 kPa and the highest swelling ratios as compared to all other conditions (Figure 6.3 (A and B)). For both the MGC-12 and MHA-14 prepolymers, the 6 % w/v concentrations (6wtMGC-12 and 6wtMHA-14) produced hydrogels with equilibrium moduli greater than 100 kPa (Figure 6.3 (A and B)). Increasing the prepolymer concentrations to 8 % w/v further increased the equilibrium moduli and decreased the swelling ratios. Therefore, for MGC and MHA a 6 % w/v concentration was selected for further study. As a result of the lower molecular weight of the MCS, higher prepolymer solution concentrations were required to produce hydrogels with an equilibrium modulus within the same range as that of the MGC and MHA hydrogels. An MGC-16 prepolymer solution concentration of 10 % w/v resulted in hydrogels with equilibrium moduli of 20.6 ± 2.0 kPa, which are comparable in value to that of the 4 % w/v MGC-12 and MHA-14 hydrogels. Doubling the MCS-16 prepolymer solution concentration to 20 % w/v increased the resulting hydrogel moduli to 271.7 ± 14.2 kPa (Figure 6.3 (C)). A further increase in concentration to 30 % w/v MCS-16 produced hydrogels with equilibrium moduli of 477.4 ± 69.2 kPa (Figure 6.3 (C)). However, an equilibrium modulus close to the targeted range of 200 ± 100 kPa was obtained using a 20 % w/v MCS-16 (20wtMCS-16) and was therefore selected for the additional MCS studies. Hydrogel swelling ratios (q) decreased as the prepolymer concentration increased and ranged from 28.4 ± 2.1 to 9.1 ± 0.4 for all the prepolymers examined.

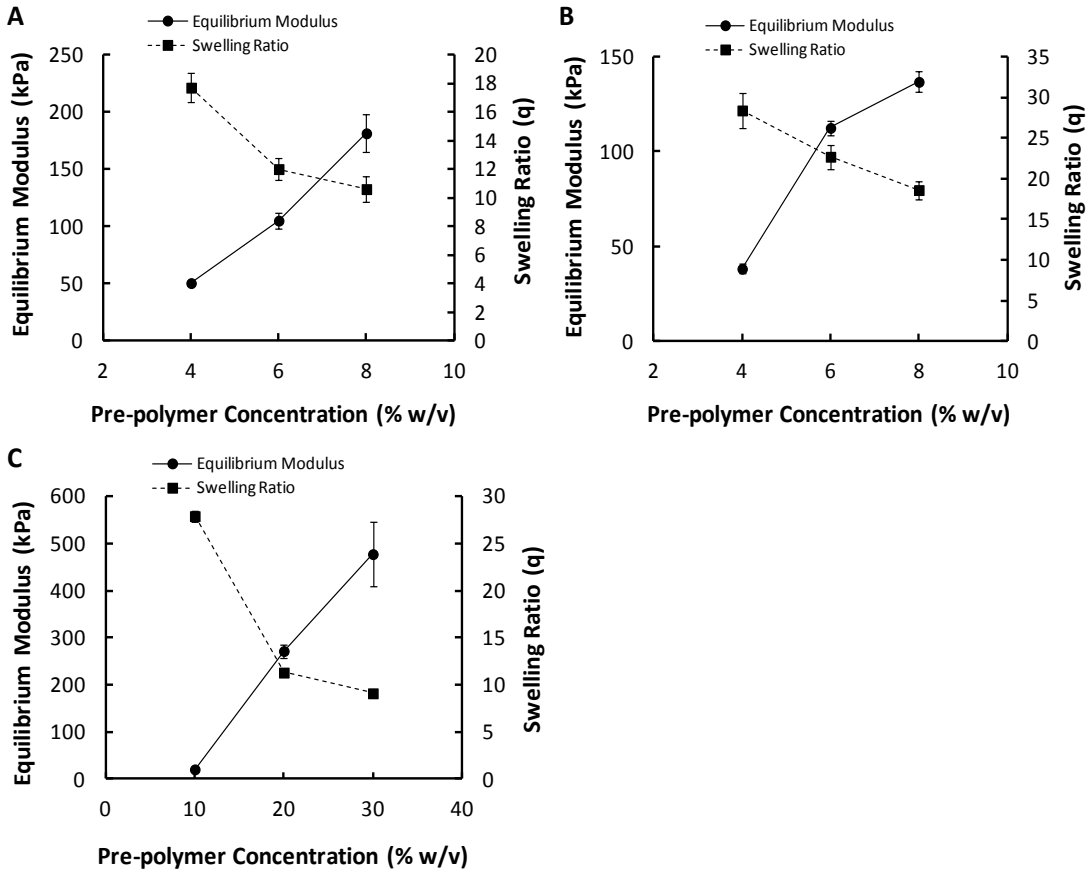

Figure 6.3: Effect of prepolymer solution concentration (% w/v) on final hydrogel properties for low degree of methacrylation for the (A) MGC-12, (B) MHA-14 and (C) MCS-16 prepolymers

6.4.3 Tuning of Hydrogel Mechanical Properties with Degree of Methacrylation

At the selected prepolymer concentrations (6wtMGC, 6wtMHA and 20wtMCS), the influence of the prepolymer degree of methacrylation on the physical properties of the resulting hydrogels (equilibrium modulus, sol content swelling ratio, equilibrium water content) was determined (Table 6.1). Interestingly, the viscosity of the MGC solutions increased with degree of methacrylation, an effect that was not observed for either the MHA or MCS solutions. Zero shear viscosities for 2 % w/v MGC-12 and MGC-58 solutions were 1.0 ± 1.1 and 288.0 ± 26.1 Pa·s,

respectively. It should also be noted that MGC-58 required much longer mixing times to dissolve, regardless of prepolymer concentration. Comparatively, the MHA-96 prepolymer dissolved readily in solution and had a zero shear viscosity of 0.2 ± 0.1 Pa·s for a 2 % w/v solution. However, at the selected prepolymer concentrations all the hydrogels were efficiently cross-linked, which was evident from the low sol contents regardless of the degree of methacrylation of the prepolymer (Table 6.1). The highest sol contents occurred in the 6wtMGC hydrogels and the lowest occurred in the 20wtMCS hydrogels, but the sol contents were not dependent on the degree of methacrylation of the prepolymer (Table 6.1). The general trends in the physical properties for each hydrogel were higher modulus, lower swelling ratio and lower equilibrium water content as the prepolymer degree of methacrylation increased (Table 6.1). The only exception to these trends was the equilibrium modulus of the hydrogels prepared with 6wtMGC, which did not increase above 104.9 ± 13.6 kPa regardless of the degree of MGC methacrylation. The hydrogels prepared with 6wtMHA-14 to -96 had a significantly wider range of equilibrium moduli and swelling ratios compared to the MGC hydrogels. Hydrogels prepared with the 20wtMCS-45 prepolymer had the highest equilibrium moduli at 624.0 ± 48.4 kPa and the lowest swelling ratios compared to the other hydrogels (Table 6.1).

Table 6.1: Effect of degree of methacrylation on hydrogel properties at selected prepolymer concentrations.

Hydrogel	Equilibrium Modulus (kPa)	Sol Content (%)	Swelling Ratio (q)	Equilibrium Water Content (%)
6wtMGC-12	104.9 ± 13.6	13.5 ± 3.3	12.0 ± 0.2	91.7 ± 0.1
6wtMGC-26	82.4 ± 5.4	11.3 ± 3.4	11.0 ± 2.8	90.5 ± 2.1
6wtMGC-58	103.7 ± 15.0	13.4 ± 7.2	8.3 ± 0.5	87.9 ± 0.7
6wtMHA-14	112.5 ± 3.6	6.7 ± 0.5	22.7 ± 1.5	95.6 ± 0.3
6wtMHA-42	165.4 ± 12.2	8.1 ± 0.4	15.8 ± 1.4	94.4 ± 0.5
6wtMHA-96	255.6 ± 9.6	9.9 ± 3.8	11.7 ± 0.8	91.5 ± 0.6
20wtMCS-16	271.7 ± 14.2	3.8 ± 1.5	13.9 ± 0.3	92.8 ± 0.2
20wtMCS-26	359.6 ± 32.2	4.6 ± 1.6	10.4 ± 0.2	90.3 ± 0.1
20wtMCS-45	624.0 ± 48.4	4.7 ± 2.1	7.8 ± 0.3	87.2 ± 0.5

6.4.4 Effect of Degree of Methacrylation on Hydrogel Failure Properties

The failure properties of the hydrogels under mechanical loading were also examined since they are important parameters in a load bearing soft tissue (LBST) application. Hydrogels prepared with the higher molecular weight prepolymers (MGC and MHA) failed between strains of 40 – 60 % and the hydrogels prepared with the lower molecular weight MCS failed between strains of 30 – 40 % (Table 6.2). Within the same strain region the modulus values determined using a constant strain rate, were significantly higher than those measured from the stress relaxation protocol (Table 6.1). Stress at failure were highest for the hydrogels prepared using prepolymers with lower degrees of methacrylation (6wtMGC-12 and 6wtMHA-14) and decreased as prepolymer degree of methacrylation increased. The MCS hydrogels exhibited an opposite trend with increasing failure stress as the prepolymer degree of methacrylation increased. Overall, the MCS hydrogels possessed the highest moduli and lowest failure strains compared to the other hydrogels.

Table 6.2: Hydrogel test to failure properties with respect to degree of methacrylation for hydrogels prepared with A) 6wtMGC, B) 6wtMHA and C) 20wtMCS prepolymers.

Hydrogel	Modulus (kPa)	Stress at Failure (kPa)	Strain at Failure (%)
6wtMGC-12	149.3 ± 5.0	326.1 ± 58.6	54.8 ± 0.5
6wtMGC-26	214.7 ± 1.2	316.4 ± 20.8	48.8 ± 0.7
6wtMGC-58	253.3 ± 11.0	209.2 ± 18.7	43.8 ± 2.8
6wtMHA-14	81.8 ± 4.8	395.3 ± 62.5	57.9 ± 0.9
6wtMHA-42	223.2 ± 9.7	350.7 ± 11.2	49.2 ± 0.6
6wtMHA-96	316.1 ± 14.4	329.4 ± 12.2	42.5 ± 1.1
20wtMCS-16	437.5 ± 17.7	203.0 ± 111.1	31.5 ± 4.7
20wtMCS-26	492.0 ± 42.4	364.9 ± 33.3	37.0 ± 0.7
20wtMCS-45	779.0 ± 329.4	551.9 ± 65.4	38.6 ± 4.5

6.4.5 Effect of Degree of Methacrylation on Hydrogel Swelling Properties

The change in hydrogel mass after swelling is considered to be important to achieve predictable hydrogel properties after an *in situ* implant scenario. The difference between the mass of the hydrogel's after cross-linking and equilibrium swelling was associated with changes in water content as the sol contents of the hydrogels were low and did not change significantly with degree of methacrylation (Table 6.1). It should also be noted that the hydrogels maintained uniform geometry during any increase or decrease in hydrogel mass. The higher degrees of prepolymer methacrylation had a significant effect on decreasing the equilibrium mass of the hydrogels (Figure 6.4). For the hydrogels prepared with the MGC-26, MGC-58 (Figure 6.4 (A)) and MHA-96 (Figure 6.4 (B)) a significant decrease in the cross-linked mass was also observed from their respective hydrogels made with the lowest prepolymer methacrylation. Hydrogels that were made with the MGC-12 (Figure 6.4 (A)), MHA-14 (Figure 6.4 (B)) and all of the MCS prepolymers (Figure 6.4 (C)) demonstrated significant increases in their equilibrium mass from

their original cross-linked mass. Only the MHA-96 hydrogels significantly decreased in mass after reaching equilibrium (Figure 6.4 (B)). Overall, the degree of prepolymer methacrylation had a significant effect on the hydrogels mass after cross-linking and equilibrium swelling. The degree of prepolymer methacrylation was beneficial in controlling the hydrogels swelling properties, in addition to modulus, through the degree of methacrylation.

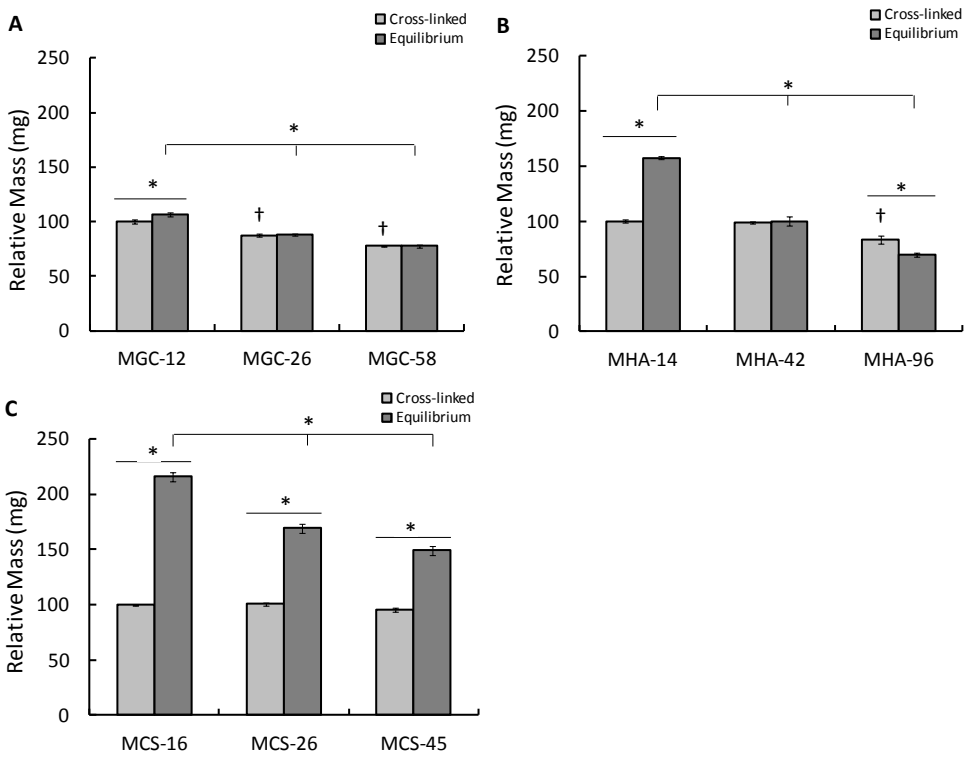

Figure 6.4: Relative mass of the hydrogels immediately after cross-linking and after equilibrium swelling for (A) 6wtMGC, (B) 6wtMHA and (C) 20wtMCS as a function of degree of methacrylation. All hydrogel masses were normalized to the post-cross-linked hydrogels prepared with prepolymers having the lowest degree of methacrylation. (*) Significant within the group, (†) significant from cross-linked mass of hydrogels prepared with the lowest degree of methacrylation ($p < 0.05$).

6.4.6 Blending MGC and MHA with MCS to Control Hydrogel Modulus

The single component MGC-12 and MHA-42 hydrogels were chosen for further investigation based on their low swelling and equilibrium moduli between 200 ± 100 kPa; however, both were on the lower end of the targeted modulus range. Blending of the higher (MGC or MHA) and lower (MCS) molecular weight components was attempted to further increase the hydrogel modulus. Specifically, the 6wtMGC-12 and 6wtMHA-42 prepolymer solutions were blended with 20wtMCS-45 at 50 and 90 % prepolymer mass fractions. The higher MCS mass fractions and degree of methacrylation were chosen to have a greater effect on the final hydrogel modulus. The addition of MCS-45 to MGC-12 or MHA-42 resulted in blended hydrogels that were significantly different from the single component hydrogels used in their construction. The equilibrium moduli increased significantly with the MCS-45 mass fraction (Figure 6.5 (A)). The equilibrium mass for the blends with MHA-42 also increased with higher amounts of MCS-45, however, the equilibrium mass for the MGC-12 blends only increased with the 90 % MCS-45 mass fraction (Figure 6.5 (B)).

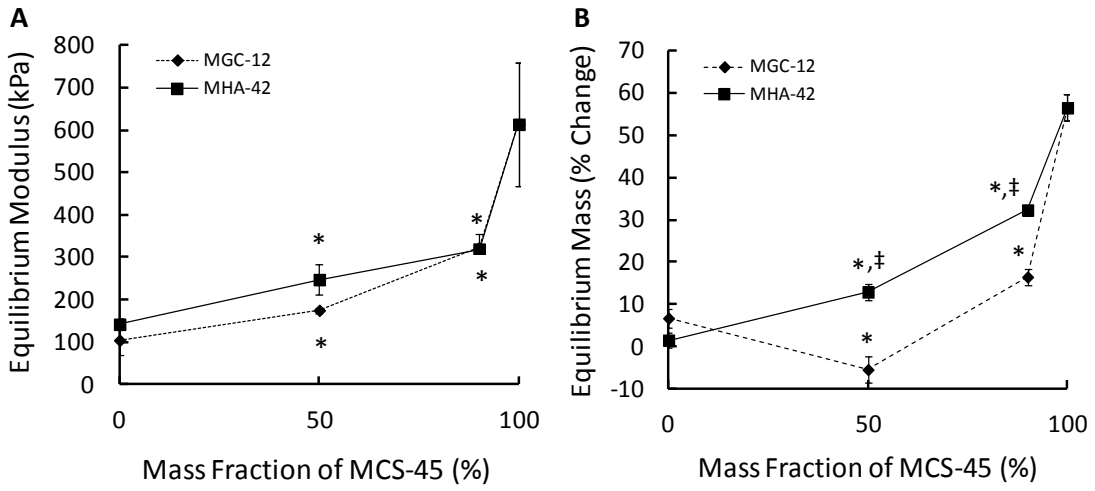

Figure 6.5: Hydrogel blends using 6wtMGC-12 and 6wtMHA-42 with 20wtMCS-45 (reported as final mass ratio) (A) equilibrium modulus and (B) change in mass from original cross-linked mass after equilibrium swelling. (*) Significant blend values from both of the single component hydrogels, (‡) significant between groups at the specific MCS-45 mass fraction ($p < 0.05$).

The total prepolymer concentrations for the blends increased from 9.5 to 13 % w/v as the mass fraction of MCS-45 increased from 50 and 90 %, which could have affected the final equilibrium modulus. To determine whether the increase in modulus was due to the total prepolymer concentration or from the degree of methacrylation, a less modified MCS-18 prepolymer produced from the longer reactions presented in Figure 6.1, was used to produce hydrogel blends with the same mass fractions as in Figure 6.5. The 20wtMCS-18 prepolymer solutions produced hydrogels with an equilibrium modulus of 128.8 ± 6.5 kPa, which was between the modulus of the 6wtMGC-12 and 6wtMHA-42 hydrogels and was also much lower than the 624.0 ± 48.4 kPa equilibrium modulus for the 20wtMCS-45 hydrogels. Only minor changes in the hydrogel moduli were observed for both the MGC-12 and MHA-42 when blended with the MCS-18 prepolymer (Figure 6.6). Therefore, the increase in mechanical properties of the

blends was attributed to the difference in degree of MCS methacrylation and not from the higher prepolymer concentrations as the MCS mass fraction was increased.

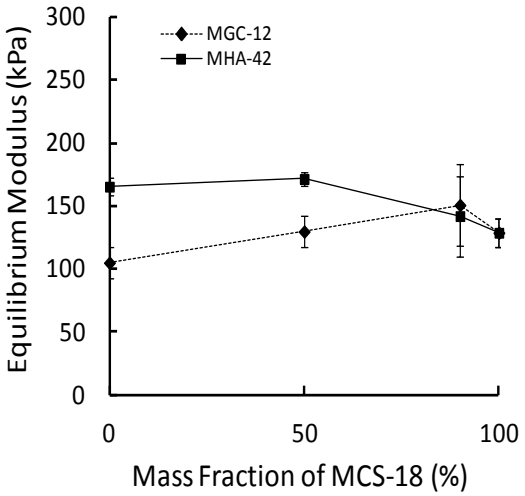

Figure 6.6: Equilibrium moduli of blended hydrogels using 6wtMGC-12 and 6wtMHA-42 with a less modified 20wtMCS-18 (lower modulus, 24 h MA reaction) prepolymer. Blends are reported as the final mass ratio.

The higher blends with 90 % MCS-45 mass fraction demonstrated much higher swelling and may also dilute any beneficial cellular effects from the MGC or MHA components. For these reasons only the 50 % MCS-45 mass fraction blends were selected for additional characterization studies. The 50 % MCS-45 blended MGC-12 (5050 MGC12MCS45) and MHA-42 (5050 MHA42MCS45) hydrogels were highly hydrated and possessed low sol contents (Table 6.3). The swelling ratios for both 5050 blends (Table 6.3) were still within the range of their respective single component hydrogels (Table 6.1). Under constant strain rate, the moduli for the 5050 hydrogel blends were slightly higher than the equilibrium modulus determined from the stress relaxation testing. In comparison to the single component MGC-12 and MHA-42 hydrogels (Table 6.2), the 5050 blends were slightly higher in compressive modulus and stress at failure, but slightly lower in failure strains (Table 6.4). Overall, the addition of the 50 % MCS-45 prepolymer

saw the maximum benefit in increasing the modulus of the hydrogel blends, while minimizing swelling. All other mechanical values for the 5050 blends were within a similar range to the single component MGC-12 or MHA-42 hydrogels.

Table 6.3: Additional equilibrium hydrogel properties of the 5050 mass ratio blends of MGC12MCS45 and MHA42MCS45.

Hydrogel	Sol Content (%)	Swelling Ratio (q)	Equilibrium Water Content (%)
5050 MGC12MCS45	6.4 ± 2.7	9.8 ± 0.5	89.8 ± 0.5
5050 MHA42MCS45	3.7 ± 3.2	14.8 ± 0.3	93.2 ± 0.2

Table 6.4: Test to failure data for 5050 mass blends of MGC12MCS45 and MHA42MCS45 hydrogels.

Hydrogel	Modulus (kPa)	Stress at Failure (kPa)	Strain at Failure (%)
5050 MGC12MCS45	192.8 ± 17.8	332.9 ± 27.2	49.6 ± 3.3
5050 MHA42MCS45	241.8 ± 29.2	391.4 ± 28.7	46.4 ± 1.8

6.4.7 Cell Characterization in Single Component Hydrogels at High and Low Degrees of Methacrylation

Following the determination of the influence of concentration and degree of methacrylation of the prepolymers on the hydrogel physical properties, the behavior of chondrocytes encapsulated within the single component hydrogels prepared with prepolymers of both low and high degrees of methacrylation was assessed. At the same cell seeding density, Live/Dead™ images demonstrated the effect of prepolymer degree of methacrylation (low and

high values) in terms of swelling size and cellular density/distribution (Figure 6.7). All hydrogels appeared to have a good distribution of live cells throughout, with the exception of the 6wtMGC-58 hydrogels. Although hydrogel swelling/shrinking affected the cell density, it did not appear to have an effect on cell viability after 1 and 7 days in culture, with cell viability within most hydrogels remaining between 80 – 90 % (Table 6.5). The one exception to this observation was the lower cell viability at both 1 and 7 days for the 6wtMGC-58 hydrogels. The higher prepolymer viscosity of this prepolymer solution may have resulted in cell death during mixing as a result of higher shear forces.

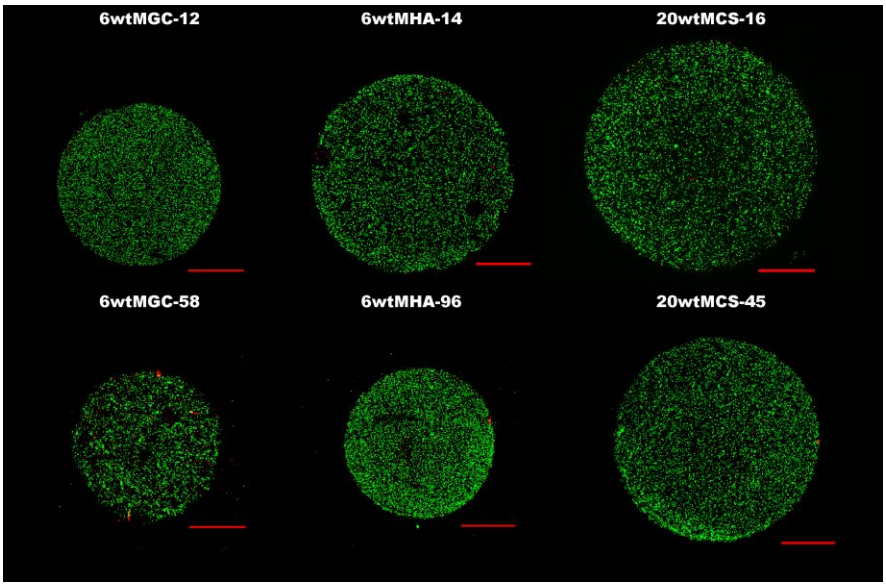

Figure 6.7: Live/Dead™ stained images after 24 h static culture of chondrocytes photoencapsulated within hydrogels prepared with prepolymers of both high and low degrees of methacrylation. Scale bar = 1000 µm.

Table 6.5: Chondrocyte viability after 24 h in the hydrogels prepared with prepolymers of low and high degrees of methacrylation (calculated from Live/Dead™ images).

Hydrogel	Day 1 Cell Viability (%)	Day 7 Cell Viability (%)
6wtMGC-12	78.8 ± 10.0	53.5 ± 16.7
6wtMGC-58	65.5 ± 3.1	66.5 ± 8.2
6wtMHA-14	87.3 ± 6.1	90.9 ± 2.4
6wtMHA-96	83.4 ± 8.4	81.1 ± 12.6
20wtMCS-16	82.5 ± 8.5	80.5 ± 18.2
20wtMCS-45	89.3 ± 2.9	79.3 ± 4.0

Metabolic activity of the encapsulated chondrocytes in hydrogels prepared with the lowest and highest methacrylated 6wtMGC, 6wtMHA and 20wtMCS prepolymers was monitored over a 7 day culture using the MTT assay (Figure 6.8). Metabolic activity in the 6wtMGC hydrogels was significantly decreased with the MGC-58 prepolymers; however, no change in metabolic activity was observed with time in either of the MGC-12 or MGC-58 hydrogels (Figure 6.8 (A)). The degree of the MHA prepolymer methacrylation did have any effect on the metabolic activity of the encapsulated chondrocytes after day 1. The metabolic activity of the encapsulated chondrocytes in the MHA hydrogels was able to increase after day 7 in culture and was significantly higher in the MHA-14 hydrogels than in the MHA-96 hydrogels (Figure 6.8 (B)). A higher degree of methacrylation between the MCS-16 and MCS-45 hydrogels resulted in a significant decrease in the day 1 chondrocyte metabolic activity. However, by day 7 the metabolic activity of the chondrocytes in the MCS-45 hydrogels was able to significantly increase and match the metabolic activity of the chondrocytes in the MCS-16 hydrogels (Figure 6.8 (C)).

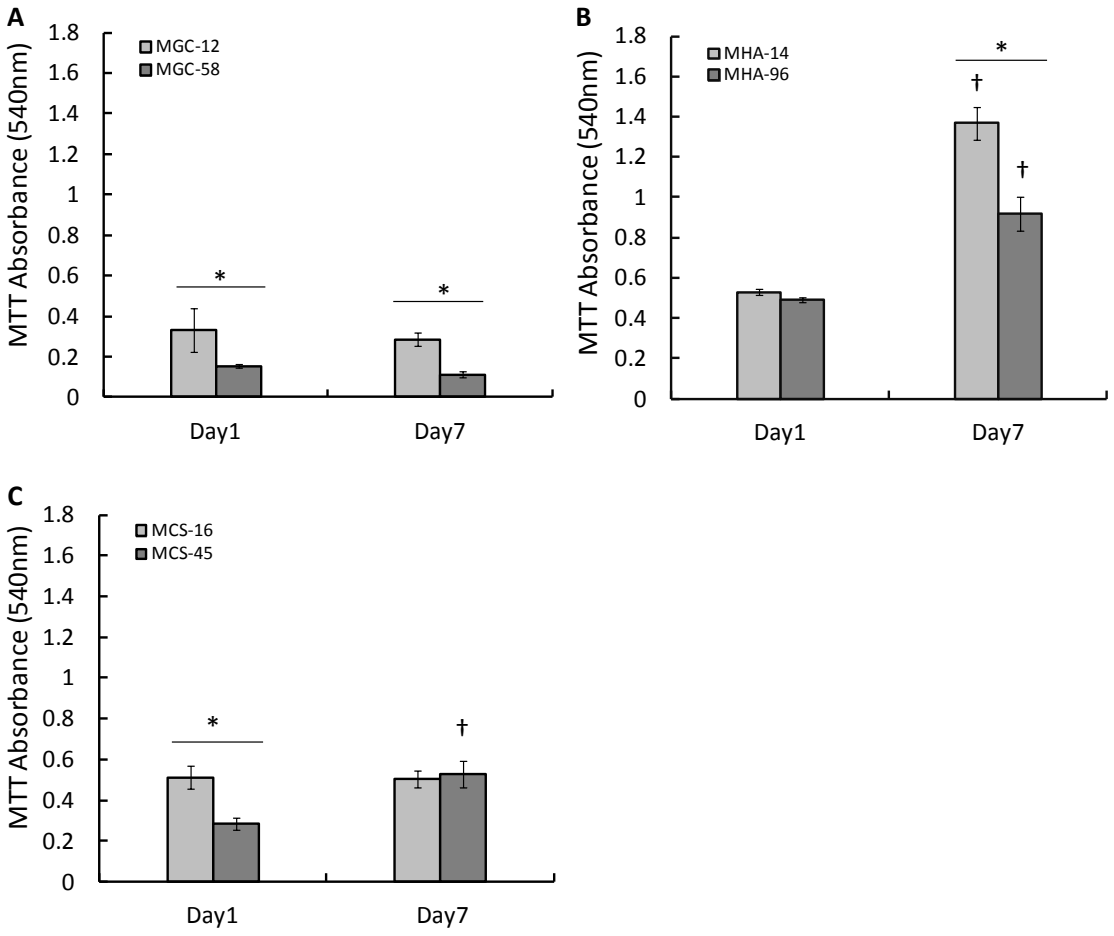

Figure 6.8: Metabolic activity of encapsulated primary chondrocytes (40 x 10^6 cells/mL) in hydrogels prepared with prepolymers of low and high degrees of methacrylation over a 7 day culture. A) 6wtMGC (12 and 58 % methacrylation), B) 6wtMHA (14 and 96 % methacrylation) and C) 20wtMCS (16 and 45 % methacrylation). (*) Significant within groups, (†) significant from day 1 values ($p < 0.05$).

6.4.8 Long-Term Metabolic Activity in Selected Single Component and Blended Hydrogels

The behavior of encapsulated primary bovine chondrocytes was investigated over a 35 day culture period in static culture *in vitro* for the selected single component (6wtMGC-12 and 6wtMHA-42) and 50 % MCS-45 mass fraction hydrogel blends (5050 MGC12MCS45 and 5050 MHA42MCS45). Although no issues with viability in the blends was expected, the day 1 MTT

values were used to ensure a sufficient number of cells remained after photo-encapsulation. The total number of active cells in the hydrogels after 24 h were determined to be 72.6 ± 9.2, 83.0 ± 5.5, 96.5 ± 3.3 and 90.4 ± 8.2 % of the number of cells originally seeded in the 6wtMGC-12, 6wtMHA-42, 5050 MGC12MCS45 and 5050 MHA42MCS45 hydrogels, respectively. The number of cells calculated with the MTT method was comparable to the numbers obtained from the Live/Dead™ assay in the previous section. The addition of the MCS-45 prepolymer in the 5050 MGC12MCS45 blends resulted in significant increases to the metabolic activity over the single component MGC-12 hydrogels at days 14 and 35 of the culture (Figure 6.9). Long-term metabolic activity increased significantly at day 35 for the blended 5050 MHA42MCS45 hydrogels, which was also the highest change in activity compared to the other hydrogels. As with the short term tests for metabolic activity, the MGC-12 hydrogels appeared to have low activity during the long-term cultures. Although a significant increase in metabolic activity with time was observed for the high modulus MHA-96 hydrogels during the shorter 7 day culture, a comparable increase in the MHA-42 hydrogels was not as significant during the longer term cultures.

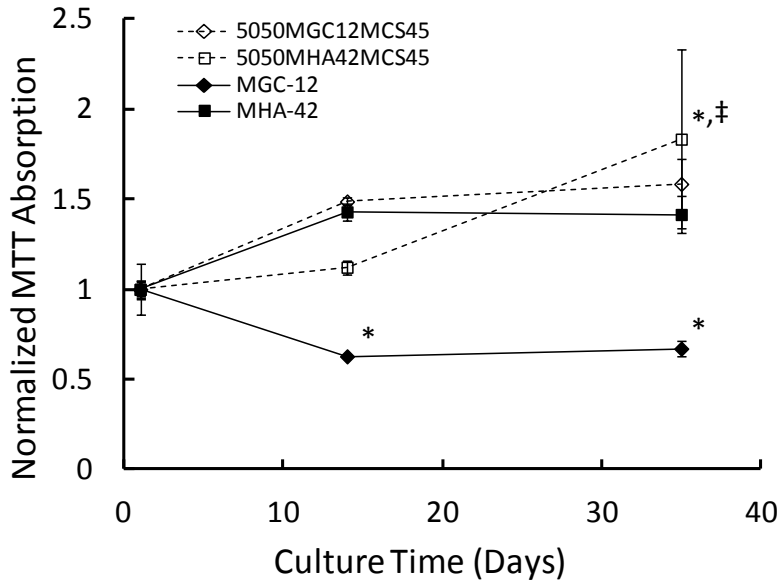

Figure 6.9: Relative change in metabolic activity of encapsulated chondrocytes over a 35 day *in vitro* static culture in hydrogels prepared with A) 6wtMGC-12 and 5050 MGC12MCS45 and B) 6wtMHA-42 and 5050 MHA42MCS45. Data was normalized to day 1 values. (*) Significant for all other gels at the specific time point, (‡) significant from all other time points for the specific gel ($p < 0.05$).

6.5 Discussion

In the current study, improvements to the methacrylic anhydride (MA) methacrylation reaction were initially conducted to produce modified hyaluronic acid (HA) and chondroitin sulfate (CS) prepolymers with predictable degree of substitutions and stable hydrogel properties (swelling) once cross-linked. Smeds *et al*. reported 3 – 17 % methacrylation of HA relative to the carbohydrate protons using a range of reaction times and excess amounts of MA. [91, 200] Similarly following this protocol, Burdick *et al*. reported 12 % methacrylation for a 50 kDa molecular weight HA using 20 fold excess of MA in a 1 % w/v HA solution and a 24 h reaction time. [203] However, the protocol suggested by Smeds *et al*. has been reported to be unpredictable and inconsistent in terms of the final degree of methacrylation, [92] a conclusion also supported by our

results (Table A.4). The unpredictable degree of methacrylation obtained with the longer, non-pH controlled MA reaction are a result of a rapid decrease in pH caused by the formation of methacrylic acid as a byproduct of the main reaction between MA and the hydroxyl groups on HA or CS and from a side reaction with water (Figure 6.1). Therefore, assuming the majority of the methacrylic acid was initially formed by the side reaction with the excess water, the lower reaction pH likely caused the hydroxyl groups on HA and CS to be less reactive to the MA molecules. In addition, the long reaction times at low pH conditions may have resulted in cleavage of the methacrylate groups and/or epimerization of the polysaccharide molecule. [218, 219] On the other hand, there is the possibility that maintaining a higher pH in the modified protocol could lead to hydrolytic cleavage of the polysaccharide backbone. [220, 221] However, no major differences were detected in the final solution viscosity when the long or short reaction protocols were used, whereas noticeable differences in the final degree of methacrylation and hydrogel stiffness were observed for the two different MA protocols (Table 6.1 and Table A.4). By reducing the reaction time and controlling the pH throughout the reaction, predictable degrees of methacrylation were achieved for both HA and CS (Figure 6.2). With higher degrees of methacrylation of the prepolymers, hydrogel physical properties increased in modulus and decreased in swelling, which is to be expected for a higher cross-link density. [94, 207] However, previous studies have not physically characterized the range of MGC, MHA and MCS hydrogels to the extent presented in this study.

The methacrylation reaction of glycol chitosan with glycidyl methacrylate (GMA) was previously optimized. [81] However, the decrease in solubility of the GMA modified MGC as the degree of methacrylation increased was an issue while preparing the prepolymers for cross-linking. Immediately after the methacrylation reaction, prepolymer solutions did not exhibit a noticeable difference in viscosity. Differences in viscosity of the prepolymer solutions only became apparent when re-dissolving the prepolymer after lyophilization. Given that this issue

was not present with the highly modified MHA-42 or -96 prepolymers, the reduction in MGC solubility with higher degree of methacrylation was likely due to methacrylate competition with the original glycol modification to make chitosan water-soluble at neutral pH. For this reason, the MGC prepolymers with reduced solubility would not form uniform hydrogel networks, which may explain the limited effect of the degree of methacrylation on the tunability of the MGC hydrogels equilibrium modulus and swelling behaviour. However, when the MGC hydrogels were tested under constant strain rates, noticeable trends were observed in the failure properties of the hydrogels. Therefore, a difference in the MGC hydrogels physical properties was only noticeable at higher strains, which may not occur at physiological loading. In addition to the limited tunability of the equilibrium properties of the MGC hydrogels, the lowest cell viabilities (55 – 67 %) and metabolic activities were observed in the different 6wtMGC hydrogels after 7 days in culture. Previous studies have reported 80 % cell viability for encapsulated chondrocytes over a 21 day culture, but in hydrogels with a much lower 2 % w/v prepolymer concentration and therefore lower moduli of approximately 5 kPa. [82] However, given that higher hydrogel modulus between 100 – 300 kPa was desired in this study, high prepolymer concentrations and degree of methacrylation were required to achieve the targeted equilibrium moduli. Therefore, further studies are required to improve the solubility of the higher methacrylated MGC-58 prepolymers and the viability of the encapsulated chondrocytes within all of the 6 % w/v MGC hydrogels.

In the case of the MHA and MCS hydrogels, whose mechanical properties could be controlled to a greater degree through the degree of methacrylation of the prepolymers, cell viability did not appear to be affected by hydrogel stiffness or swelling ratios. The 6wtMHA-14 hydrogels had the highest overall cell viability and metabolic activity followed by the much stiffer 6wtMHA-96 hydrogels after 7 days in culture. The higher cell response in the MHA hydrogels may be a result of the CD44 chondrocyte membrane receptor, which has been reported to have specific recognition and high interaction to HA. [211] The CD44 membrane receptors have

also been linked with the formation of, and anchorage to, a highly hydrated HA matrix surrounding the chondrocytes. [89, 222] These cell mediated improvements to the surrounding hydrogel may be related to the increased cell viability and metabolic activity observed with the MHA hydrogels. However, further work will be required to determine whether the higher metabolic activity is related to higher cell activity (e.g. motility, proliferation) and/or ECM production, which could also potentially lead to an increased hydrogel modulus. The stiffest MCS hydrogels, which were as high as 624.0 ± 48.4 kPa, also demonstrated high cell viabilities around 80 %, but relatively low metabolic activities. High equilibrium swelling in all of the MCS hydrogels, regardless of the degree of methacrylation resulted in increased distance between the cells from the original seeding density. The increase in cell-matrix distance in the highly swollen hydrogel network coupled with a lack of strong affinity between the cell membrane receptors of the encapsulated chondrocytes and chondroitin sulfate may have also played a role in the lower metabolic activity. [211] Therefore, in addition to the choice of polysaccharide materials and final mechanical properties of the hydrogels, future studies will need to examine the high MCS swelling effects on cell retention and ECM accumulation.

For the current study objectives, high modulus and minimal change in equilibrium mass were sought for the multiple polysaccharides examined, since unwanted changes in dimension could result in possible failure or loss of the scaffold in a LBST repair scenario. Testing the hydrogels mechanical properties near physiological conditions is beneficial in determining how the scaffold will perform under normal operating conditions. However, knowing the failure properties of the hydrogels at higher strains is also important as these properties will dictate when catastrophic failure and total loss of load bearing support will occur within the scaffold. All the hydrogels examined in this study displayed failure strains between 32 – 58 % when tested at constant strain rates. Even the lowest failure strain of 30 %, which was observed in the 20wtMCS-16 hydrogels, was still higher than most physiological strains the native tissue would

experience *in vivo*. For example, Park *et al*. reported physiological strains of 20 % for native cartilage under normal loading conditions. [175] Moreover, failure strains of approximately 30 % were reported for native cartilage in tension. [223] It should also be noted that the hydrogels were tested in unconfined compression, but *in vivo* some confinement would occur from the surrounding tissues. Therefore, the failure properties of the high modulus hydrogels reported in this study appear to be suitable for LSBT repair.

In order for a hydrogel to be successful in a LBST repair scenario, a high modulus was deemed necessary to bear the weight of the native tissue it will be replacing. Previous studies have investigated synthetic poly(ethylene glycol) (PEG) (diacrylates and dimethacrylates) prepolymers to produce cellular and acellular hydrogels with cartilage-like mechanical properties between 30 – 400 kPa and up to 2.46 MPa, respectively. [204, 224] Generally, molecular weights less than 5000 g/mol, and prepolymer concentrations between 10 – 40 % w/v were required to obtain these higher moduli. However, the PEG based hydrogels are non-degradable and require further modification with more natural and degradable components to improve their cellular interactions over time. [225] For example, blending PEG based hydrogels with MCS has been used to improve the activity of encapsulated chondrocytes or mesenchymal stem cells in LBST studies. [85-87, 214] Alternatively, natural prepolymers such as HA and CS have been used to encapsulate chondrocytes to maintain their phenotype and improve their behavior in terms of viability and ECM accumulation. [206, 226, 227] As mentioned earlier, the CD44 receptors to HA were proven beneficial to the encapsulated chondrocytes in terms of viability and metabolic activity. However, the higher molecular weights (between 1.5 – 5 MDa) and lower concentration (2 % w/v) of the MHA prepolymers have resulted in limited mechanical properties, generally below 100 kPa. [201, 228, 229] To achieve better mechanical properties from these natural prepolymers we have, in this study, used a modified reaction with methacrylic anhydride to improve the control of the degree of methacrylation achieved and examined higher prepolymer concentrations. In this manner, we

have produced single component hydrogels of 6wtMGC-12 and 6wtMHA-42 with moduli in a range of 100 – 165 kPa, which also exhibited a minimal change in cross-linked mass (± 10 %) after swelling. Blending the single component hydrogels with the lower molecular weight MCS-45 prepolymer at 50 % mass fraction further increased the moduli to between 175 – 250 kPa without sacrificing the swelling and failure characteristics of the hydrogels. Not only did the blending help improve the modulus over the single component hydrogels, but the blended hydrogels were also more conducive to the metabolic activity of the encapsulated chondrocytes. Blending with the 20wtMCS-45 prepolymer was particularly important for the 6wtMGC hydrogels, which had less tunability of the mechanical properties and inferior cellular behavior than the 6wtMHA based hydrogels. In the case of the MHA hydrogels, blending was also able to increase the modulus and enable metabolic activity to increase until the end of the culture period. Overall, the addition of MCS to each hydrogel was beneficial to the long term activity of the chondrocytes. This effect on cell behavior may be due to a cell protective property of chondroitin sulfate. Previous studies have demonstrated the addition of chondroitin sulfate to human articular chondrocytes was able to counteract the negative effect of interleukin - 1β, a cytokine involved with cartilage degradation, and was able to increase proteoglycan synthesis in culture. [230, 231] Chondroitin sulfate may have also played a protective role in improving the metabolic activity of bovine chondrocytes to *in vitro* environmental stresses (enzymatic, heat, mechanical compression, cytokine) meant to simulate *in vivo* joint stress. [232] Although, in our application chondroitin sulfate was part of the hydrogel network it was possible that it was still able to have a positive effect on the metabolic activity of the encapsulated chondrocytes. However, further work will be required to determine if these increases in cellular activity will result in sufficient ECM accumulation/localization within the hydrogel blends.

6.6 Conclusion

The method of methacrylation was shown to be important in producing a high quality prepolymer for the manufacture of tunable hydrogels. The methacrylic anhydride reaction with hyaluronic acid and chondroitin sulfate was improved by controlling the pH and shortening the reaction time. The final MHA and MCS prepolymers produced high modulus hydrogels with consistent and predictable degrees of methacrylation. It was also highlighted that there were many parameters specific for each material, such as molecular weight, prepolymer solubility, degree of methacrylation, and prepolymer concentration, to consider when tuning of the final hydrogel properties. The MGC prepolymer solution viscosity was affected by increased methacrylation, which impacted final mechanical properties. The MHA prepolymers were easily modified and offered the greatest range of hydrogel properties and the highest metabolic activity for encapsulated chondrocytes. The lower molecular weight MCS prepolymers produced the stiffest hydrogels, which also displayed the highest equilibrium swelling behavior. Blends of 6wtMGC-12 or 6wtMHA-42 with 20wtMCS-45 were able to improve mechanical properties and metabolic chondrocyte activity over the individual hydrogels. The targeted hydrogels were low swelling after cross-linking with moduli approaching that of native cartilage. Overall, we have shown that these high modulus hydrogels synthesized from natural polysaccharides offer a wide range of materials and modifications that are suitable for cell encapsulation and show great promise for use in load bearing soft tissue engineering.

Chapter 7

Primary Bovine Chondrocytes Maintain a Cartilage-Like Modulus Following Photo-Encapsulation in Methacrylated Hyaluronic Acid and Chondroitin Sulfate Hydrogel Blends

7.1 Completed Objectives

The work in Chapter 7 was to expand on the preliminary hydrogel studies conducted in Chapter 6 in order to meet Objective 4 (§ 3.2.4), which was to optimize the encapsulated chondrocyte phenotype in a high modulus hydrogel blends. The work in this chapter will be submitted to Biomacromolecules where I will be the first author as all experiments were designed and conducted by myself.

In this study, chondrocyte-seeded photo-cross-linked hydrogels were cultured *in vitro* over 35 days to assess their suitability for load bearing soft tissue repair. These hydrogels were prepared from prepolymer solutions containing methacrylated glycol chitosan (MGC) or methacrylated hyaluronic acid (MHA) and blends of these prepolymers with methacrylated chondroitin sulfate (MCS). The hydrogel blends were composed of 50 % mass fractions of each prepolymer. The photo-cross-linked hydrogels had initial equilibrium moduli between 100 - 300 kPa, which was deemed suitable for the repair of LBST. All hydrogels demonstrated a decrease in cellularity with time in culture; however, the MHAMCS blended hydrogels retained the highest cellularity, with close to 60 % viable cells remaining after 35 days. Visually, the remaining chondrocytes in the MHAMCS hydrogels expanded into well distributed multi-cellular aggregates. The pericellular-like matrices surrounding these aggregates were cartilaginous, containing aggrecan and collagen II. Additionally, the MHAMCS hydrogels maintained their modulus and increased in volume over the 35 day culture period. While the MGCMCS hydrogels also had a relatively constant modulus during culture, these hydrogels displayed poor

extracellular matrix accumulation and cell retention, with less than 10 % of the cells remaining after 35 days. This study demonstrates the potential of co-cross-linking MCS with MHA to form a hydrogel blend for use in a reparative LBST construct.

7.2 Introduction

Load bearing soft tissues (LBST), such as the articular cartilage and nucleus pulposus, are susceptible to age related changes and damage from physical injuries as these tissues do not mount an effective reparative response. [121, 138, 194, 195] Current surgical approaches for symptomatic joints include total joint arthroplasty (TJA) using permanent hardware. [32] However, limited lifetime of the implant, improper placement of the device, and potential infections can limit their long-term utility. [196, 197] Therefore, a cell based repair strategy to fill the defect at an earlier stage in the disease process could provide a much needed regenerative repair option. [40, 100, 233] One such approach that has potential to be both load bearing and regenerative is the use of cell-seeded photo-cross-linkable hydrogels. [71, 234]

The two main design criteria for a hydrogel, specific for LBST repair, are an appropriate modulus and high cellularity after cross-linking. Equilibrium compressive moduli have been reported to be between 500 – 1000 kPa for human articular cartilage depending on age and degree of degradation. [138, 198] Similarly, the confined aggregate modulus has also been reported to be between 440 ± 190 to 1010 ± 430 kPa for the degenerated and healthy human nucleus pulposus, respectively. [199] However, the means to achieve both criteria in a single component hydrogel often requires conflicting prepolymer parameters. For example, the use of higher prepolymer concentration with the maximum conjugation of photo-reactive groups ensures superior gel stiffness while the opposite conditions are generally required to improve cell viability and matrix production. Callahan *et al*. formed hydrogel gradients with moduli and swelling ratios that ranged between 1.7 to 6.5 kPa and 13 to 8, respectively, by cross-linking RGD-modified poly(ethylene

glycol)-dimethacrylate prepolymer solutions from 10 to 30 % w/v concentration. They reported that the lower modulus hydrogels (i.e. 1.7 vs. 6.5 kPa) were better at maintaining the phenotype and synthetic potential of chondrocytes isolated from the cartilage of patients undergoing total knee arthroplasty. [235] Chung *et al*. investigated photo-cross-linkable methacrylated hyaluronic acid (MHA) hydrogels with prepolymer concentrations ranging from 2 to 20 % w/v MHA. The 2 % w/v MHA prepolymer concentration produced hydrogels with moduli of 11 kPa and a swelling ratio of 42. The lower modulus 2 % w/v MHA hydrogels were beneficial in maintaining higher cell viability and accumulation of extracellular matrix than the stiffer 5, 10 and 20 % w/v MHA hydrogels with moduli ranging between 26 to 100 kPa. [95] Although the focus of those studies was to maintain high cell viability and chondrocyte phenotype within the hyaluronic acid hydrogels, it is questionable whether the low initial modulus of the 2 % w/v MHA hydrogels would be suitable for the actual repair of a LBST defect. However, with culture times between 1 – 2 months, there is potential for cell growth and ECM accumulation to increase the moduli of 1 – 2 % w/v MHA hydrogels closer to 100 kPa with chondrocytes, and to as high as 1 MPa with bone marrow derived mesenchymal stem cells. [65, 68, 96, 205] Nevertheless, the required time frame is unsuitable for an in situ repair scenario. The large swelling ratios generally associated with low modulus hydrogels is also a major concern for an implantable load bearing scaffold. Large changes in the hydrogel dimensions could lead to altered mechanical properties and cell behavior, and a higher likelihood of implant failure with the surrounding tissue. [73, 207, 236]

Producing a hydrogel with a modulus in the range of native LBSTs is not difficult; however, producing one that can also encapsulate viable and active cells can be challenging. Few studies have explored this need for a cell encapsulating hydrogel to match the mechanical properties of LBSTs. One approach is to utilize a high prepolymer solution concentration. For example, Bryant *et al*. utilised high concentrations (10 – 30 % w/v) of 3400 g/mol poly(ethylene glycol) dimethacrylate (PEGDM) to produce cellular hydrogels with moduli between 30 to 400

kPa and swelling ratios between 12.6 to 5.2 to mimic the properties of native cartilage. [204] Chondrocytes within the lower modulus hydrogels with swelling ratios greater than 7.9 produced a uniform distribution of GAG as opposed to the localized lacunae staining in the stiffer hydrogels after 4 weeks in culture. [204] To enhance the distribution of ECM with time in culture, hydrolytically degradable lactide linkages were added to the otherwise non-degradable PEGDM network. However, the effects of extracellular matrix (ECM) accumulation and distribution on the hydrogel modulus with time was not reported. [204]

Another method to improve a hydrogel's mechanical properties is to co-cross-link a high molecular weight prepolymer with a lower molecular weight component to increase the cross-link density. Khanlari *et al*. examined 13 % w/v solutions of a 20-30 kg/mol methacrylated chondroitin sulfate (MCS) prepolymer with a 34 % degree of methacrylation as the primary material and 0.6 mol % of a 700 g/mol poly(ethylene glycol) (PEG) diacrylate to produce stiff, low swelling, hydrogels. The addition of the PEG diacrylate cross-linker lowered the swelling ratio of the MCS hydrogels from 45 to 13 and increased the modulus from 142 to 785 kPa. [84] However, low molecular weight PEG diacrylates are known to be cytotoxic. [237] Another study by Lee *et al*. investigated alginate with a molecular weight of 1.7×10^5 g/mol as the primary material with different molecular weights and concentrations of a covalent PEG diamine cross-linker. Increasing the concentration of either a 1000 or 3400 g/mol PEG diamine cross-linker resulted in a maximum modulus of 37 and 30 kPa and swelling ratios of 78 and 198, respectively. [213] Although adequate control over the hydrogels mechanical properties was demonstrated, the maximum moduli were too low for our intended purpose. Moreover, the large swelling ratios and lack of natural enzymes in the body that can degrade alginate, may limit their use as a repair device for LBST.

Other studies have also used blending to incorporate polymers that can enhance the viability and biosynthesis of the encapsulated cells. For example, chondroitin sulfate, when

blended and cross-linked into PEG based hydrogels, increased the proliferation of the encapsulated chondrocytes in addition to the accumulation of extracellular matrix over a 6 week period. [214] However, the initial cell viability and the hydrogel compressive moduli decreased from 97 to 55 % and 130 to 91 kPa after 6 weeks in culture, respectively. [87] In another study, Varghese *et al*. demonstrated that the MCS cross-linked into PEG hydrogels could be degraded by encapsulated mesenchymal stem cells, which then allowed for the formation of cartilage-like outgrowths on the surface of the hydrogels. [86] Bryant *et al*. also used MCS to increase modulus and swelling, and to act as degradable linkages in poly(vinyl alcohol) (PVA) hydrogels. [85] The potential issue with these approaches is the use of non-degradable synthetic polymers (PEG or PVA) that typically have a low degree of interaction with the encapsulated cells requiring the need to graft ECM derived components to the prepolymers to enhance their bioactivity. [238] A few studies have examined hydrogels prepared from blends of extracellular matrix specific polymers to allow for an improved cellular response and a greater chance of complete scaffold regeneration. Guo *et al*. demonstrated the potential of photo-cross-linking methacrylated hyaluronic acid and chondroitin sulfate in the presence of a self assembled collagen network to increase the overall modulus to a maximum of 40 kPa. [226] Levett *et al*. used a completely photo-cross-linkable mixture of methacrylated gelatin, chondroitin sulfate and hyaluronic acid to produce hydrogels with an initial modulus close to 50 kPa. The addition of hyaluronic acid to the gelatin hydrogels enhanced chondrogenesis and matrix distribution, which also corresponded to an increase in the hydrogels modulus up to 150 kPa after 8 weeks in culture. [206] Although these results are encouraging, the initial moduli of these hydrogels were low relative to native load bearing tissues and insufficient for immediate load bearing following implantation.

To form hydrogels with moduli closer to those of load bearing soft tissues, we previously proposed the use of co-cross-linked blends composed of 100 kg/mol methacrylated hyaluronic acid (MHA) or methacrylated glycol chitosan (MGC) with 50 kg/mol methacrylated chondroitin

sulfate (MCS). The hydrogel blends, composed of 50 % mass fraction of each prepolymer, possessed equilibrium moduli of 200 ± 100 kPa and minimal equilibrium swelling after cross-linking. [239] In this study, primary bovine articular chondrocytes were photoencapsulated within these blends and cultured over a 35 day *in vitro* static culture. The goal was to assess the suitability of the hydrogel blends for use in a load bearing soft tissue repair application by examining the modulus, cellularity and extracellular matrix accumulation with time in culture. A hydrogel that can maintain an active cell population in a high modulus environment would benefit the design of an *in situ* load bearing device for the repair and regeneration of cartilaginous soft tissues.

7.3 Methods and Materials

7.3.1 Materials

High purity (99.8 %, HPLC) sodium hyaluronate produced by microbial fermentation (M_n = 116 kg/mol, $Đ$ = 1.3) was obtained from Lifecore Biomedical (St. Paul, MN, USA) and used as received. Chondroitin sulfate (≥ 90 %) from bovine ($M_n \approx 50$ kg/mol) was purchased from LKT Laboratories (St. Paul, MN, USA) and used as received. Glycol chitosan (M_n = 93 kg/mol, $Đ$ = 1.2 and 60 % purity) was obtained from Wako Chemicals (Richmond, VA, USA) and purified by dialysis with 50 kg/mol MWCO tubing and lyophilized prior to use. Collagen type I antibody (mouse anti-bovine, ab90395) was obtained from Abcam (Cambridge, MA, USA). Collagen type II (mouse anti-bovine II-II6B3) and aggrecan (mouse anti-bovine 1C6s) primary antibodies were obtained from the Iowa Hybridoma Bank (University of Iowa). All other materials were obtained from Sigma-Aldrich (Oakville, ON, Canada) and were used as received unless otherwise noted.

7.3.2 Prepolymer Synthesis and Characterization

N-Methacrylated glycol chitosan (MGC) was prepared according to previously published work. [81] Briefly, glycol chitosan was dissolved in Type I water at 2 % w/v and reacted with 0.1 molar equivalents of glycidyl methacrylate to the repeating monomer unit of glycol chitosan. The reaction was initially adjusted to pH 9 with 1 M NaOH and allowed to react for 24 h at room temperature with constant stirring. The MGC solution was purified by dialysis in 50 kDa MWCO tubing with water and membranes changed twice during a 4 h period. The purified products were lyophilized and stored at -20 ˚C.

Methacrylated hyaluronic acid and methacrylated chondroitin sulfate were prepared by dissolving at 2 % w/v in Type I water and reacted at 5 and 10 molar equivalents of methacrylic anhydride to the repeating dimer units of the prepolymers, respectively. The reactions were conducted at room temperature for 1 h with constant stirring while maintaining the pH at 9 with the addition of 5 N NaOH throughout the reaction. The prepolymer solutions were purified by precipitating in 100 % ethanol, followed by dissolution in Type I water and dialysing with 14 kDa MWCO tubing for a total of 2 days with multiple water changes. After dialysis, the solutions were neutralized with 1 M NaOH before lyophilization and storage at -20 ˚C.

^{1}H NMR spectra of the prepolymers were collected on a Bruker Avance-400 MHz spectrometer from 0.7 mL samples dissolved at 20 mg/mL in deuterium oxide. The degree of *N*-methacrylation of glycol chitosan (GC) was confirmed by ^{1}H NMR analysis, and calculated based on the number of *N*-methacrylated monomer units. [150] The ratio of the integrated signal of the vinyl protons on the *N*-methacrylate group (average of the chemical shifts at δ = 6.2 and 5.9 ppm) over the integrated signals for the C1 protons present on every glycol chitosan residue (δ = 5.1 ppm) was used to calculate the degree of methacrylation. The degree of methacrylation for hyaluronic acid and chondroitin sulfate was similarly confirmed by ^{1}H NMR analysis following the method used by Van Vlierberghe *et al.* [216] The ratio of the integrated signals associated with the methyl protons on the methacrylate group (δ = 2.0 ppm) over the methyl protons from the N-

acetyl groups on each repeating dimer at δ = 1.9 ppm was used to calculate the degree of methacrylation. The vinyl protons (δ = 6.1 and 5.7 ppm) were used to determine the methacrylate contribution to the two overlapping methyl signals.

7.3.3 Cell Isolation and Hydrogel Fabrication

Primary chondrocytes from the articulating surfaces of bovine metacarpal joints were isolated as described previously. [150] The prepolymer solutions were dissolved (% w/v) in Ham's F12 culture medium with Irgacure 2959 photo-initiator (0.1 % w/v final concentration). Prepolymer solutions were mixed manually with a spatula in a 2 mL micro-centrifuge tube until completely dissolved. If necessary, a final centrifugation (100 g for 10 s) step was used to facilitate the removal of entrapped air bubbles. Cellular hydrogels were made by mixing concentrated cell and prepolymer suspensions, both in F12 culture medium, to obtain a final cell concentration of 4 x 10^7 cells/mL and the desired prepolymer concentration. Ham's F12 solution was used in place of the cellular suspension to produce the acellular scaffolds of the same prepolymer concentration as the cellular scaffolds. A cylindrical Teflon tube was used to fabricate the hydrogels (3.2 mm I.D. and 2.2 mm height). The molds were placed on a glass coverslip, the solution was transferred by pipet to the molds in excess and another coverslip was placed on top and clamped using a two pronged clip, which left the top and bottom view of the mold exposed. The whole assembly was then secured between two light guides placed 1 cm axially from each end of the mold (intensity at base of the mold = 10 mW/cm^2) and photo-cross-linked for 60 s by exposure to UV light filtered at 320 – 390 nm. The hydrogels formed were then transferred to a 24 well culture plate containing 2 mL of Ham's F12 culture media supplemented with 10 % fetal bovine serum (FBS), 0.1 % ascorbate and 1 X antibiotics/antimycotics. Acellular and cellular hydrogels were maintained in culture in an incubator at 37 ˚C with an atmosphere supplemented

with 5 % CO_2 and 95 % relative humidity. Media were changed every other day for up to 35 days.

7.3.4 Mechanical Characterization

Throughout the 35 day culture, both acellular and cellular scaffolds were harvested at 1, 14 and 35 days for mechanical testing. Prior to mechanical testing, the hydrogels were weighed and their heights and diameters were measured at different locations with digital calipers. The measured dimensions of the hydrogels were used to calculate their apparent volume. Compressive stress relaxation measurements were conducted on both the acellular and cellular hydrogels to determine their equilibrium modulus values (n = 4 – 5). Testing was performed on a micro-mechanical tester (MACH-1, Biomomentum Inc. Laval, QC) equipped with a 1 kg load cell all housed in a 37 ˚C incubator. Unconfined scaffold samples (3.2 mm diameter x 2.2 mm height) were immersed in a Ham's F12 culture medium bath with a solid base and moving upper platen (1 cm diameter each). Stress relaxation tests were conducted at 2 % strain increments, to a total strain of 20 %. Step strains were applied at a rate of 6 %/s. The resulting force decay was recorded until equilibrium was reached, which was defined as a change in force of less than 0.2 g/min. The equilibrium modulus was obtained from the slope by linear regression of the linear region of the decayed stress versus applied stain curve (10 – 20 % strain).

The measured volumes of both the cellular and acellular hydrogels were used to determine the percent change from the original mold volume (17.7 mm^3) with time in culture (n = 5). The hydrogel mass was also tracked with time in culture and swelling ratios (q) were calculated from the ratio of the wet mass over dry mass. Equilibrium water content was calculated as the difference in equilibrium wet mass and dry mass over the equilibrium wet mass (% w/w).

7.3.5 Analysis of Cellularity and Extracellular Matrix Accumulation

Cell tracking near the surface of the hydrogels was accomplished by staining the chondrocytes using the PKH26 (Sigma) membrane dye prior to encapsulating within the different hydrogels. The dye was applied to the cells following the manufacturer suggested protocol. For this purpose, cells (10×10^6 cells) were re-suspended in 1 mL of the supplied Diluent C and mixed with 1 mL of the PKH26 dye (4×10^{-6} M) solution. Cells and dye were incubated for 5 min and stopped by adding 2 mL of 10 % FBS supplemented Ham's F12 medium. The stained cells were centrifuged at 700 g for 5 min and the supernatant was aspirated leaving the cell pellet undistributed. The cell pellets were re-suspended in their respective prepolymer solutions at the required cellular concentrations and cross-linked according the protocols described above. The hydrogels were cultured for up to 35 days in culture and imaged as cultured at 1, 14 and 35 days. Fluorescent images were taken on a FluoView FV1000 laser scanning confocal microscope (inverted) using the 10x objective and FV10-ASW software (Olympus America Inc. Center Valley, PA). The entire surface of the hydrogel was scanned up to a maximum depth of 200 μm at 10 μm slices in the z-direction. The FV10-ASW Olympus software was used to compile stitched mosaic images, which were compressed for the entire z-stack depth.

Cell numbers within the centre of the hydrogels were counted from the 8 μm paraffin embedded hydrogel sections, which were used for immunohistochemistry. Cell nuclei stained with DAPI were imaged under a Zeiss Imager M1 fluorescent microscope. Images were counted for cells using ImageJ software over a 0.25 mm^2 area and the total cellular area was divided by an average cell size to account for multi-cell aggregates at the later time points. A total of 4 areas from 4 separate sections were used to count the cells for the full depth of the section. The data was normalized to day 1 values for each hydrogel over a 1, 14 and 35 day culture period.

Assays for sulfated glycosaminoglycan (GAG), collagen and DNA contents were performed on entire acellular (controls) and cellular scaffolds ($n = 5 – 6$) at days 1, 14 and 35.

Samples were removed at the designated time points and stored at -85 ˚C until analysis. The fresh frozen samples were thawed, individually crushed, and digested by papain (80 mg /mL in 0.020 M ammonium acetate, 10^{-3} M ethylenediaminetetraacetic acid and 2 x 10^{-3} M dithiothreitol all in type-1 water) for 3 days at 65 ˚C. The supernatant was collected and used in the following biochemical assays. DNA content was measured using the Hoechst 33258 dye-binding assay. [134] Sulfated GAG content in the papain digest was measured using the dimethylmethylene blue (DMMB) absorbance assay. [135] Collagen content was determined from the hydroxyproline (OH-pro) assay assuming that OH-pro accounted for 10 % of the total collagen mass. [136] OH-pro was measured using a chloramine T and Ehrlich's reagent assay after hydrolysis in 6 N HCl at 110 ˚C for 18 h. [137]

7.3.6 Immunohistochemical Staining

Hydrogels were harvested after 1, 14 and 35 days of culture and fixed in 4 % paraformaldehyde for 24 h followed by paraffin embedding. Sections for each hydrogel were cut at 8 µm using a rotary microtome (Thermo Scientific, Shandon Finesse ME+) and mounted on superfrost™ plus slides. Sections were de-paraffinized in toluene and hydrated using graded series of ethanol solutions. The sections were then immunostained with antibodies for collagen type I, collagen type II and aggrecan. For the aggrecan staining, the sections were pre-treated with a 10 mM dithiothreitol reducing solution for 2 h at 37 ˚C, 40 mM iodoacetamide alkylating solution for 1 h at 37 ˚C, and 0.25 U/mL chondroitinase ABC antigen retrieval solution for 1 h at 37 ˚C. For the collagen staining, the sections were pre-treated for 30 min at 37 ˚C with a 0.05 % trypsin solution for antigen retrieval. All sections were then blocked for 30 min with 1.5 % v/v horse serum (S-2000, Vector Labs, Burlington, Ontario). Sections were rinsed with 1 X PBS and the appropriate primary antibodies were added for overnight incubation in a humid chamber at 4 ˚C at the following dilutions: collagen type I antibody (ab90395) at a 1:100 dilution, collagen

type II (II-II6B3) at a 1:10 dilution, and aggrecan (1C6s) antibody at a 1:10 dilution. Following primary antibody incubation, Texas red conjugated secondary antibodies (TI-2000, Vector Labs) were added at 1:100 dilution in a 2 % w/v BSA solution for 2 h. Negative controls were prepared by substituting the primary antibody with additional blocking using the appropriate host sera. After staining, a drop of Vectashield® mounting media containing DAPI (H-1200, Vector Labs) was added to each section and finally mounted with a coverslip. The sections were visualized immediately after staining using a Zeiss Imager M1 fluorescent microscope equipped with an AxioCam Mrm camera and Axiovision Rel. 4.7 software.

7.3.7 Statistical Analyses

All results are expressed as the mean ± the standard deviation and were analyzed using statistical software (SigmaStat 1.0, SPSS Science, Chicago, IL). Physical, biochemical, and mechanical characterization results as a function of time were analyzed using a 2-way ANOVA and the Fisher's LSD post-hoc test with pairwise comparisons. Significance was associated with p values less than 0.05.

7.4 Results

7.4.1 Prepolymer Characterization

The degree of methacrylation of the glycol chitosan was 6 %, while the degree of methacrylation of the hyaluronic acid and the chondroitin sulfate was 42 and 45 %, respectively. These degrees of methacrylations were chosen to provide hydrogels with a targeted equilibrium modulus of 200 ± 100 kPa and minimum equilibrium swelling after cross-linking for solution concentrations of 6 % w/v for MGC and MHA, and 20 % w/v for MCS, based on our previous work. [239]

7.4.2 Degree of Swelling in Culture

The MGCMCS and MHAMCS blends along with single component hydrogels made with MGC or MHA were cultured *in vitro* under static conditions for 1, 14 and 35 days. The change in equilibrium volume from the original mold dimensions at each time point is reported in Table 7.1, for the blended and single component hydrogels. The acellular and cellular MGCMCS hydrogels decreased in volume from the original mold dimensions at day 1 and with the exception of the acellular MGCMCS day 14 value, did not change after 35 days in culture. The acellular MHAMCS hydrogels increased approximately 20 % in volume from the original volume of the cross-linking mold after 1 day in culture. Following this initial increase in volume only the day 14 volume was significantly higher than the day 1 values. The volume of the cellular MHAMCS hydrogels increased significantly with time at day 14 and 35 to a maximum value of 31 % of the original mold dimensions (Table 7.1). The increase in the cellular MHAMCS hydrogels was significantly higher than the acellular MHAMCS at days 14 and 35 of the culture.

The single component MGC and MHA hydrogels were also examined to monitor the effect of time in culture on their change in volume (Table 7.1). The MGC hydrogels markedly decreased in volume with time, by up to 42 % at the end of the culture period. The reduction in volume was significantly suppressed with the addition of chondrocytes at days 14 and 35 of the culture. The cellular MGC gels reached a 24 % reduction in size by day 35. By contrast, the day 35 acellular and cellular MHA hydrogels were only slightly lower in volume, by 3 and 0.5 %, respectively, from the volume of the molds (Table 7.1).

Table 7.1: Change in acellular and cellular hydrogel volume between equilibrium and original mold dimensions (%) for the single component and blended hydrogels over a 35 day culture period. (*) Significant from other points with respect to time, (†) significant from day 1 values, (‡) significant between acellular hydrogel at respective time point ($p < 0.05$).

		Change from Mold Volume (%)	
Hydrogel	Culture Time (Day)	Acellular	Cellular
MGCMCS	1	-11.1 ± 10.3	-16.6 ± 3.4
	14	-17.9 ± 1.5†	-12.7 ± 1.9
	35	-16.8 ± 3.9	-16.9 ± 2.3
MHAMCS	1	16.1 ± 5.8	20.2 ± 2.5*
	14	21.1 ± 1.1†	25.2 ± 3.2*
	35	20.7 ± 4.1	30.7 ± 1.7*,‡
MGC	1	-11.5 ± 1.6*	-13.8 ± 1.2*
	14	-29.2 ± 2.7*	-20.1 ± 0.7*,‡
	35	-41.9 ± 2.3*	-24.2 ± 2.2*,‡
MHA	1	-8.7 ± 5.2	-6.5 ± 2.5
	14	-6.0 ± 3.8	-2.0 ± 2.6†,‡
	35	-3.0 ± 1.5†	-0.5 ± 2.4†

Swelling ratios and equilibrium water content (EWC) for the cellular MHA (single component or blended) hydrogels were greater than the MGC (single component or blended) hydrogels at each time point (Figure 7.1). Moreover, the single component hydrogels had slightly higher swelling ratios and EWC compared to their respective blends for most of the culture. The cellular MHA and MHAMCS hydrogels' swelling ratios and equilibrium water contents remained relatively stable over the 35 day culture period. The single component MGC hydrogels displayed significant decreases in their swelling ratios and EWC after day 1 (Figure 7.1 (A and B)). A significant drop from the day 1 values was also observed in the EWC of the MGCMCS hydrogels by the end of the culture (Figure 7.1 (B)).

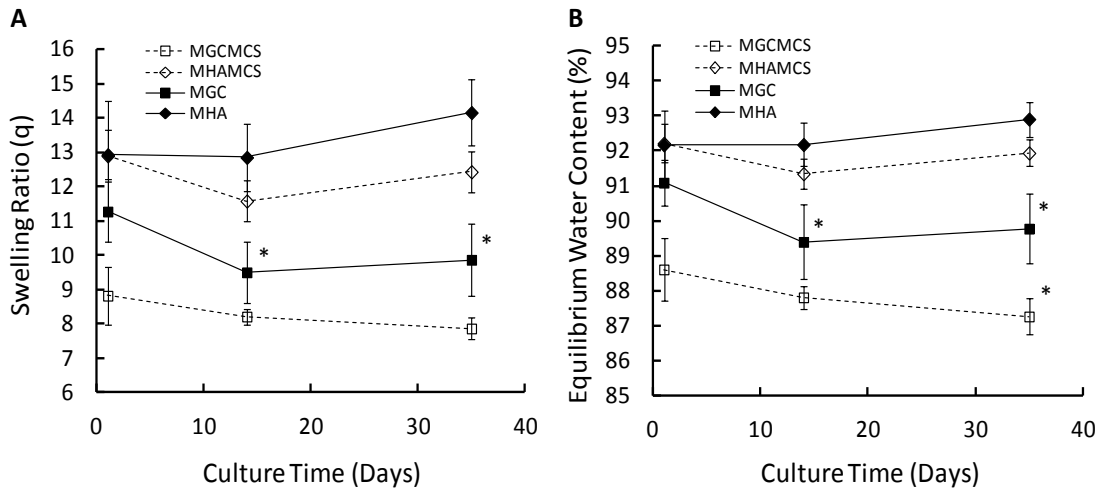

Figure 7.1: Cellular swelling ratios and equilibrium water contents for the single component (MGC and MHA) and blended (MGCMCS and MHAMCS) hydrogels with time in culture. (*) Significant from day 1 value ($p < 0.05$).

7.4.3 Hydrogel Modulus with Culture Time

The initial equilibrium modulus for both the cellular and acellular MGCMCS hydrogels was slightly less than 200 kPa (Figure 7.2 (A)). A significant decrease in the original modulus was observed for the acellular MGCMCS hydrogels at day 14, but by day 35 the modulus was comparable to the day 1 values. The modulus of the cellular MGCMCS hydrogels did not change with time. However, at day 14 and day 35 the differences between the two groups were significant. The initial modulus of 250 kPa for the cellular MHAMCS hydrogels was maintained throughout the 35 day culture (Figure 7.2 (B)). A significant decrease in the acellular MHAMCS day 1 modulus was observed at days 14 and 35. The modulus for the cellular MHAMCS hydrogels was both significantly higher than their acellular controls at day 14 and day 35. The effect of time and cells was significant in increasing the modulus of the cellular MHAMCS hydrogels at day 35 when compared to the day 1 values.

The MGC hydrogels had the lowest initial equilibrium modulus of around 100 kPa, which significantly increased at days 14 and 35 (Figure 7.2 (C)). The cellular MGC hydrogel moduli were also significantly higher than those of the acellular hydrogels at days 1 and 35. However, no significant interactions were observed between cellularity and time for the MGC hydrogels. The cellular MHA hydrogels maintained a constant equilibrium modulus close to 200 kPa for the entire culture period, which was significantly higher than the acellular controls at day 35 (Figure 7.2 (D)).

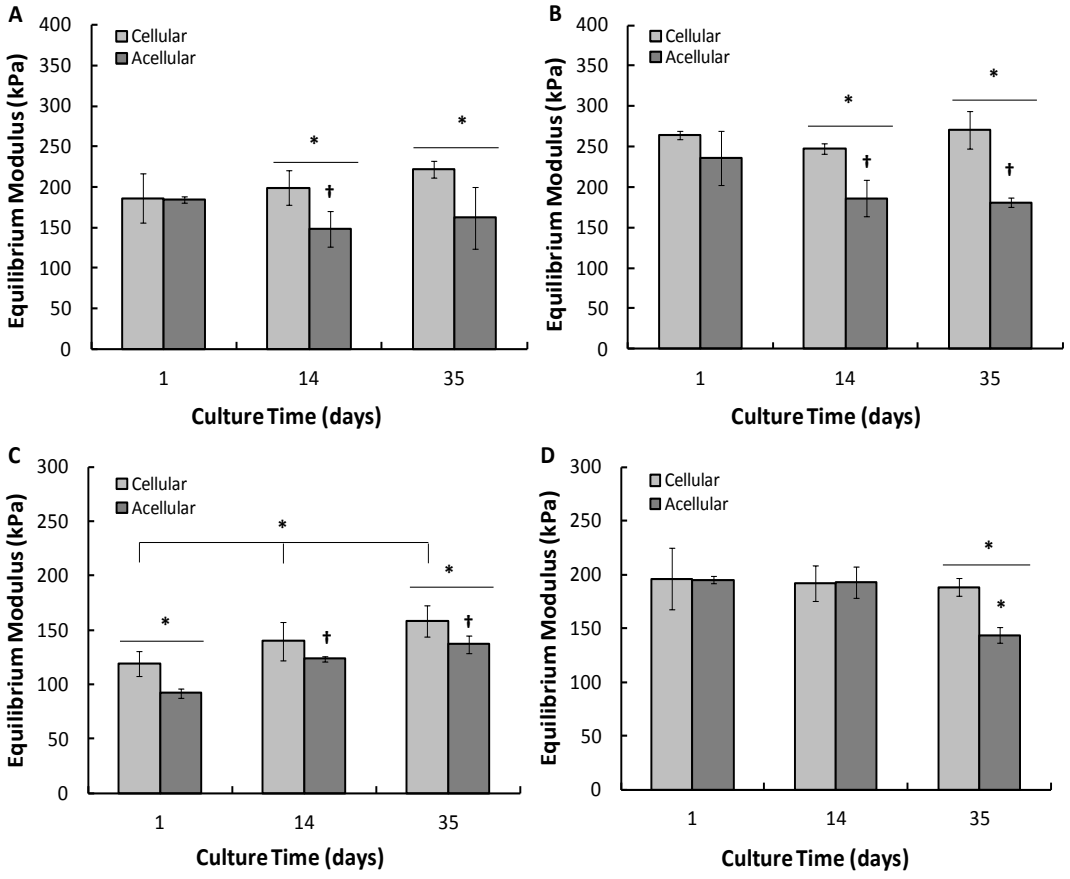

Figure 7.2: Equilibrium modulus of acellular and cellular scaffolds over a 35 day culture period for A) MGCMCS and B) MHAMCS blended hydrogels along with single component hydrogels C) MGC and D) MHA (*) Significant from other points within the group, (†) significant from day 1 values ($p < 0.05$).

7.4.4 Sub-Surface Cell Distribution in the Hydrogels

Large scale mosaic-stitched images of the entire gel surface, at a depth of 200 μm, were used to monitor the location and distribution of PKH26 labeled chondrocytes over a 35 day culture period (Figure 7.3). The PKH26 stain intensity is halved with each cell division, therefore areas that appeared to be cellular, but which did not fluoresce, were assumed to be a result of highly proliferative cell growth. By day 14 chondrocytes in the MGCMCS hydrogels formed what appeared to be areas of non-stained cellular aggregates just below the surface (Figure 7.3 (A)). With an additional 3 weeks in culture, an interconnected network of the non-stained cellular aggregates could be observed on the surface of the MGCMCS hydrogels. Individually stained cells could still be observed below the surface of the hydrogel not masked by the cellular outgrowths. The MHAMCS hydrogels did not have any noticeable cellular outgrowths on their surfaces, but appeared to form stained cell clusters within the hydrogels after 35 days of culture (Figure 7.3 (B)). For the single component hydrogels, the decrease in size of the MGC hydrogels with time was observable from the PKH26 images (Figure 7.3 (C)). With the observed decrease in MGC hydrogel size, an increase in stained cell intensity was likely due to a higher cell density. In addition, strong background fluorescence was apparent in the non-cellular regions of the shrinking MGC hydrogels, which was most noticeable at day 35. No apparent changes in cell density or distribution were observed in the MHA hydrogels with time (Figure 7.3 (D)).

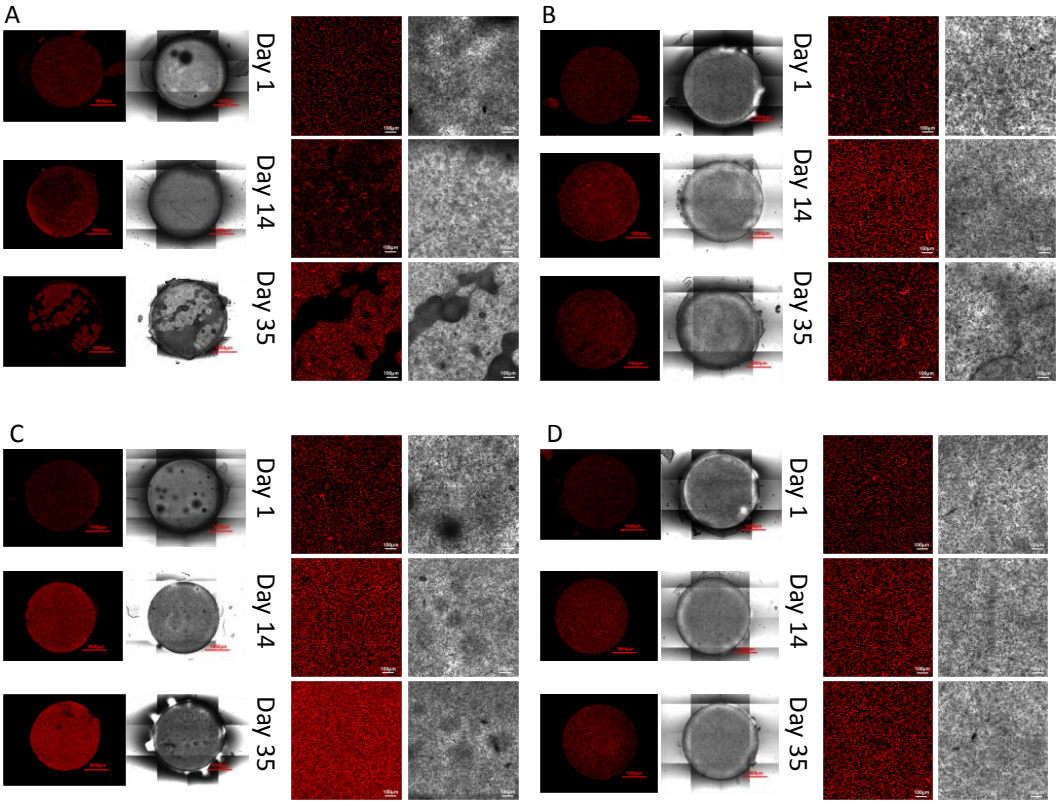

Figure 7.3: Encapsulated chondrocytes pre-stained with PKH26 cell tracker (red). Fluorescent and DIC confocal images for the blended hydrogels A) MGCMCS and B) MHAMCS along with the single component hydrogels C) MGC, darker spots in day 1 brightfield images were due to bubbles and D) MHA. Mosaic images of full hydrogels (left) with 1000 µm scale bar (red) and 100 X images (right) with 100 µm scale bar (white).

7.4.5 Cellularity within the Hydrogels

Limitations in depth penetration with the confocal laser scanning microscope prevented the tracking of the cells through the entire depth of the hydrogels. Therefore, the cellularity within each hydrogel was also investigated by imaging DAPI stained nuclei within hydrogel sections (Figure 7.4). In a previous study, we demonstrated that the MGCMCS, MHAMCS, MGC and MHA hydrogels were able to maintain 90.4 ± 8.2, 96.5 ± 3.3, 72.6 ± 9.2 and 83.0 ± 5.5 % of the number of cells originally seeded cells, respectively. [239] After photo-encapsulation and 24 h of

culture, the chondrocytes were shown to be evenly distributed in all of the hydrogels (Figure 7.4 (Day 1)). A marked reduction in the cell density was observed in both the MGCMCS and MGC hydrogels over the 35 day culture (Figure 7.4 (MGCMCS and MGC)). The few cells that were remaining after 35 days appeared to be in small rounded clusters. On the other hand, the cells within the MHAMCS and MHA hydrogels appeared to change from being isolated and individual at day 1 to large, multi-cell clusters by day 35. The number of these enlarged cellular clusters in the MHA based hydrogels decreased with time, but remained well distributed throughout the sections (Figure 7.4 (MHAMCS and MHA)).

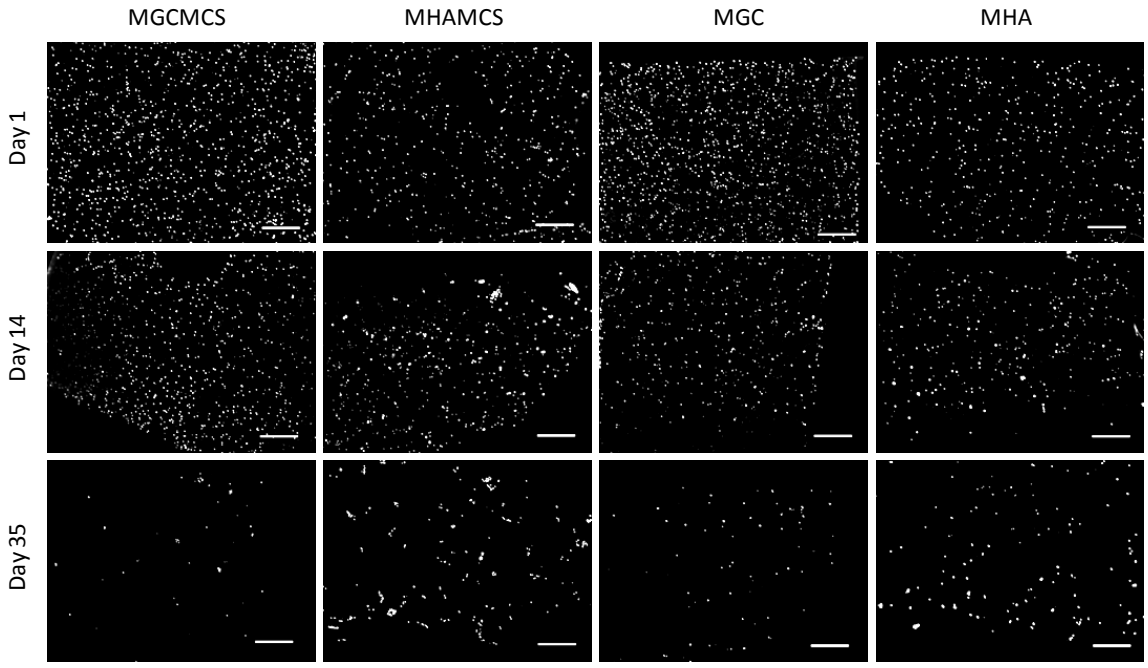

Figure 7.4: DAPI images (cells highlighted in white) from hydrogel sections for all single component and blended hydrogels over 35 days, highlighting cell localization and tracking movement/growth patterns. Images were taken at 100 X magnification, 200 µm scale bar.

The cellularity of the hydrogels was calculated from the DAPI images shown in Figure 7.4. All the hydrogels demonstrated a significant drop in cellularity with time (Figure 7.5). The

MHAMCS hydrogels maintained the highest cellularity over the entire culture as compared to the other hydrogel compositions, with approximately 60 % of the cells present at day 1 remaining at 35 days. The single component MHA hydrogels maintained a higher cellularity than the single component and blended MGC hydrogels by the end of the culture. Although chondrocytes were present on the surface of the MGCMCS hydrogels, as determined from the PKH26 images, the internal cell numbers by day 35 were less than 10 % of the day 1 values.

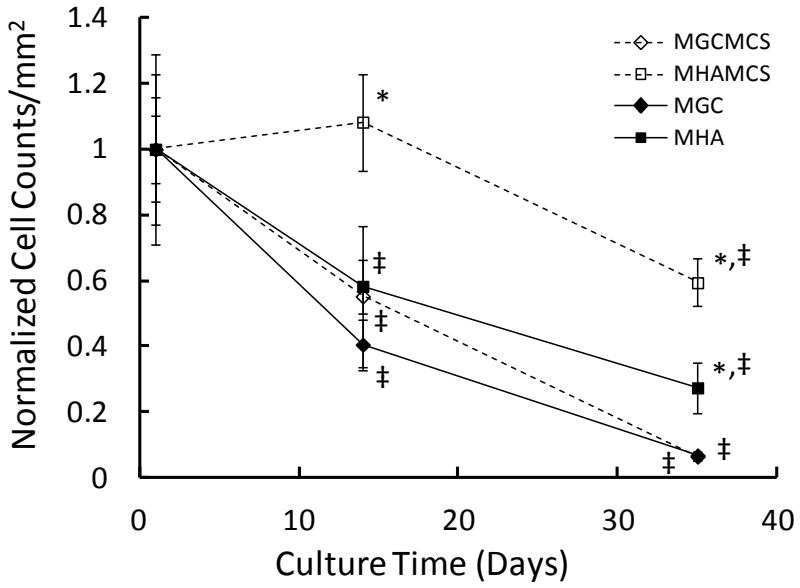

Figure 7.5: Normalized cell counts from DAPI images over time for the single component and blended hydrogels. (*) Significant from all other gels at the specific time point, (‡) significant from all other time points for specific gel ($p < 0.05$).

7.4.6 Biochemical Characterization of the Accumulated Tissue within the Hydrogels

The entire cellular hydrogels were analysed directly from culture for sulfated GAG and collagen accumulation, which was normalized to the DNA values after 1, 14, and 35 days. Significantly higher accumulation of sulfated GAG occurred in the single component and blended MHA hydrogels compared to the MGC based hydrogels at days 14 and 35 of the culture (Figure

7.6 (A)). The addition of MCS to the MHA hydrogels did not have any effect on GAG production over the single component MHA hydrogels. However, the production of GAG increased significantly with time in both the MHA and MHAMCS hydrogels. Alternatively, the addition of MCS to the MGC hydrogels significantly increased the amount of GAG over that obtained in the single component MGC hydrogels at day 14 and 35. The single component MGC hydrogels did not show any change in GAG production with time. Collagen production was also higher in each of the MHA and MHAMCS hydrogels than in all other gels after 35 days in culture. At day 35, the addition of MCS to the MHA gels yielded significantly increased collagen content than obtained in the single component MHA hydrogels. The MHAMCS hydrogels also demonstrated significant increase in collagen production at days 14 and 35. Neither of the MGC or MGCMCS hydrogels incurred any significant increase in collagen production with time in culture or through the addition of MCS in the blends (Figure 7.6 (B)).

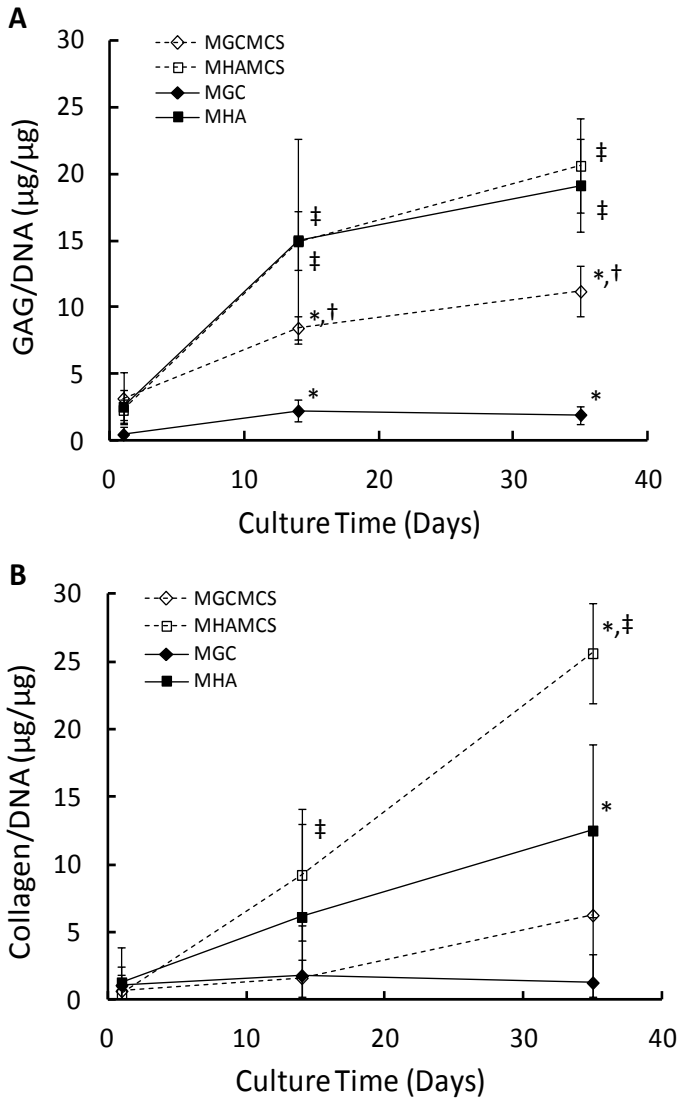

Figure 7.6: Biochemistry data, total GAG and collagen, normalized to the DNA content for the single component and blended hydrogels over the 35 day culture. (*) Significant from all other gels at specific time point, (†) Significant from day 1 values for specific gel, (‡) significant from all other time points for specific gel ($p < 0.05$).

7.4.7 Immunohistochemical Appearance of the de novo Tissue within the Hydrogels

Immunohistochemistry was utilized to localize and identify the specific cartilaginous extracellular matrix proteins in each of the hydrogels (Figure 7.7). Staining for collagen II and

aggrecan was used to assess whether a chondrocyte-like phenotype was maintained while collagen I was used as a marker of dedifferentiation. For all hydrogels (single component and blended), collagen I staining was minimal after 35 days in culture. Aggrecan and collagen II were localized into smaller cell clusters in the MGC and MHA hydrogels. The addition of MCS to the MHA hydrogels resulted in the greatest increase in aggrecan and collagen II staining, with the staining occurring in larger and more distributed cell clusters.

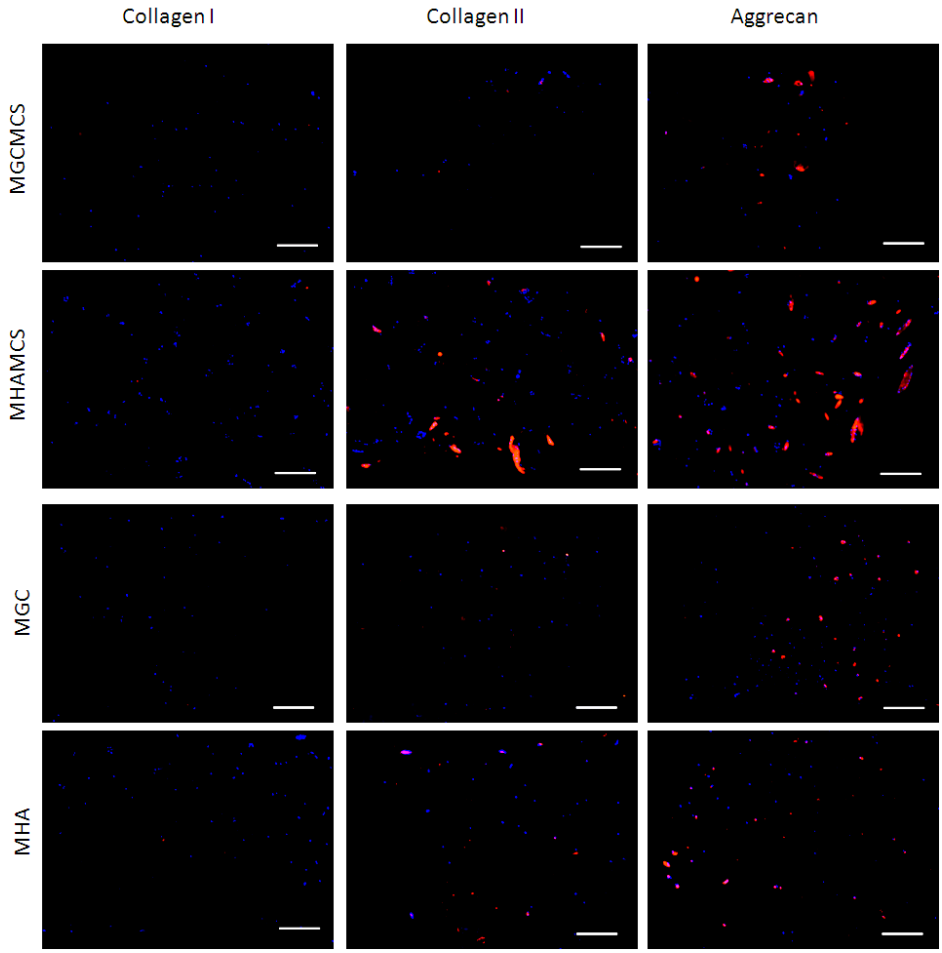

Figure 7.7: Immunohistochemistry for collagen I, collagen II and aggrecan for all single component and blended hydrogels over a 35 day culture period. Cell nuclei were stained with DAPI and are shown in blue. The respective staining for the collagens and aggrecan is shown in red. 100 X magnification and 200 µm scale bar.

Under higher magnifications, a low amount of collagen I was observed in some of the cell clusters for all of the hydrogel conditions (Figure 7.8 (A)). While the presence of collagen II was confirmed for all the cellular hydrogels, closer inspection of the cell clusters revealed differences in the location of the collagen II. In the MGCMCS and MGC hydrogels, collagen II staining was limited to the centre of the cell clusters whereas in the MHAMCS and MHA hydrogels the staining was observed surrounding the entire cell cluster (Figure 7.8 (B)). This effect was not as evident with the aggrecan staining, which was present in all hydrogels at the surface of the cell clusters (Figure 7.8 (C)). Interestingly, the multi-cellular aggregates appeared to have higher cellularity, were larger in size and also displayed a more spindle-like shape in the MHAMCS hydrogels compared to the smaller and more rounded shape in the other hydrogels. In addition, the DIC images of the MGCMCS hydrogels displayed a high density of individual cells that were smaller in size compared to the other hydrogels (Figure 7.8 (A – C)). Generally, chondrocytes in the DIC images of the MHAMCS and MHA hydrogels appeared to be larger than those in the MGCMCS and MGC hydrogels.

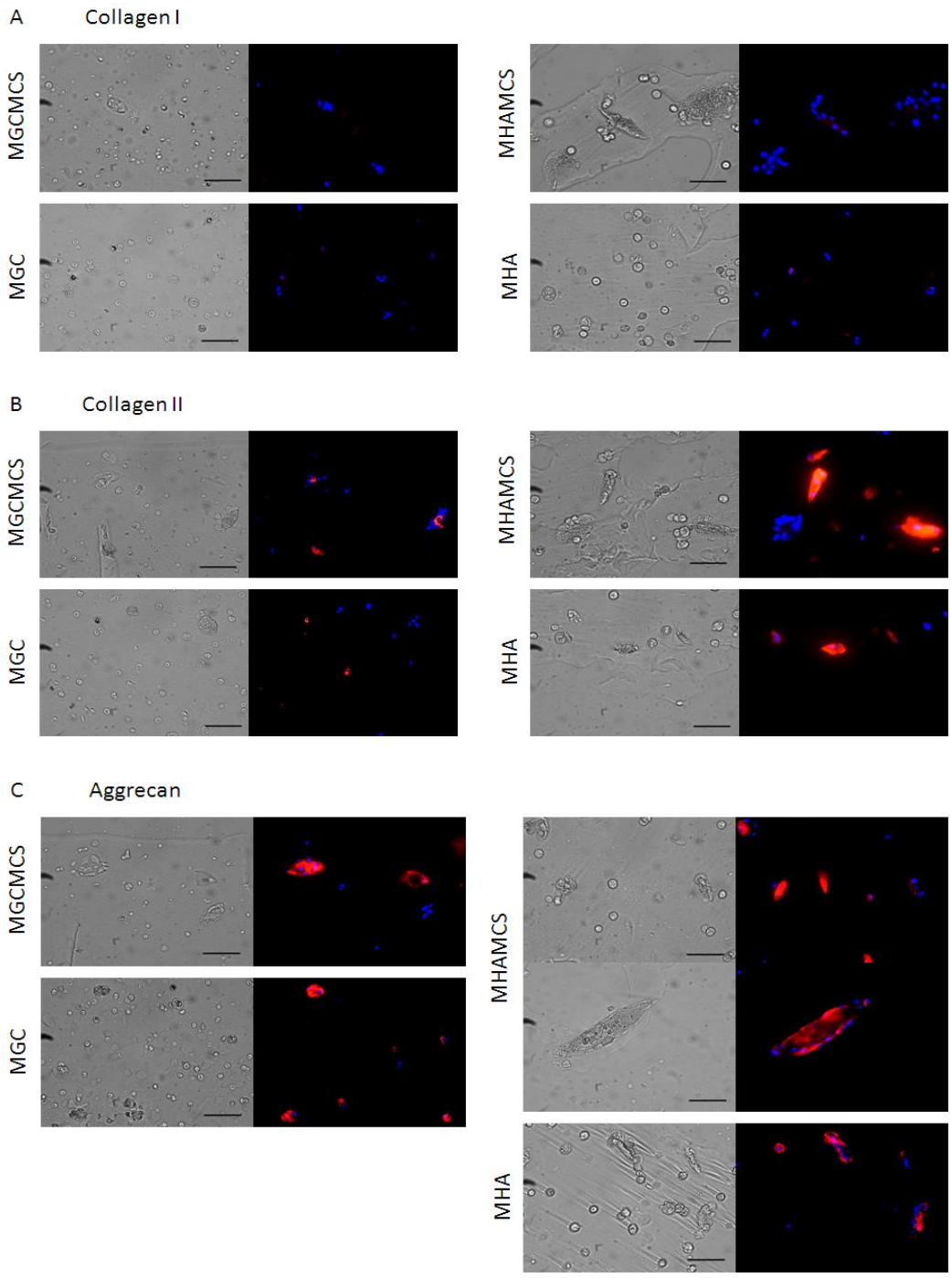

Figure 7.8: High (500 X) magnification images of day 35 time point for all individual and blended hydrogels for A) collagen I, B) collagen II and C) aggrecan. Matrix is highlighted in red and counter-stained using DAPI (blue). 50 µm scale bar

7.5 Discussion

Cell-seeded hydrogels with initial moduli approaching that of native tissue would be of great significance for the repair and regeneration of LBSTs. In a previous study, we demonstrated cell viabilities between 54 – 91 % for bovine articular chondrocytes after 1 week in culture in a variety of single component hydrogels (MGC, MHA and MCS) with high degrees of prepolymer methacrylation and moduli between 100 – 624 kPa. [239] In this study, we demonstrated that mixing and co-cross-linking the lower molecular MCS component into the higher molecular weight MGC or MHA hydrogels improved the initial modulus and cellular response with time in culture. The MHAMCS blends, which were the closest in chemical nature to native LBST extracellular matrix components, had the highest initial modulus and the highest cellularity and synthesis of GAG and collagen throughout the culture compared to the other hydrogels. The increase in cellular activity and functional matrix production from the encapsulated chondrocytes in the hydrogel blends was essential for the maintenance of the initial modulus until the end of the culture period.

Although not native to LBST extracellular matrices, methacrylated glycol chitosan is similar in structure and molecular weight to the hyaluronic acid used in this study ($M_n \approx 100$ kg/mol) and it is degradable by lysozyme. [81] Moreover, chitosan has been used in many other studies to form hydrogel scaffolds for the regeneration of articular cartilage and the nucleus pulposus tissues. [80, 82, 126, 149] However, in this study, the acellular single component MGC hydrogels displayed a noticeable decrease in volume with time, while retaining form stability. The decrease in the MGC hydrogel volume appeared to be a result of a change in the MGC's material property as while the size, swelling ratio and equilibrium water content of the hydrogels decreased, the modulus increased with time. The colour of these hydrogels (acellular and cellular) changed from clear to golden yellow during the 35 day culture period. These findings suggest that the glycol chitosan may have crystallized with time in culture as a result of the relatively high 6

% w/v prepolymer concentration used in this study compared to previous studies which typically examined lower 1 – 2 % w/v MGC hydrogels. [82, 126] The fact that these changes were reversible after soaking in a 1 % acetic acid solution, without dissolution of the gel, support this crystallization explanation (Figure A.12). Crystallization of glycol chitosan and the stiffening effect on the hydrogel network would explain the significant increase in equilibrium modulus of the MGC hydrogels with time. Additionally, crystallization and shrinkage of the MGC hydrogels may have impeded nutrient delivery throughout the gels resulting in a drastic reduction of cellularity (< 10 % remaining after day 35) and the limited matrix accumulation with time. While the shrinkage of the MGC hydrogels was suppressed with the addition of the MCS prepolymer, the low cellularity within the MGCMCS blends did not improved with time. However, less shrinkage and crystallization of the MGCMCS hydrogel network, compared to the MGC hydrogels, may have allowed cells closer to the surface to receive more nutrients from the surrounding media and form large cellular tissue growths, which eventually protruded from the hydrogel surface after 35 days in culture. Varghese *et al*. reported similar findings with bone marrow derived mesenchymal stem cells (MSC) in MCS containing poly(ethylene glycol) (PEG) hydrogels after 42 days in culture. [86] The MCS component in the PEG hydrogels was degradable by the encapsulated MSCs, which promoted cellular aggregation within the hydrogels that eventually grew beyond the original hydrogel surface. Large chondrocyte outgrowths have also been reported with the addition of physically entrapped aggrecan to poly(ethylene glycol) hydrogel networks. The addition of aggrecan enhanced cell proliferation and migration from the interior to the exterior of the hydrogels. [87] It was suggested that these cellular outgrowths may be beneficial at enhancing the integration of the implant due to higher seeded-cell interactions with the surrounding native tissue. In this study, the mechanical properties of the cellular MGC and MGCMCS hydrogels increased significantly over their acellular controls by day 35, which suggest a possible link to the accumulation of tissue within the hydrogel. However, the significant

loss of cellularity at the centre of the gels, and that cell growth only occurred at the gel surface, may be an indication that any of the positive cellular effects on the mechanical properties of the MGC and MGCMCS hydrogels could be short-lived. Therefore, to consider the MGC based hydrogels for further use will require improvements to internal cell retention and reduction in the possible crystallization effect, since crystallized regions may not be as susceptible to enzymatic degradation.

The acellular MHA based hydrogels displayed significant decreases from their day 1 equilibrium moduli after 35 days for the single component MHA and 14 and 35 days for the MHAMCS hydrogels. These decreases in the acellular moduli are most likely due to hydrolysis of the ester linkages of the methacrylate groups since the hyaluronic acid molecules are mainly degraded through an enzymatic mechanism. [203] It is possible that a similar hydrolysis occurred on the methacrylate groups on the chondroitin sulfate molecules, which may have contributed to the loss of modulus in the acellular MHAMCS controls with time. Although the decreases in equilibrium moduli were significant for the MHA based hydrogels, they remained within the targeted range of 200 ± 100 kPa throughout the entire culture period. Over 35 days of culture, it was apparent that the encapsulated chondrocytes were active within the hydrogels, as indicated by the increased volume and modulus of the cellular hydrogels over their respective acellular controls.

The remaining cellularity within the single component MHA hydrogels was close to 27 % after 35 days in culture. Chung *et al*. reported similar findings for auricular chondrocytes encapsulated in 2 to 20 % w/v MHA hydrogels, which had roughly 30 to 7 % of the initial 2 x 10^6 cells after 6 weeks *in vivo*, respectively. [95] In the current study, even though the number of chondrocytes within these scaffolds was decreasing, the remaining cells remained active and produced significant amounts of cartilaginous extracellular matrix over the 35 day culture period. It was also likely that the cells closer to the surface of the hydrogels, which did not appear to

decrease in number with time as indicated in the PKH26 images, were responsible for a large portion of the extracellular matrix production. This accumulation of cartilaginous tissue within the cellular MHA hydrogels may have served to suppress the loss of modulus seen in the acellular MHA hydrogel controls at day 35. However, longer studies will be required to determine if the diminishing cell population observed within the MHA hydrogels can rebound and/or stabilize, or continue to produce functional ECM.

The addition of MCS to the MHA hydrogel increased the initial modulus to approximately 250 kPa. This modulus was maintained with time in culture in the presence of the encapsulated chondrocytes in contrast to the decreasing modulus of the acellular controls. The cellular MHAMCS hydrogels increased in volume significantly with time, from 20 % initially to 31 % by day 35. Comparatively, the acellular MHAMCS controls were stable and maintained an initial 20 % swelling for the entire culture. Given that the cellular MHAMCS modulus was maintained as the volume of the hydrogels increased indicated cells were able to remodel the hydrogel environment with time. Although the MHAMCS hydrogels decreased in cellularity after 35 days, they maintained the highest number of cells (60 % of the day 1 value) compared to the other hydrogels investigated. The ability of the MHAMCS hydrogels to retain a higher cellularity during the culture was a likely reason for the higher accumulation of extracellular matrix with larger and well distributed pericellular-like tissues throughout the gels. Therefore, the higher cellularity and resulting matrix synthesis in the MHAMCS hydrogel compared to the single component MHA hydrogels indicates that MCS had a stimulatory effect on the encapsulated chondrocytes. Chondroitin sulfate has been shown to enhance the anabolic response of chondrocytes *in vitro* and is also able to inhibit the effects of interleukin – 1β, a cytokine involved in cartilage inflammation and degradation. [230-232] Although not explicitly investigated, it was possible that a similar anabolic response occurred with the addition of MCS to the hydrogels. The presence of the MHA in the MHAMCS blends improved cell retention and the *de novo* tissue

surrounding them, compared to the MGCMCS hydrogels. Given that no cellular outgrowths were detected on the surface, it was assumed that the stiffening of the cellular MHAMCS networks was due to the higher matrix production from the MCS component and better cell retention and more specifically the formation of the PCM-like tissue from the MHA components of the hydrogels. The tissue formations produced in the MHAMCS hydrogels, displayed unique shapes which were spindle and comet-like in appearance. Pericellular (PCM) matrices similar in size and shape to those in the MHAMCS hydrogels, have been reported in native articular cartilage, which also varied with location in the tissue. [240] This suggests a higher interaction of the encapsulated cells with the hydrogel and a potential attempt by the chondrocytes to re-organize the *de novo* tissue within the hydrogels. The *de novo* tissues formed in the other hydrogels appeared to be trapped in smaller pockets with no defined shape. This higher chondrocyte interaction with the MHA based hydrogels may be related to the CD44 cellular membrane receptor, which principally recognizes and binds to hyaluronate. [211] This same interaction with CD44 is also responsible for the ability of chondrocytes to internalize hyaluronic acid where it can fuse with lysosomes and thus be degraded. [90] Knudson *et al*. also reported hyaluronan-like cell receptors were responsible for the self-assembly of an aggrecan rich PCM, which anchored the PCM to the chondrocytes membrane. [89] Guilak *et al*. reported that the PCM plays a functional role in the biomechanics of articular cartilage, which in turn dictates the behavior of the chondrocytes. [241] Therefore, future studies will need to examine the relationship between the chondrocyte and PCM, and PCM to the hydrogel network and how these interactions can affect the mechanical properties of the MHAMCS hydrogels.

7.6 Conclusions

High modulus and low swelling hydrogel blends were able to maintain their initial mechanical properties throughout the 35 day culture, as a result of the cell mediated response

within the hydrogels. The use of polysaccharides native to cartilaginous soft tissues, specifically hyaluronic acid and chondroitin sulfate to form the hydrogels, had beneficial effects on the encapsulated chondrocytes. The high cellular interaction of chondrocytes with both the MHA and MCS components in the MHAMCS hydrogels allowed for greater cellularity and ECM synthesis than the MGC based hydrogels throughout the culture. The accumulation, distribution and possible remodeling of cartilaginous tissue within the MHAMCS hydrogels maintained the overall modulus while the material network weakened with time. Therefore, the high modulus MHAMCS hydrogels and synthetic cell phenotype within make them well suited for *in situ* LBST repair and regeneration applications, and warrants further studies to better understand the mechanisms between tissue production and hydrogel mechanical properties. Although a significant drop in cellularity was observed in the MHAMCS hydrogels, they were able to retain the highest number of the cells, with close to 60 % of the cells remaining after 35 days in culture. Further studies will be required to improve the cellularity within the MHAMCS hydrogels over time, which may be accomplished through dynamic culture conditions and mechanical stimulation of the scaffolds.

Chapter 8

Conclusions

8.1 Formation of a Co-continuous Morphology

The formation of the co-continuous morphology was possible by mixing two immiscible phases with a single photo-cross-linking mechanism. The morphology was dependent on the molecular weight of the 100 % tri-acrylated *star*-copolymer with 50:50 molar ratio of D,L-lactide and ε-caprolactone monomers and the prepolymer concentration of an *N*-methacrylated glycol chitosan solution. The morphology of each phase (mono- or co-continuous) was important for the final mechanical properties of the composite scaffolds. The co-continuous morphology in the elastomer-hydrogel composite had significantly higher mechanical properties than the single phase hydrogel, and the chondrocytes were able to survive the formation of the co-continuous morphology and the photo-cross-linking reaction. Metabolic activity and DNA accumulation increased in the cell-laden hydrogel phase of the co-continuous scaffolds. The co-continuous hydrogel-elastomer design allowed for the formation of a high modulus cell encapsulating scaffold, which has currently been lacking in the field of load bearing soft tissue repair.

8.2 Improvements to the Elastomer phase

Long-term stability of the mechanical properties of the co-continuous scaffolds was improved with the use of a 70:30 molar ratio trimethylene carbonate and ε-caprolactone based copolymer for the elastomer phase. The resultant high modulus confirmed the continuity of the elastomer phase within the co-continuous morphology. Complete diffusion of an aqueous based dye in the hydrogel phase of the co-continuous scaffolds created contrast between the two phases, which also demonstrated continuity of the hydrogel phase. The co-continuous scaffolds were injectable, resistant to physiological loading and able to regenerate *de novo* tissue in the *N*-

methacrylated glycol chitosan hydrogel phase. This study confirmed the tunability of the elastomer phase and the potential of co-continuous scaffolds for use in the repair of cartilaginous load bearing soft tissues.

8.3 Improvements to the Hydrogel Phase

A modified methacrylation protocol with methacrylic anhydride allowed for faster reaction times and greater control of the final degree of methacrylation of the hyaluronic acid and chondroitin sulfate prepolymers not yet reported in the literature. The potential of these new hydrogels to possess superior mechanical properties and improved cellular responses was demonstrated in comparison to the previously investigated N-methacrylated glycol chitosan hydrogels.

8.4 Improvements to Cellular Response in the Hydrogel Phase

The cellular response was greatly improved when a blend of hyaluronic acid and chondroitin sulfate prepolymers was used to culture the chondrocytes. The initial mechanical properties of the hydrogels were high enough to approach that of native cartilaginous load bearing soft tissues, while still supporting chondrocyte viability and phenotype. The encapsulated chondrocytes remained well distributed and formed pericellular matrices similar to that of native cartilaginous load bearing soft tissues, which was able to maintain the initial modulus of the hydrogels over time.

Chapter 9

Future Research Directions

9.1 Formation of Co-continuous Morphology with Hyaluronic Acid, Chondroitin Sulfate and Their Blends

The potential reparative abilities of the co-continuous scaffolds are evidenced through the range of materials that have been demonstrated to tune the final physical properties of the scaffolds. Objectives 3 and 4 focused solely on improving the hydrogel phase in terms of both the mechanical properties and cellular response. Additionally, the prepolymer concentrations necessary to form the targeted hydrogel modulus were also able to form a co-continuous morphology in the 7030TMCCL ASCP with equilibrium modulus ranging from 570 to 1000 kPa (Figure 9.1). Although slightly different in appearance, the co-continuous morphology of the MHA, MCS and select blends resulted in comparable moduli to the initial MGC based co-continuous scaffolds (around 1000 kPa).

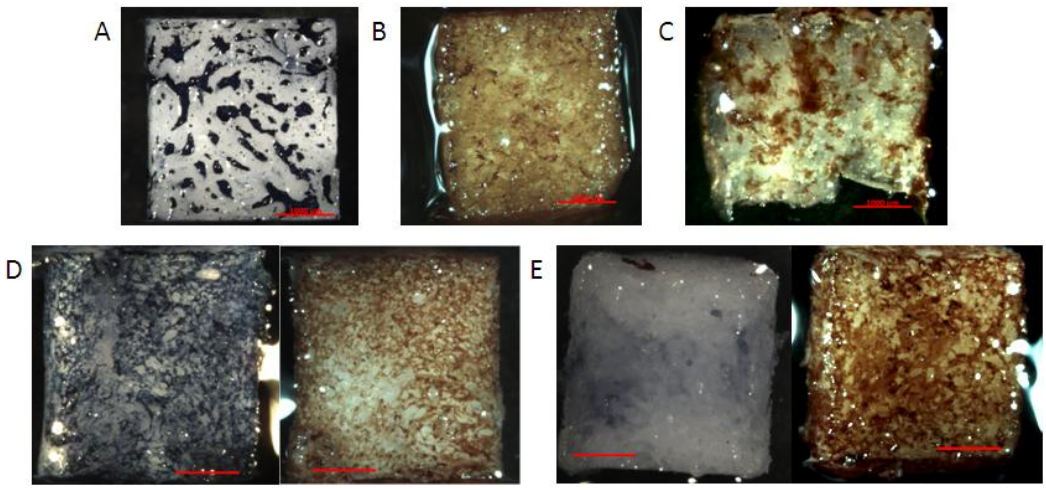

Figure 9.1: Morphology of co-continuous scaffolds with different hydrogel phases in 7030TMCCL elastomer for A) 30 % loading of 8 % w/v MGC, B) 25 % loading of 6 % w/ MHA, C) 25 % loading of 20 % w/v MCS, D) 25 % loading of 9.5 % w/v MGCMCS and C) 25 % loading of 9.5 % w/v MHAMCS. MGC phase stained with trypan blue and MHA and MCS phases stained with safranin-o to highlight their location within the elastomer. Equilibrium modulus for co-continuous scaffolds were 1168, 569, 806, 1004 and 699 kPa for each respective image. 1000 µm scale bar

9.2 Preliminary *Ex Vivo* Reparative Abilities of Co-continuous and Hydrogel Scaffolds

In a preliminary study, the adhesive abilities of a representative co-continuous scaffold were able to withstand the swelling force of the native bovine NP tissue. However, additional work will be required to determine the actual mechanism for adhesion of the scaffolds (co-continuous or hydrogel only) to the native NP tissue and if cells in culture can further increase the interfacial bond between them.

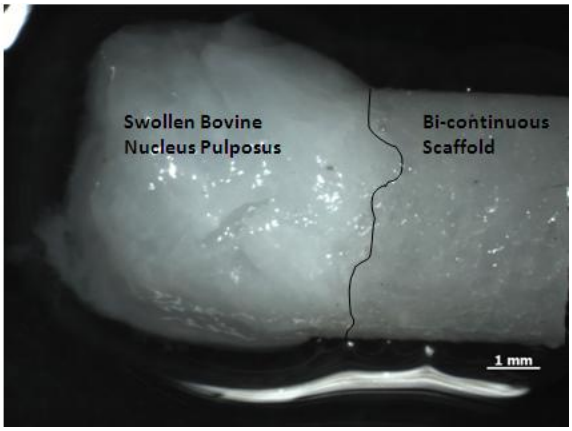

Figure 9.2: 5446DLLACL co-continuous scaffold photo-cross-linked in the presence of swollen bovine nucleus pulposus using radial cross-linking setup. Approximate interfacial zone outlined in black.

The high modulus hydrogels examined in this thesis also demonstrated the potential to form a stand-alone repair for the NP in bovine caudal discs (Figure 9.3). Overall, multiple scaffold designs and materials have been demonstrated for regenerative repairs of the cartilaginous load bearing soft tissues of the intervertebral discs. These approaches ranged from utilizing synthetic materials, which possess superior mechanical properties for longer-term support and regeneration, to natural materials which potentially better mimic the native environment and cell behaviour.

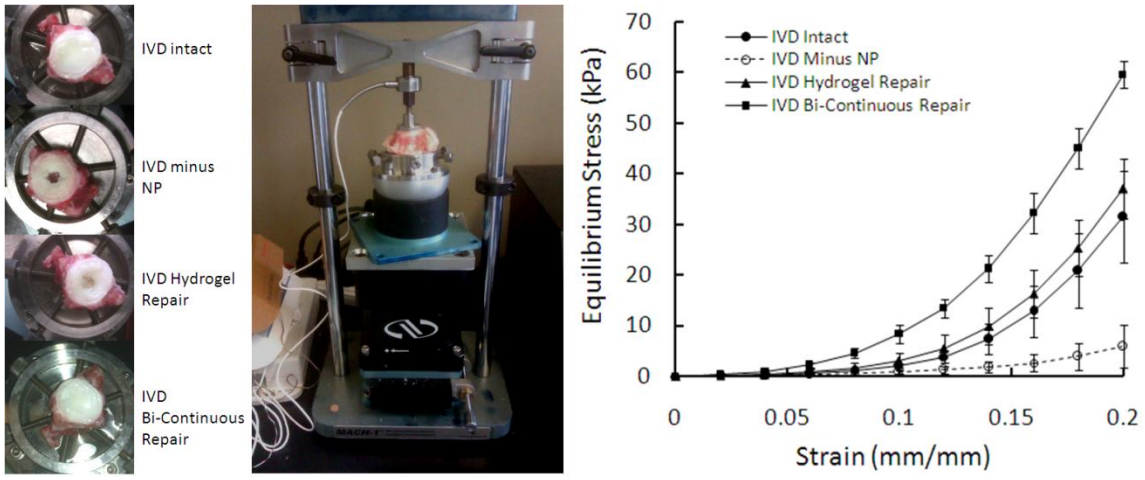

Figure 9.3: Repair of a bovine caudal intervertebral disc with a hydrogel and co-continuous scaffold. Intervertebral discs were tested intact, minus NP, NP repaired with 6 % w/v MGC hydrogel and NP repaired with 30 % loading of 6 % w/v MGC co-continuous scaffold.

9.3 Recommendations for Future Work

The focus of this study was on the design and development of cell laden biomaterials that could be used for an innovative injectable, load bearing soft tissue replacement with regenerative capabilities. It is recommended that a protocol and mixing device be developed to aid in the manufacture of the co-continuous scaffolds, which could also be used as a self contained device suitable for the sterile delivery of the scaffolds to the repair site. Consultation with an orthopedic surgeon is also highly recommended to determine a suitable surgical approach for a minimally invasive repair of the affected disc. The use of an appropriate organ culture model of the human intervertebral discs would also benefit the developmental stages of the delivery and repair approach. [242]

The next step of the project will be to investigate further the long-term *in vitro* behaviour of the co-continuous TMC:CL based scaffolds in combination with the MHAMCS hydrogels. Improvements to the encapsulated cell performance may be enhanced with the use of a dynamic culture system to assist with nutrient delivery to the centre of the scaffolds. Mechanical

stimulation (tensile, compression and hydrostatic) has also been shown to be beneficial for load bearing cell types in terms of stimulating matrix production. [96,243,244] Therefore, studies should investigate an appropriate loading regime that can used to improve the behavior of the cells from the static culture conditions used in this study.

Chondrocytes were chosen as a cell source that was abundant, robust and active compared to the NP cell population and were therefore deemed suitable for our purposes. However, in addition to improving the *in vitro* culture conditions, studies should also be conducted in parallel to determine the most effective cell source for use in the co-continuous scaffolds. A cell source that is easily isolated, effective at synthesizing cartilaginous matrix and more suited for an actual repair model/approach is desired. Therefore, methods should also be examined to improve the senescent mature NP cell population, which may be accomplished with the use of co-culturing with a mesenchymal stem cell population (bone or adipose derived). [54, 245] Cartilaginous phenotype markers can be used to identify the differentiation of the stem cells. [17] Moreover, human adipose derived stem cells have been identified as an appropriate cell type to differentiate into a more NP specific cell, compared to chondrocytes, based on gene profiling. [246] Therefore, a well characterized NP and stem cell source should be examined for their regenerative potential within the co-continuous scaffolds.

After sufficient characterization of the co-continuous scaffolds in an *in vitro* culture environment, the behaviour of the scaffolds (mechanical stability and regenerative abilities of the encapsulated cells) will then need to be assessed in an appropriate animal IVD model. [247,248] Initial biocompatibility and degradation studies can be carried out in smaller models (rat or rabbit) without load bearing or subcutaneously. However, a larger animal model such as sheep may be more suitable for an actual replacement of the NP material with the co-continuous scaffolds.[249,250] The larger animal models will help provide information on the biomechanical and regenerative abilities of the co-continuous scaffolds in an actual IVD space.

References

1. Druss, D. G.; Marcus, S. C.; Olfson, M.; Pincus, H. A. *Health Affairs* **2002**, *21*, 105-111.

2. Katz, J. N. *Journal of Bone and Joint Surgery (Am.)* **2006**, *88 (Suppl 2)*, 21-24.

3. Freemont, A. J. *Rheumatology* **2009**, *48*, 5-10.

4. Bawa, M.; Boden, S. D. The epidemiology and economics of intervertebral disc disease. In *The lumbar intervertebral disc;* Phillips, F. M., Lauryssen, C., Eds.; Thieme Medical Publishers, Inc.: New York, NY, 2010; pp 3-8.

5. Lee, C. K. *Spine* **1988**, *13*, 375-377.

6. Etebar, S.; Cahill, D. W. *Journal of Neurosurgery: Spine* **1999**, *90*, 163-169.

7. Freeman, B. J.; Davenport, J. *European Spine Journal* **2006**, *15*, 439-447.

8. Antoniou, J.; Steffen, T.; Nelson, F.; Winterbottom, N.; Hollander, A. P.; Poole, R. A.; Aebi, M.; Alini, M. *Journal of Clinical Investigation* **1996**, *98*, 996-1003.

9. Marchand, F.; Ahmed, A. M. *Spine* **1990**, *15*, 402-410.

10. Roberts, S.; Menage, J.; Urban, J. P. G. *Spine* **1989**, *14*, 166-174.

11. Holm, S.; Maroudas, A.; Urban, J.; Selstam, G.; Nachemson, A. *Connective Tissue Research* **1981**, *8*, 101-119.

12. Brodin, H. *Acta Orthopaedica Scandinavica* **1955**, *24*, 177-183.

13. Urban, J. P.; Smith, S.; Fairbank, J. C. *Spine* **2004**, *29*, 2700-2709.

14. Bobechko, W. P.; Hirsh, C. *Journal of Bone and Joint Surgery (Br.)* **1965**, *47*, 574-580.

15. Gertzbein, S. D.; Tait, J. H.; Devlin, S. R. *Clinical Orthopaedics* **1977**, *123*, 149-154.

16. Takada, T.; Nishida, K.; Doita, M.; Kurosaka, M. *Spine* **2002**, *27*, 1526-1530.

17. Mwale, F.; Roughley, P.; Antoniou, J. *European Cells and Materials* **2004**, *8*, 58-64.

18. Hunter, C. J.; Matyas, J. R.; Duncan, N. A. *Spine* **2004**, *29*, 1099-1104.

19. Aguiar, D.; Johnson, S.; Oegema, T. *Experimental Cell Research* **1999**, *246*, 129-137.

20. Guehring, T.; Wilde, G.; Sumner, M.; Grunhagen, T.; Karney, G.; Tirlapur, U.; Urban, J. *Arthritis & Rheumatism* **2009**, *60*, 1026-1034.

21. Adams, M. A.; Roughley, P. J. *Spine* **2006**, *31*, 2151-2161.

22. Adams, M. A. Anatomy and physiology of the lumbar intervertebral disc and endplates. In *The lumbar intervertebral disc;* Phillips, F. M., Lauryssen, C., Eds.; Thieme Medical Publishers, Inc.: New York, NY, 2010; pp 9-19.

23. kerttula, L. I.; Serlo, W. S.; Tervonen, O. A.; Paakko, E. L.; Vanharanta, H. V. *Spine* **2000**, *25*, 1104-1108.

24. Holm, S.; Holm, A. K.; Ekstrom, L.; Karladani, A.; Hansson, T. *Journal of Spinal Disorders & Techniques* **2004**, *17*, 64-71.

25. Jones, P.; Gardner, L.; Menage, J.; Williams, G.; Roberts, S. *Arthritis Research & Therapy* **2008**, *10*, R86.

26. Kim, K.; Chung, H.; Ha, K.; Lee, J.; Kim, Y. *The Spine Journal* **2009**, *9*, 658-666.

27. Battie, M. C.; Videman, T.; Parent, E. *Spine* **2004**, *29*, 2679-2690.

28. Boos, N.; Weissbach, S.; Rohrbach, H.; Weiler, C.; Spratt, K. F.; Nerlich, A. G. *Spine* **2002**, *27*, 2631-2644.

29. Heine, J. *Virchows Archive - A: Pathological Anatomy & Histopathology* **1926**, *260*, 521-663.

30. Sambrook, P. N.; MacGregor, A. J.; Spector, T. D. *Arthritis & Rheumatism* **1999**, *42*, 366-372.

31. Battie, M. C.; Videman, T.; Gibbons, L. E.; Fisher, L. D.; Manninen, H.; Gill, K. *Spine* **1995**, *20*, 2601-2612.

32. Weinstein, J. N.; Lurie, J. D.; Olson, P. R.; Bronner, K. K.; Fisher, E. S. *Spine* **2006**, *31*, 2707-2714.

33. Denozière, G.; Ku, D. N. *Journal of Biomechanics* **2006**, *39*, 766-775.

34. Meakin, J. R.; Hukins, D. W. L. *Journal of Materials Science: Materials in Medicine* **2001**, *12*, 207-213.

35. Carl, A.; Ledet, E.; Yuan, H.; Sharon, A. *The Spine Journal* **2004**, *4*, 325S-329S.

36. Klara, P.; Ray, C. *Spine* **2002**, *27*, 1374-1377.

37. Di Martino, A.; Vaccaro, A. R.; Lee, J. Y.; Denaro, V.; Lim, M. R. *Spine* **2005**, *30*, 16S-22S.

38. Stella, J. A.; D'Amore, A.; Wagner, W. R.; Sacks, M. A. *Acta Biomaterialia* **2010**, *6*, 2365-2381.

39. Kandel, R.; Roberts, S.; Urban, J. *European Spine Journal* **2008**, *17*, S480-S491.

40. Yang, X.; Li, X. *European Spine Journal* **2009**, *1811*, 1564-1572.

41. Wilke, H.; Neef, P.; Caimi, M.; Hoogland, T.; Claes, L. E. *Spine* **1999**, *24*, 755-762.

42. Perie, D.; Korda, D.; Iatridis, J. *Journal of Biomechanics* **2005**, *38*, 2164-2171.

43. Cloyd, J.; Malhotra, N.; Weng, L.; Chen, W.; Mauck, R.; Elliott, D. *European Spine Journal* **2007**, *16*, 1892-1898.

44. Iatridis, J.; Setton, L.; Weidenbaum, M.; Mow, V. *Journal of Orthopaedic Research* **1997**, *15*, 318-322.

45. Umehara, S.; Tadano, S.; Abumi, K.; Katagiri, K.; Kaneda, K.; Ukai, T. *Spine* **1996**, *21*, 811-819.

46. Rundell, S.; Guerin, H.; Auerbach, J.; Kurtz, S. *Spine* **2009**, *34*, 2022-2032.

47. Miyazaki, T.; Kobayashi, S.; Takeno, K.; Meir, A.; Urban, J.; Baba, H. *Tissue Engineering Part A* **2009**, *15*, 3835-3846.

48. He, B.; Wang, Y.; Yang, J.; Peng, F.; Li, F. *Journal of Huazhong University of Science and Technology [Medical Sciences]* **2013**, *33*, 228-233.

49. Yuan, M.; Leong, K. W.; Chan, B. P. *The Spine Journal* **2011**, *11*, 947-960.

50. Wei, A.; Chung, S.; Tao, H.; Brisby, H.; Lin, Z.; Shen, B.; Ma, D.; Diwan, A. *Tissue Engineering Part A* **2009**, *15*, 2581-2593.

51. Zeiter, S.; van der Werf, M.; Ito, K. *Journal of Tissue Engineering and Regenerative Medicine* **2009**, *3*, 310-320.

52. Sobajima, S.; Vadala, G.; Shimer, A.; Kim, J.; Gilbertson, L.; Kang, J. *The Spine Journal* **2008**, *8*, 888-896.

53. Leung, V.; Chan, D.; Cheung, K. *European Spine Journal* **2006**, *15*, S406-S413.

54. Risbud, M.; Shapiro, I.; Vaccaro, A.; Albert, T. *The Spine Journal* **2004**, *4*, 348S-353S.

55. Sakai, D.; Mochida, J.; Yamamoto, Y.; Nomura, T.; Okuma, M.; Nishimura, K.; Nakai, T.; Ando, K.; Hotta, T. *Biomaterials* **2003**, *24*, 3531-3541.

56. Le Maitre, C.; Baird, P.; Freemont, A.; Hoyland, J. *Arthritis Research & Therapy* **2009**, *11*, R20.

57. Kim, D.; Kim, S.; Heo, S.; Shin, J.; Lee, S.; Park, S.; Shin, J. *Journal of Bioscience and Bioengineering* **2009**, *108*, 63-67.

58. Yang, S. H.; Wu, C. C.; Shih, T. T.; Sun, Y. H.; Lin, F. H. *Spine* **2008**, *33*, 1951-1957.

59. Vadala, G.; Studer, R. K.; Sowa, G.; Spiezia, F.; Iucu, C.; Denaro, V.; Gilbertson, L. G.; Kang, J. D. *Spine* **2008**, *33*, 870-876.

60. Hoogendoorn, R. J. W.; Lu, Z. F.; Kroeze, R. J.; Bank, R. A.; Wuisman, P. I.; Helder, M. N. *Journal for Cellular and Molecular Medicine* **2008**, *12*, 2205-2216.

61. Gaetani, P.; Torre, M.; Klinger, M.; Faustini, M.; Crovato, F.; Bucco, M.; Marazzi, M.; Chlapanidas, T.; Levi, D.; Tancioni, F.; Vigo, D.; Baena, R. *Tissue Engineering: Part A* **2008**, *14*, 1415-1423.

62. Lu, Z. F.; Doulabi, B. Z.; Wuisman, P. I.; Bank, R. A.; Helder, M. N. *Journal of Cellular and Molecular Medicine* **2008**, *12*, 2812-2822.

63. Lu, Z. F.; Zandieh, D. B.; Wuisman, P. I.; Bank, R. A.; Helder, M. N. *Biochemical and Biophysical Research Communications* **2007**, *359*, 991-996.

64. Zhang, Y.; Phillips, F. M.; Thonar, E. J.; Oegema, T.; An, H. S.; Roman-Blas, J. A.; He, T. C.; Anderson, D. G. *Spine* **2008**, *33*, 831-838.

65. Chung, C.; Erickson, I. E.; Mauck, R. L.; Burdick, J. A. *Tissue Engineering Part A* **2008**, *14*, 1121-1131.

66. Zeiter, S.; der Werf, M. v.; Ito, K. *Journal of Tissue Engineering and Regenerative Medicine* **2009**, *3*, 310-320.

67. Erickson, I. E.; Huang, A. H.; Chung, C.; Li, R. T.; Burdick, J. A.; Mauck, R. L. *Tissue Engineering Part A* **2008**, *15*, 1041-1052.

68. Mauck, R.; Yuan, X.; Tuan, R. *Osteoarthritis and Cartilage* **2006**, *14*, 179-189.

69. Mauck, R. L.; Seyhan, S. L.; Ateshian, G. A.; Hung, C. T. *Annals of Biomedical Engineering* **2002**, *30*, 1046-1056.

70. Hong, Y.; Song, H.; Gong, Y.; Mao, Z.; Gao, C.; Shen, J. *Acta Biomaterialia* **2007**, *3*, 23-31.

71. Nguyen, K. T.; West, J. L. *Biomaterials* **2002**, *23*, 4307-4314.

72. Elisseeff, J.; Anseth, K.; Sims, D.; McIntosh, W.; Randolph, M.; Yaremchuk, M.; Langer, R. *Plastic and Reconstructive Surgery* **1999**, *104*, 1014-1022.

73. Nicodemus, G. D.; Bryant, S. J. *Tissue Engineering: Part B* **2008**, *14*, 149-165.

74. Chou, A. I.; Nicoll, S. B. *Journal of Biomedical Materials Research Part A* **2009**, *91*, 187-194.

75. Collin, E. C.; Grad, S.; Zeugolis, D. I.; Vinatier, C. S.; Clouet, J. R.; Guicheux, J. J.; Weiss, P.; Alini, M.; Pandit, A. S. *Biomaterials* **2011**, *32*, 2862-2870.

76. Moss, I. L.; Gordon, L.; Woodhouse, K. A.; Whyne, C. M.; Yee, A. J. M. *Spine* **2011**, *36*, 1022-1029.

77. Chou, A.; Nicoll, S. *Journal of Biomedical Materials Research* **2009**, *91A*, 187-194.

78. Fedorovich, N.; Oudshoorn, M.; van Geemen, D.; Hennink, W.; Alblas, J.; Dhert, W. *Biomaterials* **2009**, *30*, 344-353.

79. Williams, C.; Malik, A.; Kim, T.; Manson, P.; Elisseeff, J. *Biomaterials* **2005**, *26*, 1211-1218.

80. Di Martino, A.; Sittingerc, M.; Risbud, M. V. *Biomaterials* **2005**, *26*, 5983-5990.

81. Amsden, B. G.; Sukarto, A.; Knight, D. K.; Shapka, S. N. *Biomacromolecules* **2007**, *8*, 3758-3766.

82. Park, H.; Choi, B.; Hu, J.; Lee, M. *Acta Biomaterialia* **2013**, *9*, 4779-4786.

83. Wang, L.; Shen, S.; Lu, S. *Carbohydrate Polymers* **2003**, *52*, 389-396.

84. Khanlari, A.; Detamore, M. S.; Gehrke, S. H. *Macromolecules* **2013**, *46*, 9609-9617.

85. Bryant, S. J.; Davis-Arehart, K. A.; Luo, N.; Shoemaker, R. K.; Arthur, J. A.; Anseth, K. S. *Macromolecules* **2004**, *37*, 6726-6733.

86. Varghese, S.; Hwang, N. S.; Canver, A. C.; Theprungsirikul, P.; Lin, D. W.; Elisseeff, J. *Matrix Biology* **2008**, *27*, 12-21.

87. Ingavle, G. C.; Frei, A. W.; Gehrke, S. H.; Detamore, M. S. *Tissue Engineering Part A* **2013**, *19*, 1349-1359.

88. Ingavle, G. C.; Dormer, N. H.; Gehrke, S. H.; Detamore, M. S. *Journal of Materials Science: Materials in Medicine* **2012**, *23*, 157-170.

89. Knudson, C. B. *The Journal of Cell Biology* **1993**, *120*, 825-834.

90. Knudson, W.; Chow, G.; Knudson, C., B. *Matrix Biology* **2002**, *21*, 15-23.

91. Smeds, K. A.; Pfister-Serres, A.; Hatchell, D. L.; GRINSTAFF, M. W. *Journal of Macromolecular Science-Pure and Applied Chemistry* **1999**, *36*, 981-989.

92. Oudshoorn, M. H.; Rissmann, R.; Bouwstra, J. A.; Hennink, W. E. *Polymer* **2007**, *48*, 1915-1920.

93. Van Dijk-Wolthuis, W.; Kettenes-Van Den Bosch, J.; Van der Kerk-Van Hoof, A; Hennink, W. *Macromolecules* **1997**, *30*, 3411-3413.

94. Bencherif, S. A.; Srinivasan, A.; Horkay, F.; Hollinger, J. O.; Matyjaszewski, K.; Washburn, N. R. *Biomaterials* **2008**, *29*, 1739-1749.

95. Chung, C.; Mesa, J.; Randolph, M. A.; Yaremchuk, M.; Burdick, J. A. *Journal of Biomedical Materials Research Part A* **2006**, *77*, 518-525.

96. Erickson, I. E.; Kestle, S. R.; Zellars, K. H.; Farrell, M. J.; Kim, M.; Burdick, J. A.; Mauck, R. L. *Acta biomaterialia* **2012**, *8*, 3027-3034.

97. Serrano, M. C.; Chung, E. J.; Ameer, G. A. *Advanced Functional Materials* **2010**, *20*, 192-208.

98. Kang, Y.; Yang, J.; Khan, S.; Anissian, L.; Ameer, G. A. *Journal of Biomedical Materials Research Part A* **2006**, *77*, 331-339.

99. Gerecht, S.; Townsend, S. A.; Pressler, H.; Zhu, H.; Nijst, C. L. E.; Bruggeman, J. P.; Nichol, J. W.; Langer, R. *Biomaterials* **2007**, *28*, 4826-4835.

100. Boyd, L. M.; Carter, A. J. *European Spine Journal* **2006**, *15*, 414S-421S.

101. Milner, R. S.; Arrowsmith, P. H.; Edith Jane, M. M. United States Patent US6187048B1.

102. Chia, S. L.; Gorna, K.; Gogolewski, S.; Alini, M. *Tissue Engineering Part A* **2006**, *12*, 1945-1953.

103. Yang, S.; Leong, K. F.; Du, Z.; Chua, C. K. *Tissue Engineering* **2001**, *7*, 679-689.

104. Hollister, S. J. *Nature Materials* **2005**, *4*, 518-524.

105. Gerecht, S.; Townsend, S.; Pressler, H.; Zhu, H.; Nijst, C.; Bruggeman, J.; Nichol, J.; Langer, R. *Biomaterials* **2007**, *28*, 4826-4835.

106. Chapanian, R.; Amsden, B. *European Journal of Pharmaceutics and Biopharmaceutics* **2010**, *74*, 172-183.

107. Chapanian, R.; Tse, M. Y.; Pang, S. C.; Amsden, B. G. *Biomaterials* **2009**, *30*, 295-306.

108. Amsden, B. G.; Tse, M. Y.; Turner, N. D.; Knight, D. K.; Pang, S. C. *Biomacromolecules* **2006**, *7*, 365-372.

109. Amsden, B. G.; Misra, G.; Gu, F.; Younes, H. M. *Biomacromolecules* **2004**, *5*, 2479-2486.

110. Chapanian, R.; Tse, M. Y.; Pang, S. C.; Amsden, B. G. *Journal of Biomedical Materials Research Part A* **2010**, *92A*, 830-842.

111. Pego, A. P.; Poot, A. A.; Grijpma, D. W.; Feijen, J. *Macromolecular Bioscience* **2003**, *2*, 411-419.

112. Lind, M.; Larsen, A.; Clausen, C.; Osther, K.; Everland, H. *Knee Surgery, Sports Tramatology, Arthroscopy* **2008**, *16*, 690-698.

113. Moutos, F. T.; Guilak, F. *Biorheology* **2008**, *45*, 501-512.

114. Mikos, A.; Temenoff, J. *Electronic Journal of Biotechnology* **2000**, *3*, 1-6.

115. Peng, H. T.; Martineau, L.; Shek, P. N. *Journal of Material Science: Materials in Medicine* **2007**, *18*, 975-986.

116. Peng, H.; Mok, M.; Martineau, L.; Shek, P. *Journal of Material Science: Materials in Medicine* **2007**, *18*, 1025-1035.

117. Peng, H.; Martineau, L.; Shek, P. *Journal of Material Science: Materials in Medicine* **2008**, *19*, 997-1007.

118. Leckie, A. E.; Akens, M. K.; Woodhouse, K. A.; Yee, A. J. M.; Whyne, C. M. *Spine* **2012**, *37*, E1296-E1303.

119. Hayami, J. W. S.; Waldman, S. D.; Amsden, B. G. *Macromolecular bioscience* **2011**.

120. Roberts, S.; Evans, H.; Trivedi, J.; Menage, J. *The Journal of Bone and Joint Surgery* **2006**, *88A*, 10S-14S.

121. Buckwalter, J. A. *Journal of Orthopaedic & Sports Physical Therapy* **1998**, *28*, 192-202.

122. O'Driscoll, S. W. *Journal of Bone and Joint Surgery (Am.)* **1998**, *80*, 1795-1812.

123. Arnoczky, S. P.; Warren, R. F. *American Journal of Sports Medicine* **1983**, *11*, 131-141.

124. Bono, C. M.; Garfin, S. R. *The Spine Journal* **2004**, *4*, 145S-150S.

125. Lee, C. K.; Langrana, N. A. *The Spine Journal* **2004**, *4*, 173S-176S.

126. Hong, Y.; Song, H.; Gong, Y.; Mao, Z.; Gao, C.; Shen, J. *Acta Biomaterialia* **2007**, *3*, 23-31.

127. Hayami, J. W. S.; Surrao, D. C.; Waldman, S. D.; Amsden, B. G. *Journal of Biomedical Materials Research Part A* **2010**, *92*, 1407-1420.

128. Shen, J. Y.; Pan, X. Y.; Lim, C. H.; Chan-Park, M. B.; Zhu, X.; Beuerman, R. W. *Biomacromolecules* **2007**, *8*, 376-385.

129. Choi, A. P. C.; Zheng, Y. P. *Medical & Biological Engineering & Computing* **2005**, *43*, 258-264.

130. Jin, H.; Lewis, J. *Journal of Biomechanical Engineering* **2004**, *126*, 130-145.

131. Hayes, W. C.; Keer, L. M.; Herrmann, G.; Mockros, L. F. *Journal of Biomechanics* **1972**, *5*, 541-551.

132. Waldman, S. D.; Couto, D. C.; Grynpas, M. D.; Pilliar, R. M.; Kandel, R. A. *European Cells and Materials* **2007**, *13*, 66-75.

133. Suzuki, S.; Yamamuro, T.; Okumura, H.; Yamamoto, I. *The British Journal of Radiology* **1991**, *64*, 1001-1006.

134. Kim, Y.; Sah, R.; Doong, J.; Grodzinsky, A. *Analytical Biochemistry* **1988**, *174*, 168-176.

135. Goldberg, R.; Kolibas, L. *Connective Tissue Research* **1990**, *24*, 265-275.

136. Heinegard, D.; Bayliss, M.; Lorenzo, P. Biochemistry and metabolism of normal and osteoarthritic cartilage. In *Osteoarthritis;* Brandt, K., Doherty, M. and Lohmander, L., Eds.; Oxford University Press: New York, 1998; pp 74-84.

137. Woessner Jr, J. *Archieves of Biochemistry and Biophysics* **1961**, *93*, 440-447.

138. Armstrong, C.; Mow, V. *The Journal of Bone & Joint Surgery* **1982**, *64*, 88-94.

139. Grizzuti, N.; Buonocore, G.; Iorio, G. *Journal of Rheology* **2000**, *44*, 149-164.

140. Willemse, R. C.; Posthuma de Boer, A.; van Dam, J.; Gotsis, A. D. *Polymer* **1999**, *40*, 827-834.

141. Sundararaj, U.; Macosko, C. W. *Macromolecules* **1995**, *28*, 2647-2657.

142. Lee, H. M.; Park, O. O. *Journal of Rheology* **1994**, *38*, 1405-1425.

143. Anastasiadis, S. H.; Gancarz, I.; Koberstein, J. T. *Macromolecules* **1988**, *21*, 2980-2987.

144. Grace, H. P. *Chemical Engineering Communications* **1982**, *14*, 225-277.

145. Utracki, L. A. *Journal of Rheology* **1991**, *35*, 1615-1637.

146. Pearson, D. S.; Helfand, E. *Macromolecules* **1984**, *17*, 888-895.

147. Willemse, R. C.; Ramaker, E. J. J.; van Dam, J.; Posthuma de Boer, A. *Polymer* **1999**, *40*, 6651-6659.

148. Freed, L. E.; Martin, I.; Vunjak-Novakovic, G. *Orthopaedics and Related Research* **1999**, *367*, 46S-58S.

149. Roughley, P.; Hoemann, C.; DesRosiers, E.; Mwale, F.; Antoniou, J.; Alini, M. *Biomaterials* **2006**, *27*, 388-396.

150. Hayami, J. W.; Waldman, S. D.; Amsden, B. G. *Biomacromolecules* **2013**, *14*, 4236-4247.

151. Bogduk, N. *Radiologic Clinics of North America* **2012**, *50*, 613-628.

152. Modic, M. T.; Ross, J. S. *Radiology* **2007**, *245*, 43-61.

153. Fitzgerald, G. K.; Piva, S. R.; Irrgang, J. J. *Arthritis Care & Research* **2004**, *51*, 941-946.

154. Buckwalter, J.; Mankin, H. *Instructional Course Lectures* **1998**, *47*, 487.

155. Leone, A.; Guglielmi, G.; Cassar-Pullicino, V. N.; Bonomo, L. *Radiology* **2007**, *245*, 62-77.

156. Fujiwara, A.; Tamai, K.; An, H. S.; Kurihashi, A.; Lim, T. H.; Yoshida, H.; Saotome, K. *Journal of Spinal Disorders & Techniques* **2000**, *13*, 444-450.

157. Karppinen, J.; Shen, F. H.; Luk, K. D. K.; Andersson, G. B. J.; Cheung, K. M. C.; Samartzis, D. *Orthopedic Clinics of North America* **2011**, *42*, 513.

158. Luoma, K.; Riihimäki, H.; Luukkonen, R.; Raininko, R.; Viikari-Juntura, E.; Lamminen, A. *Spine* **2000**, *25*, 487-492.

159. Setton, L. A.; Elliott, D. M.; Mow, V. C. *Osteoarthritis and Cartilage* **1999**, *7*, 2-14.

160. Zhang, W.; Moskowitz, R.; Nuki, G.; Abramson, S.; Altman, R.; Arden, N.; Bierma-Zeinstra, S.; Brandt, K.; Croft, P.; Doherty, M. *Osteoarthritis and Cartilage* **2008**, *16*, 137-162.

161. Siepe, C. J.; Mayer, H. M.; Wiechert, K.; Korge, A. *Spine* **2006**, *31*, 1923-1932.

162. Schlegel, J. D.; Smith, J. A.; Schleusener, R. L. *Spine* **1996**, *21*, 970-981.

163. Lemaire, J. P.; Carrier, H.; Ali, E. H. S.; Skalli, W.; Lavaste, F. *Journal of spinal disorders & techniques* **2005**, *18*, 353-359.

164. Abbushi, A.; Endres, M.; Cabraja, M.; Kroppenstedt, S. N.; Thomale, U. W.; Sittinger, M.; Hegewald, A. A.; Morawietz, L.; Lemke, A. J.; Bansemer, V. G. *Spine* **2008**, *33*, 1527-1532.

165. Joshi, A.; Fussell, G.; Thomas, J.; Hsuan, A.; Lowman, A.; Karduna, A.; Vresilovic, E.; Marcolongo, M. *Biomaterials* **2006**, *27*, 176-184.

166. Spiller, K. L.; Laurencin, S. J.; Charlton, D.; Maher, S. A.; Lowman, A. M. *Acta biomaterialia* **2008**, *4*, 17-25.

167. Urban, J. *Rheumatology* **1994**, *33*, 901-908.

168. Urban, J. P. G.; Smith, S.; Fairbank, J. C. T. *Spine* **2004**, *29*, 2700-2709.

169. Kock, L.; van Donkelaar, C. C.; Ito, K. *Cell and Tissue Research* **2012**, *347*, 613-627.

170. Nesic, D.; Whiteside, R.; Brittberg, M.; Wendt, D.; Martin, I.; Mainil-Varlet, P. *Advanced Drug Delivery Reviews* **2006**, *58*, 300-322.

171. Hutmacher, D. W. *Biomaterials* **2000**, *21*, 2529-2543.

172. Slaughter, B. V.; Khurshid, S. S.; Fisher, O. Z.; Khademhosseini, A.; Peppas, N. A. *Adv Mater* **2009**, *21*, 3307-3329.

173. Kisiday, J.; Jin, M.; Kurz, B.; Hung, H.; Semino, C.; Zhang, S.; Grodzinsky, A. *Proceedings of the National Academy of Sciences* **2002**, *99*, 9996-10001.

174. Di Martino, A.; Vaccaro, A. R.; Lee, J. Y.; Denaro, V.; Lim, M. R. *Spine* **2005**, *30*, S16.

175. Park, S.; Hung, C.; Ateshian, G. *Osteoarthritis and Cartilage* **2004**, *12*, 65-73.

176. Yang, S.; Leong, K.; Du, Z.; Chua, C. *Tissue Engineering* **2001**, *7*, 679-689.

177. Rungseevijitprapa, W.; Bodmeier, R. *European Journal of Pharmaceutical Sciences* **2009**, *36*, 524-531.

178. Woessner, J. *Archives of Biochemistry and Biophysics* **1961**, *93*, 440-447.

179. Pego, A.; Siebum, B.; Van Luyn, M.; Gallego y Van Seijen, XJ; Poot, A.; Grijpma, D.; Feijen, J. *Tissue Engineering* **2003**, *9*, 981-994.

180. Cilurzo, F.; Selmin, F.; Minghetti, P.; Adami, M.; Bertoni, E.; Lauria, S.; Montanari, L. *AAPS PharmSciTech* **2011**, *12*, 604-609.

181. Mansour, J. M. *Kinesiology: the mechanics and pathomechanics of human movement* **2004**, *2*, 66-79.

182. Fujita, Y.; Duncan, N. A.; Lotz, J. C. *Journal of orthopaedic research* **1997**, *15*, 814-819.

183. Teoh, S. *Int. J. Fatigue* **2000**, *22*, 825-837.

184. Bertagnoli, R.; Sabatino, C. T.; Edwards, J. T.; Gontarz, G. A.; Prewett, A.; Parsons, J. R. *The Spine Journal* **2005**, *5*, 672-681.

185. Frank, E. H.; Jin, M.; Loening, A. M.; Levenston, M. E.; Grodzinsky, A. J. *Journal of Biomechanics* **2000**, *33*, 1523-1527.

186. Ishizaki, Y.; Burne, J. F.; Raff, M. C. *The Journal of Cell Biology* **1994**, *126*, 1069-1077.

187. Malin, M.; Hiljanen‐Vainio, M.; Karjalainen, T.; Seppälä, J. *Journal of Applied Polymer Science* **1996**, *59*, 1289-1298.

188. Zhu, K.; Hendren, R.; Jensen, K.; Pitt, C. *Macromolecules* **1991**, *24*, 1736-1740.

189. Pitt, G.; Gratzl, M.; Kimmel, G.; Surles, J.; Sohindler, A. *Biomaterials* **1981**, *2*, 215-220.

190. Pego, A.; Van Luyn, M.; Brouwer, L.; Van Wachem, P.; Poot, A.; Grijpma, D.; Feijen, J. *Journal of Biomedical Materials Research Part A* **2003**, *67*, 1044-1054.

191. Grizzi, I.; Garreau, H.; Li, S.; Vert, M. *Biomaterials* **1995**, *16*, 305-311.

192. Li, S.; McCarthy, S. *Biomaterials* **1999**, *20*, 35-44.

193. Hoemann, C. D.; Sun, J.; Chrzanowski, V.; Buschmann, M. D. *Analytical Biochemistry* **2002**, *300*, 1-10.

194. Buckwalter, J. A.; Mankin, H. J. *Instructional Course Lectures* **1998**, *47*, 487-504.

195. Buckwalter, J. A. *Spine* **1995**, *20*, 1307-1314.

196. Van Ooij, A.; Oner, F. C.; Verbout, A. J. *Spine* **2003**, *28*, 369-383.

197. Fehring, T. K.; Odum, S.; Griffin, W. L.; Mason, J. B.; Nadaud, M. *Clinical Orthopaedics and Related Research* **2001**, *392*, 315-318.

198. Korhonen, R.; Laasanen, M.; Töyräs, J.; Rieppo, J.; Hirvonen, J.; Helminen, H.; Jurvelin, J. *Journal of Biomechanics* **2002**, *35*, 903-909.

199. Johannessen, W.; Elliott, D. M. *Spine* **2005**, *30*, E724-E729.

200. Smeds, K. A.; Grinstaff, M. W. *Journal of Biomedical Materials Research* **2001**, *54*, 115-121.

201. Leach, J. B.; Bivens, K. A.; Patrick Jr, C. W.; Schmidt, C. E. *Biotechnology and bioengineering* **2003**, *82*, 578-589.

202. Li, Q.; Williams, C. G.; Sun, D. D.; Wang, J.; Leong, K.; Elisseeff, J. H. *Journal of Biomedical Materials Research Part A* **2004**, *68*, 28-33.

203. Burdick, J. A.; Chung, C.; Jia, X.; Randolph, M. A.; Langer, R. *Biomacromolecules* **2005**, *6*, 386-391.

204. Bryant, S. J.; Anseth, K. S. *Journal of Biomedical Materials Research* **2002**, *59*, 63-72.

205. Kisiday, J.; Jin, M.; Kurz, B.; Hung, H.; Semino, C.; Zhang, S.; Grodzinsky, A. *Proceedings of the National Academy of Sciences* **2002**, *99*, 9996-10001.

206. Levett, P. A.; Melchels, F. P.; Schrobback, K.; Hutmacher, D. W.; Malda, J.; Klein, T. J. *Acta Biomaterialia* **2014**, *10*, 214-223.

207. Anseth, K. S.; Bowman, C. N.; Brannon-Peppas, L. *Biomaterials* **1996**, *17*, 1647-1657.

208. Hu, X.; Li, D.; Zhou, F.; Gao, C. *Acta biomaterialia* **2011**, *7*, 1618-1626.

209. Muzzarelli, R. A.; Greco, F.; Busilacchi, A.; Sollazzo, V.; Gigante, A. *Carbohydrate Polymers* **2012**, *89*, 723-739.

210. Knudson, C. B.; Knudson, W. In *In Cartilage proteoglycans;* Seminars in cell & developmental biology; Elsevier: 2001; Vol. 12, pp 69-78.

211. Aruffo, A.; Stamenkovic, I.; Melnick, M.; Underhill, C. B.; Seed, B. *Cell* **1990**, *61*, 1303-1313.

212. Li, Q.; Wang, D.; Elisseeff, J. H. *Macromolecules* **2003**, *36*, 2556-2562.

213. Lee, K. Y.; Rowley, J. A.; Eiselt, P.; Moy, E. M.; Bouhadir, K. H.; Mooney, D. J. *Macromolecules* **2000**, *33*, 4291-4294.

214. Ingavle, G. C.; Dormer, N. H.; Gehrke, S. H.; Detamore, M. S. *Journal of Materials Science: Materials in Medicine* **2012**, *23*, 157-170.

215. Yu, F.; Cao, X.; Li, Y.; Zeng, L.; Yuan, B.; Chen, X. *Polymer Chemistry* **2014**, *5*, 1082-1090.

216. Van Vlierberghe, S.; Dubruel, P.; Lippens, E.; Masschaele, B.; Van Hoorebeke, L.; Cornelissen, M.; Unger, R.; Kirkpatrick, C.; Schacht, E. *Journal of Materials Science: Materials in Medicine* **2008**, *19*, 1459-1466.

217. Bayliss, M. T.; Osborne, D.; Woodhouse, S.; Davidson, C. *The Journal of Biological Chemistry* **1999**, *274*, 15892-15900.

218. Volpi, N.; Mucci, A.; Schenetti, L. *Carbohydrate Research* **1999**, *315*, 345-349.

219. Maleki, A.; Kjøniksen, A.; Nyström, B. In *Effect of pH on the behavior of hyaluronic acid in dilute and semidilute aqueous solutions;* Macromolecular symposia; Wiley Online Library: 2008; Vol. 274, pp 131-140.

220. Tømmeraas, K.; Melander, C. *Biomacromolecules* **2008**, *9*, 1535-1540.

221. Tokita, Y.; Okamoto, A. *Polymer Degradation and Stability* **1995**, *48*, 269-273.

222. Toole, B. P. In *In Hyaluronan in morphogenesis;* Seminars in Cell & Developmental Biology; Elsevier: 2001; Vol. 12, pp 79-87.

223. Sasazaki, Y.; Shore, R.; Seedhom, B. B. *Journal of Anatomy* **2006**, *208*, 681-694.

224. Nguyen, Q. T.; Hwang, Y.; Chen, A. C.; Varghese, S.; Sah, R. L. *Biomaterials* **2012**, *33*, 6682-6690.

225. Bryant, S. J.; Bender, R. J.; Durand, K. L.; Anseth, K. S. *Biotechnology and Bioengineering* **2004**, *86*, 747-755.

226. Guo, Y.; Yuan, T.; Xiao, Z.; Tang, P.; Xiao, Y.; Fan, Y.; Zhang, X. *Journal of Materials Science: Materials in Medicine* **2012**, *23*, 2267-2279.

227. Kim, I. L.; Mauck, R. L.; Burdick, J. A. *Biomaterials* **2011**, *32*, 8771-8782.

228. Masters, K. S.; Shah, D. N.; Leinwand, L. A.; Anseth, K. S. *Biomaterials* **2005**, *26*, 2517-2525.

229. Seidlits, S. K.; Khaing, Z. Z.; Petersen, R. R.; Nickels, J. D.; Vanscoy, J. E.; Shear, J. B.; Schmidt, C. E. *Biomaterials* **2010**, *31*, 3930-3940.

230. Imada, K.; Oka, H.; Kawasaki, D.; Miura, N.; Sato, T.; Ito, A. *Biological and Pharmaceutical Bulletin* **2010**, *33*, 410-414.

231. Nerucci, F.; Fioravanti, A.; Cicero, M. R.; Collodel, G.; Marcolongo, R. *OsteoArthritis and Cartilage* **2000**, *8*, 279-287.

232. Lippiello, L. *OsteoArthritis and Cartilage* **2003**, *11*, 335-342.

233. Temenoff, J. S.; Mikos, A. G. *Biomaterials* **2000**, *21*, 431-440.

234. Ifkovits, J. L.; Burdick, J. A. *Tissue Engineering* **2007**, *13*, 2369-2385.

235. Smith Callahan, L. A.; Ganios, A. M.; Childers, E. P.; Weiner, S. D.; Becker, L. M. *Acta Biomaterialia* **2013**, *9*, 6095-6104.

236. Vahdati, A.; Wagner, D. R. *Journal of Biomechanics* **2013**, *46*, 1554-1560.

237. Shin, H.; Temenoff, J. S.; Mikos, A. G. *Biomacromolecules* **2003**, *4*, 552-560.

238. Zhu, J. *Biomaterials* **2010**, *31*, 4639-4656.

239. Hayami, J. W. S.; Waldman, S. D.; Amsden, B. G. *Manuscript in preparation* **2014**.

240. Guilak, F.; Alexopoulos, L. G.; Upton, M. L.; Youn, I.; Choi, J. B.; Cao, L.; Setton, L. A.; Haider, M. A. *Annals of the New York Academy of Sciences* **2006**, *1068*, 498-512.

241. Guilak, F.; Jones, W. R.; Ting-Beall, H. P.; Lee, G. M. *Osteoarthritis and Cartilage* **1999**, *7*, 59-70.

242. Risbud, M. V.; Izzo, M. W.; Adams, C. S.; Arnold, W. W.; Hillibrand, A. S.; Vresilovic, E. J.; Vaccaro, A. R.; Albert, T. J.; Shapiro, I. M. *Spine* **2003**, 28, 2652-2659.

243. Matsumoto, T.; Kawakami, M.; Kuribayashi, K.; Takenaka, T.; Tamaki, T. *Spine* **1999**, 24, 315-319.

244. Sah, R. L.; Kim, Y. J.; Doong, J. Y.; Grodzinsky, A. J.; Plaas, A. H.; Sandy, J. D. *Journal of Orthopaedic Research* **1989**, 7, 619-636.

245. Leung, V. Y.; Chan, D.; Cheung, K. M. *European Spine Journal* **2006**, 15, 406-413.

246. Minogue, B. M.; Richardson, S. M.; Zeef, L. A.; Freemont, A. J.; Hoyland, J. A. *Arthritis & Rheumatism* **2010**, 62, 3695-3705.

247. Alini, M.; Eisenstein, S. M.; Ito, K.; Little, C.; Kettler, A. A.; Masuda, K.; Melrose, J.; Ralphs, J.; Stokes, I.; Wilke, H. J. *European Spine Journal* **2008**, 17, 2-19.

248. Beckstein, J. C.; Sen, S.; Schaer, T. P.; Vresilovic, E. J.; Elliott, D. M. *Spine* **2008**, 33, E166-E173.

249. Reid, J. E.; Meakin, J. R.; Robins, S. P.; Skakle, J. M. S.; Hukins, D. W. L. *Clinical Biomechanics* **2002**, 17, 312-314.

250. Wilke, H. J.; Kettler, A.; Claes, L. E. *Spine* **1997**, 22, 2365-2374.

Appendix

Controlled Diameter with Variable Height Cross-Linking Setup

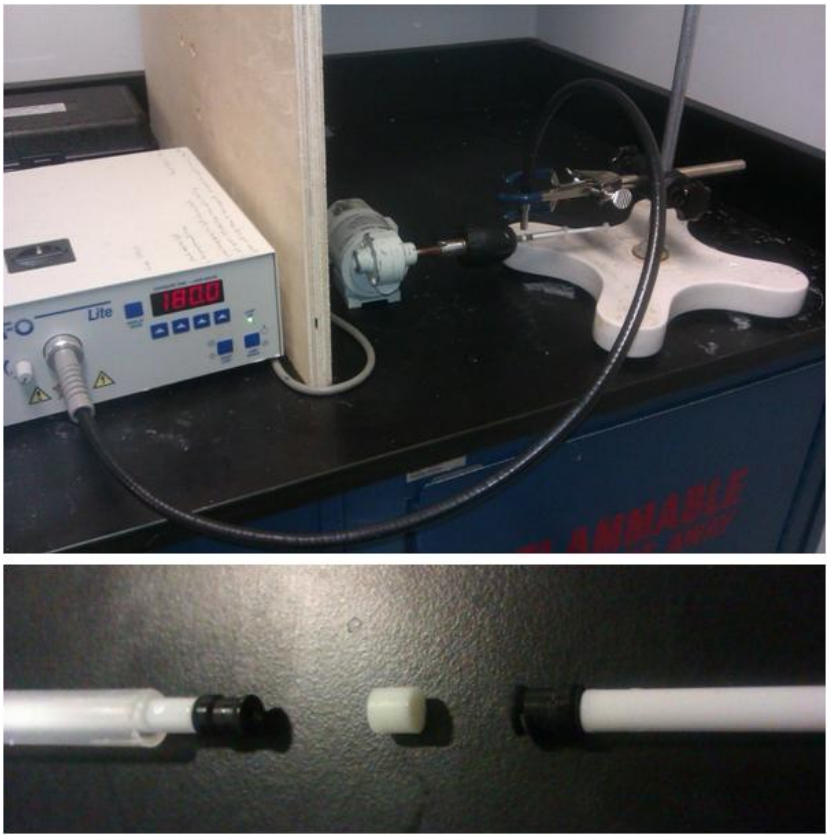

Figure A.1: Radial photo-cross-linking apparatus

Stress Relaxation Testing

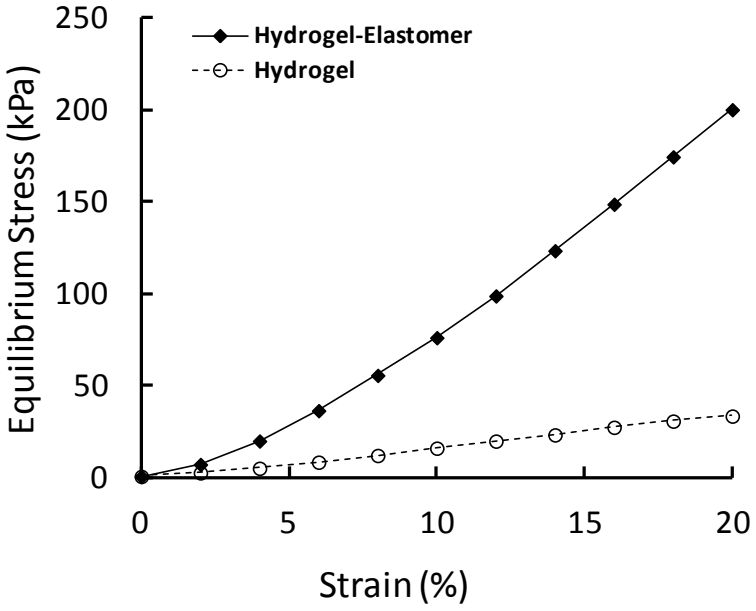

Figure A.2: Representative stress vs. strain plots of hydrogel-elastomer and hydrogel alone scaffolds that were used to calculate the equilibrium moduli.

Determination of degree of cross-linker substitution

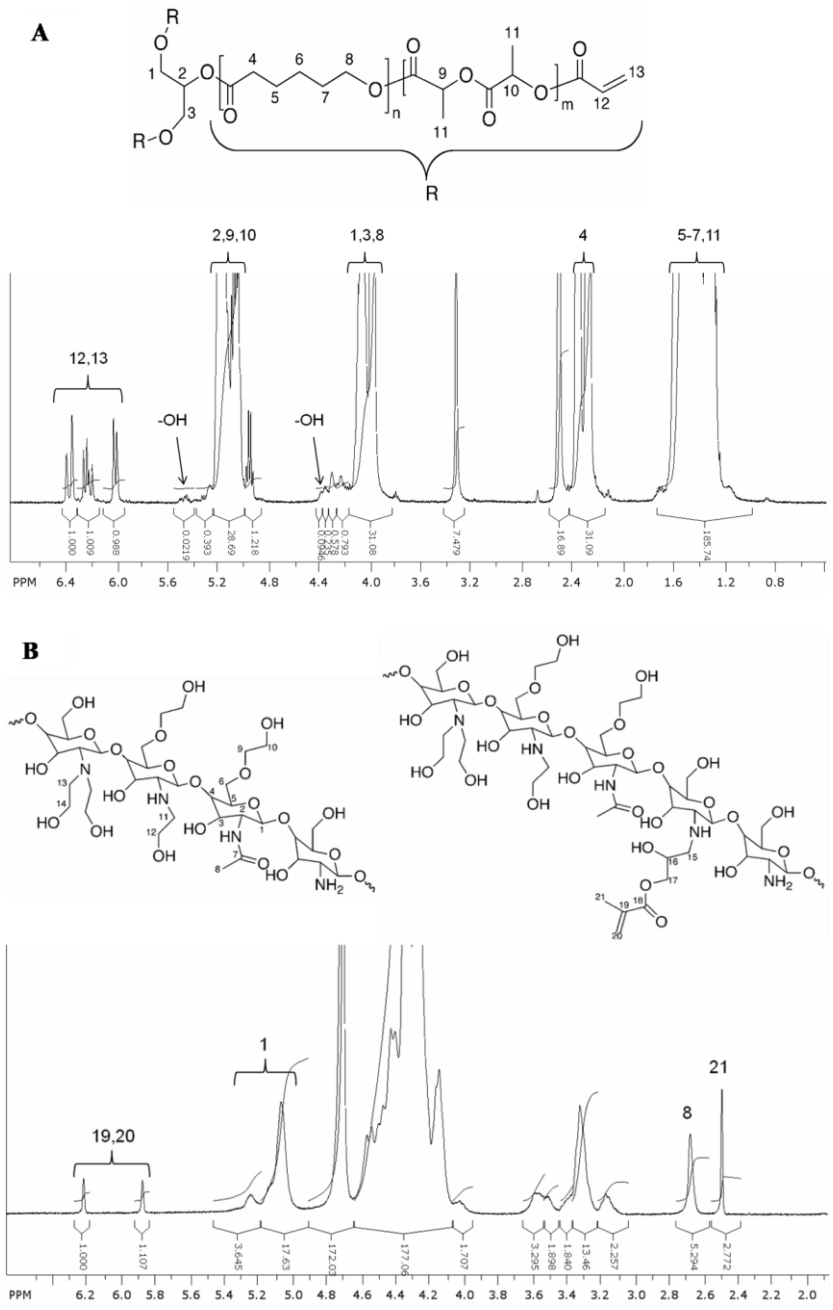

Figure A.3: Structure and ^{1}H NMR spectra of (A) 9.3K ASCP and (B) MGC pre-polymers. Degree of acrylation for the ASCP was determined from the ratio of the area under the peaks for the acrylate groups (peak 12 and 13) over the total area for the acrylate and unreacted –OH peaks. Degree of substitution for the MGC was calculated from the ratio of N-methacrylate groups (average of peak 19 and 20) over the total monomer groups (peak 1).

FTIR confirmation of degree of photo-cross-linking

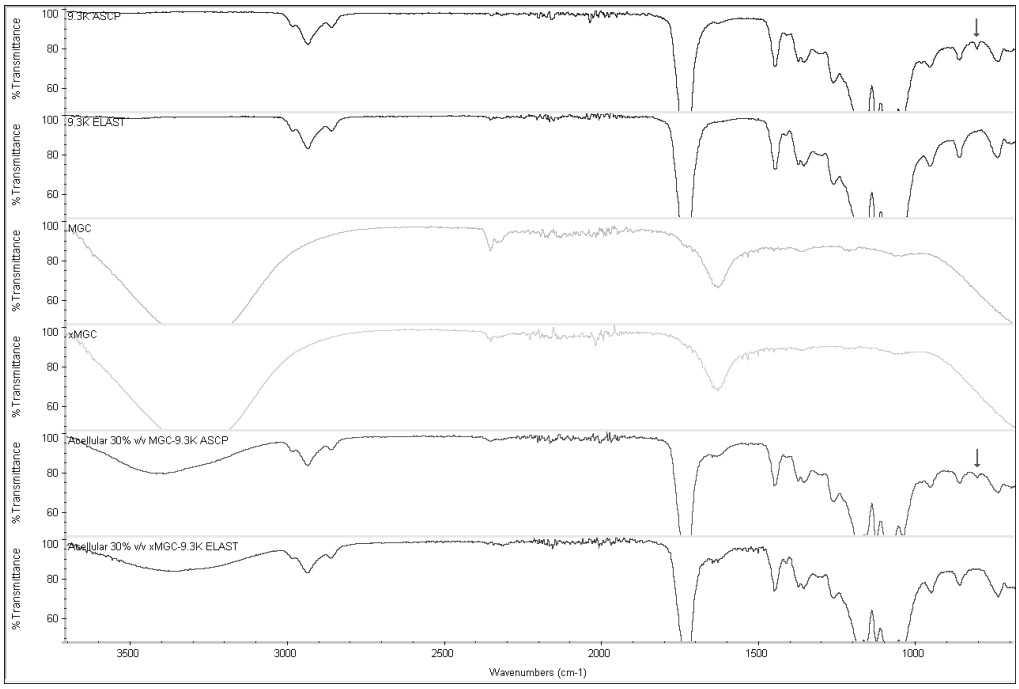

Figure A.4: FTIR of the individual components and acellular 30% v/v MGC-9.3KELAST scaffold before and after cross-linking. In order from top to bottom; 9.3K ASCP, 9.3K ELAST, MGC, MGC, acellular 30% v/v MGC-9.3KASCP and acellular 30% v/v MGC-9.3KELAST. Disappearance of –CH=CH_2 peak at 810 cm^{-1} (arrows) shows cross-linking of ASCP phase.

Morphology of Lower MGC Solution Loading on Co-continuous Morphology

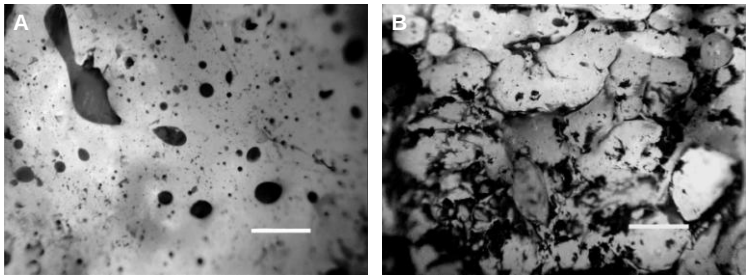

Figure A.5: Trypan blue stained images for lower MGC loading in 9.3KELAST scaffolds. (A) 15% v/v MGC and (B) 20% v/v MGC. Images were converted to black and white for better contrast; black for MGC and white for elastomer. Scale bar 100 μm.

Effect of Coarsening on Co-continuous Morphology

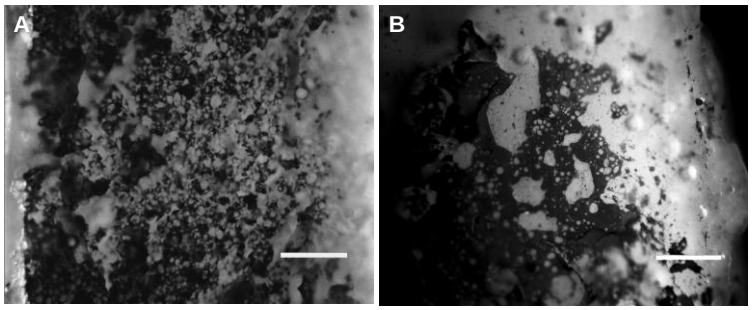

Figure A.6: Trypan blue stained images of the 30% v/v MGC-9.3KELAST scaffold to determine the effect of coarsening. (A) cross-linked immediately after mixing and (B) cross-linked after 1 hour at 37 ºC. Images were converted to black and white for better contrast; black for MGC and white for elastomer. Scale bar 100 μm.

GAG complexation with MGC hydrogel studies

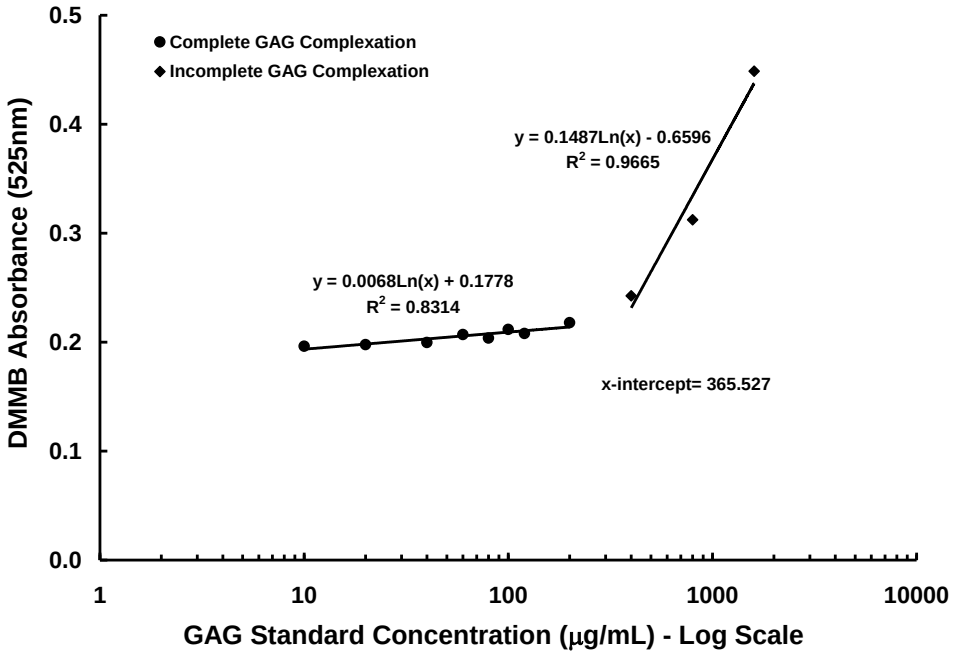

Figure A.7: DMMB absorbance readings used to detect amount of free GAG after complexation assay with MGC samples and various GAG standards. Plot of complete GAG standard adsorption and incomplete GAG standard adsorption. The intersection point of the two lines indicates the GAG standard complexation limit for a 21.7 ± 0.5 mg sample of MGC.

Injection Testing Setup

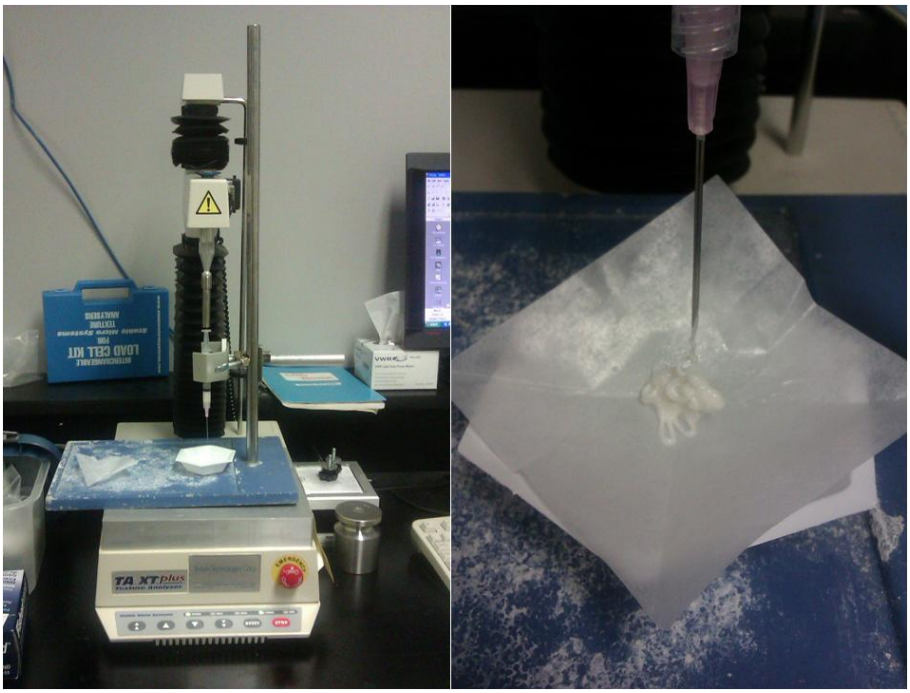

Figure A.8: Apparatus to measure force of injection in conventional syringe and needle combinations

Controlled Diameter with Variable Height Cross-Linking Setup

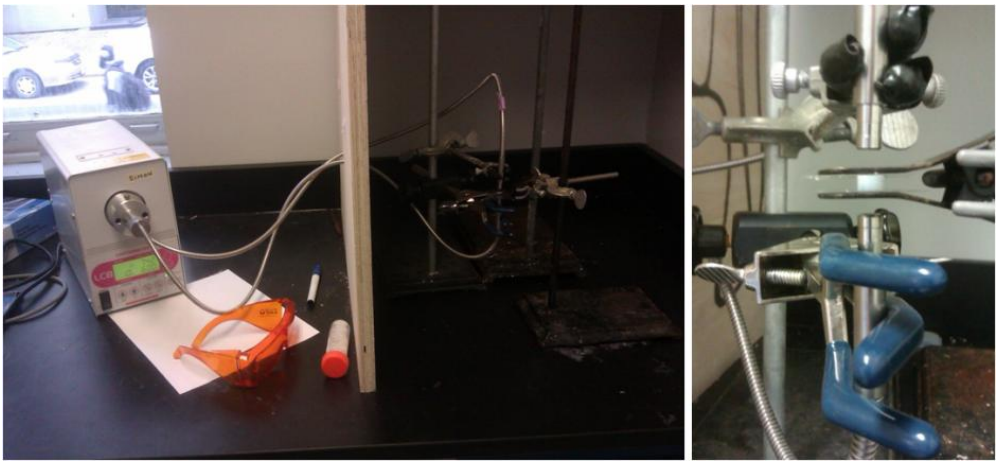

Figure A.9: Axial photo-cross-linking apparatus

Fatigue Testing Setup

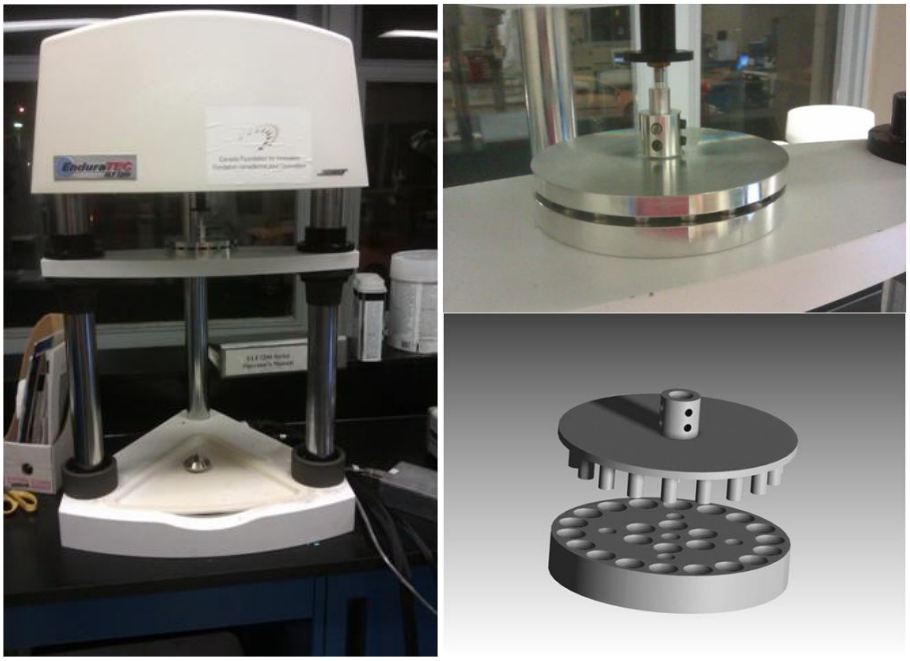

Figure A.10: Multi-platen apparatus for cyclic loading under physiological conditions

Co-continuous Scaffold Mass and Volume Pre- and Post-Fatigue

Table A.1: Change (%) in mass and volume data pre- and post-fatigue for 20 and 30% amplitudes for the 5446DLLACL and 7030TMCCL scaffolds. (*) Significant from all other values ($p < 0.05$)

	% change from initial values			
	Amplitude – Scaffold	Post-fatigue ($1x10^5$ cycles)	Post-fatigue ($5x10^5$ cycles)	Post-fatigue ($1x10^6$ cycles)
Mass	20% - DLLACL	1.4 ± 1.1	1.7 ± 0.5	0.4 ± 0.2
	30% - DLLACL	0.01 ± 0.7	1.4 ± 0.7	1.1 ± 1.4
	20% - TMCCL	0.5 ± 0.5	-0.1 ± 0.6	-0.1 ± 0.7
	30% - TMCCL	1.2 ± 0.3	0.1 ± 0.5	1.1 ± 0.3
Volume	20% - DLLACL	0.1 ± 0.1	-0.1 ± 0.1	-0.3 ± 0.3
	30% - DLLACL	1.6 ± 0.3	2.2 ± 0.3	1.6 ± 0.5
	20% - TMCCL	-0.1 ± 0.2*	-1.1 ± 0.3	-1.0 ± 0.1
	30% - TMCCL	-0.9 ± 0.1	-0.6 ± 0.3	-0.5 ± 0.4

Determination of DNA Content per Chondrocyte

Table A.2: DNA content as a function of cell number for primary bovine chondrocytes

Cell Number	DNA content (µg)	DNA (pg)/Cell Number
100000	0.59	5.87
400000	2.28	5.69
700000	3.86	5.51
1000000	5.21	5.21

Co-continuous Scaffold Mass and Volume Pre- and Post-Culture

Table A.3: Change (%) in mass and volume data pre- and post-culture for acellular and cellular scaffolds. (*) Significant from all other values, (**) significant from day 7 values ($p < 0.05$).

		% change from initial values			
	Scaffold	Post-culture (day 7)	Post-culture (day 21)	Post-culture (day 35)	Post-culture (day 56)
Mass	Acellular - DLLACL	-1.5 ± 0.3	-1.2 ± 1.1	0.9 ± 0.8**	10.1 ± 0.4*
	Cellular - DLLACL	0.6 ± 0.3	2.6 ± 0.6	3.2 ± 0.9**	7.7 ± 1.0*
	Acellular - TMCCL	-0.4 ± 0.5	-1.2 ± 0.4	-1.5 ± 0.7	-1.9 ± 0.6
	Cellular - TMCCL	1.9 ± 0.1	-1.3 ± 1.0	0.1 ± 0.4	0.1 ± 1.1
Volume	Acellular - DLLACL	0.0 ± 0.0	0.0 ± 0.0	0.0 ± 0.0	9.2 ± 0.7*
	Cellular - DLLACL	0.0 ± 0.0	0.0 ± 0.0	0.0 ± 0.0	8.0 ± 1.0*
	Acellular - TMCCL	-1.0 ± 0.4	-0.7 ± 0.3	-0.9 ± 0.4	-0.9 ± 0.2
	Cellular - TMCCL	0.1 ± 0.1	1.3 ± 0.4	-0.4 ± 0.3	-2.3 ± 0.4*

^{1}H NMR Spectra of Methacrylated Hyaluronic Acid and Chondroitin Sulfate

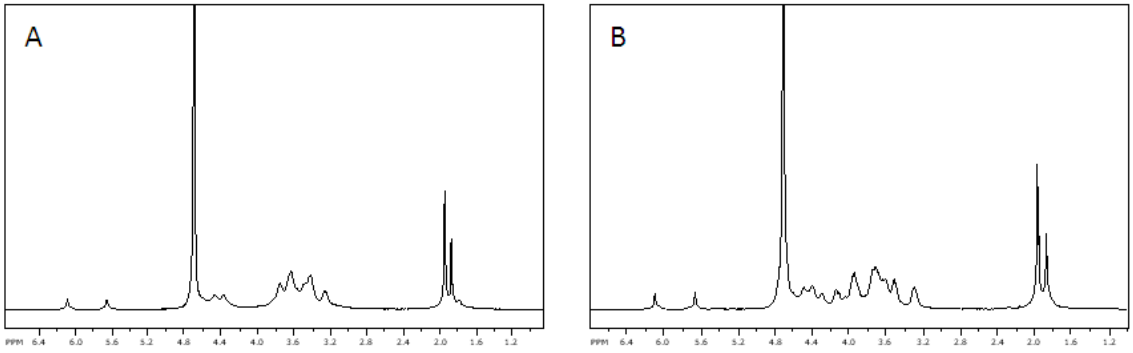

Figure A.11: Representative ^{1}H NMR spectra for A) methacrylated hyaluronic acid (MHA) and B) methacrylated chondroitin sulfate (MCS).

24 h Prepolymer Methacrylation and Hydrogel Characterization

Table A.4: Degree of methacrylation after 24 h reaction with no pH control for additional MHA and MCS prepolymers and equilibrium properties of their hydrogels

Hydrogel	Molar Ratio (MA:Dimer)	Degree of Methacrylation (%)	Equilibrium Modulus (kPa)	Swelling Ratio (q)
MHA-3	2.5	3	N/A	N/A
MCS-18	10	18	128.8 ± 6.5	11.6 ± 1.5
MCS-10	20	10	31.6 ± 4.4	23.4 ± 1.1

Crystallization of MGC Hydrogels

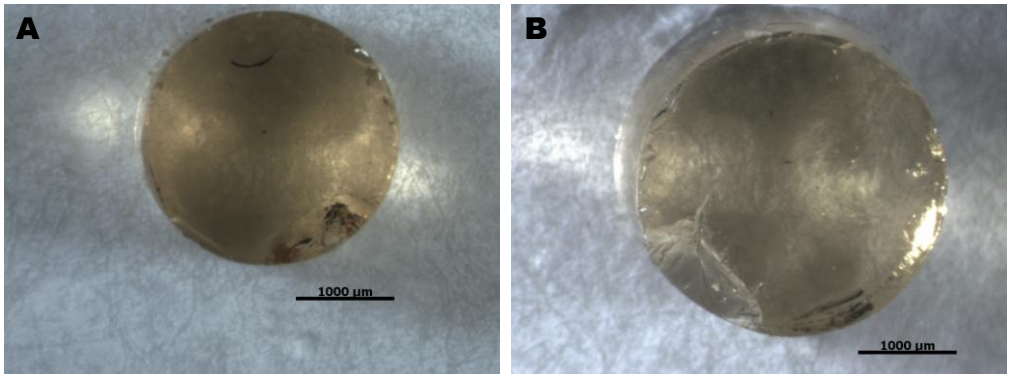

Figure A.12: Acellular 6wtMGC-12 hydrogel after 35 days in culture A) immediately after removal and B) after a 24 h soak in 1% acetic acid